NCAT Report 12-07

EVALUATION OF MIXTURE PERFORMANCE AND STRUCTURAL CAPACITY OF PAVEMENTS UTILIZING SHELL THIOPAVE®

Phase II:
Construction, Laboratory Evaluation and Full-Scale Testing of Thiopave® Test Sections – Final Report

By
Dr. David H. Timm
Mary M. Robbins
Dr. J. Richard Willis
Dr. Nam Tran
Adam J. Taylor

August 2012

National Center for Asphalt Technology
NCAT
at AUBURN UNIVERSITY

277 Technology Parkway ■ Auburn, AL 36830

NCAT Report 12-07

EVALUATION OF MIXTURE PERFORMANCE AND STRUCTURAL CAPACITY OF PAVEMENTS UTILIZING SHELL THIOPAVE®

Phase II:
Construction, Laboratory Evaluation and Full-Scale Testing
of Thiopave® Test Sections – Final Report

By
Dr. David H. Timm
Mary M. Robbins
Dr. J. Richard Willis
Dr. Nam Tran
Adam J. Taylor

National Center for Asphalt Technology
Auburn University

Sponsored by
Shell Oil Products, USA

August 2012

ACKNOWLEDGEMENTS

This project was sponsored by Shell Oil Products, USA. The project team appreciates and thanks Shell Oil Products, USA for their sponsorship of this project. Richard May deserves special recognition for providing detailed technical and editorial review of this document.

DISCLAIMER

The contents of this report reflect the views of the authors who are responsible for the facts and accuracy of the data presented herein. The contents do not necessarily reflect the official views or policies of Shell Oil Products, USA or the National Center for Asphalt Technology, or Auburn University. This report does not constitute a standard, specification, or regulation. Comments contained in this paper related to specific testing equipment and materials should not be considered an endorsement of any commercial product or service; no such endorsement is intended or implied.

TABLE OF CONTENTS

LIST OF TABLES

LIST OF FIGURES

1. INTRODUCTION

1.1 Background

In 2009, Shell Sulfur Solutions sponsored two full-scale experimental test sections at the National Center for Asphalt Technology (NCAT) pavement Test Track to evaluate the laboratory and structural characteristics of a newly-developed pelletized sulfur modified asphalt formulation called Thiopave[1] (Figure 1.1) As documented in an earlier report (Timm et al., 2011), the Thiopave system features sulfur pellets combined with a warm mix additive (WMA) that allows for production at temperatures around 275°F (135°C). At this temperature, hydrogen sulfide emissions are reduced to an acceptably low level. When fabricating laboratory mixes, the compaction aid is preblended with the virgin binder while sulfur pellets are added to the mixture immediately after the binder/compaction aid and aggregate have been combined. When plant-producing Thiopave mixes, the compaction aid is added to the asphalt stream before it reaches the aggregate. The pellets are added through the reclaimed asphalt pavement (RAP) collar or just after the asphalt binder entry point, away from the flame.

Figure 1.1 Thiopave Pellets and Compaction Aid (Timm et al., 2009)

The two sections were designed and constructed at the same time as a control section that did not feature any Thiopave materials (Figure 1.2). The control section, S9, had 7 inches (178 mm) of asphalt concrete (AC) over approximately 6 inches (152 mm) of aggregate base. This was also the case for one of the two Thiopave sections, section N6. The other Thiopave section, N5, had 2 inches (51 mm) more AC for a total AC depth of 9 inches (229 mm).

The materials and mix design for each AC lift were previously documented (Timm et al., 2009; Timm et al., 2011), while only a summary is provided here. There were five mixtures in this study that can be subdivided into "Thiopave-modified" and "control" mixtures. The control mixtures included surface, intermediate and base courses while the Thiopave mixtures were intermediate and base courses. The aggregate gradations were a blend of granite, limestone and sand using locally-available materials. Distinct gradations were developed for each control mixture (surface, intermediate and base) to achieve the necessary volumetric targets as the binder grade and nominal maximum aggregate size (NMAS) changed between layers. The Thiopave mixture gradations matched the intermediate control mixture gradation.

[1] Shell Thiopave is a trade mark of the Shell Group of Companies

The Thiopave base mixture was designed with 30% Thiopave replacing virgin binder and 2% air voids to potentially improve the fatigue cracking properties and durability through increased asphalt content. The intermediate Thiopave mixture was designed at 40% Thiopave and 3.5% air voids for better durability and to somewhat offset the stiffening effect of 40% binder replacement. The control materials mixtures were all designed at 4% air voids. It should be noted that during plant production of the mixtures, less-than-designed Thiopave contents were achieved. The 40% mixture was produced at 33% to 39% Thiopave while the 30% mixture was produced at 22% (Timm et al., 2011). Discussions between the NCAT researchers and Shell Sulfur Solutions engineers concluded in proceeding with the experiment with these Thiopave contents. Further details regarding mix design and construction of each lift are in Appendix A and previous reports (Timm et al., 2009; Timm et al., 2011).

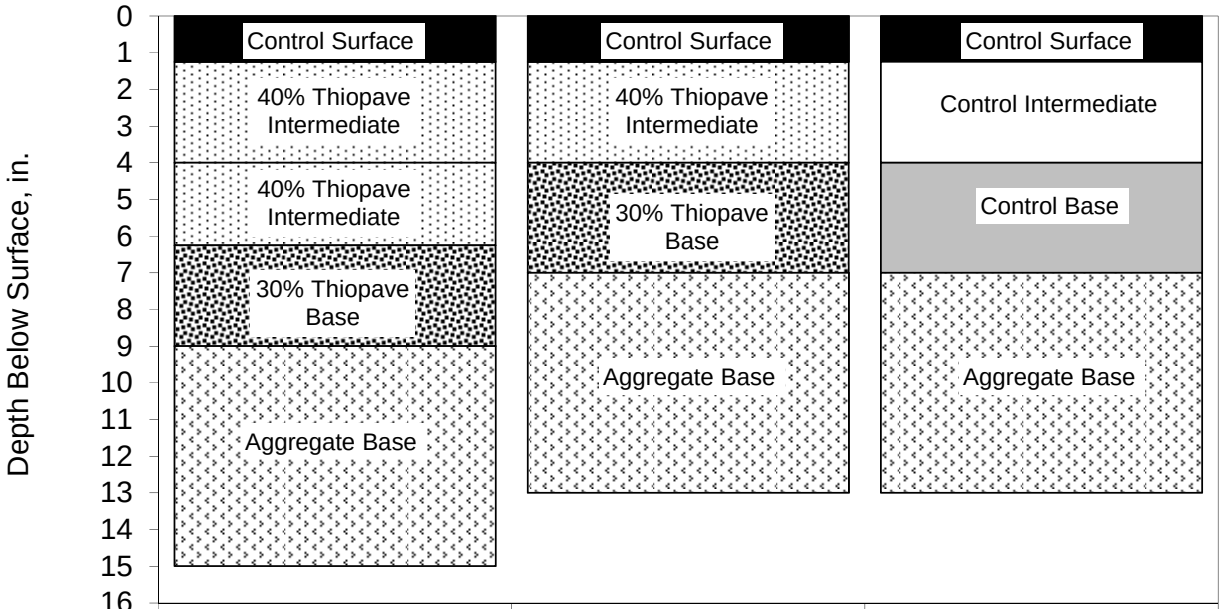

	Thiopave 9" (N5)	Thiopave 7" (N6)	Control 7" (S9)
Agg Base	6	6	6
Lift4	2.75		
Lift3	2.25	3	3
Lift2	2.75	2.75	2.75
Lift1	1.25	1.25	1.25

Figure 1.2 Cross-Section Design: Materials and Lift Thicknesses

During construction, sensors were embedded in each section to measure horizontal strain at the bottom of the AC, vertical pressure at the top of the aggregate base, vertical pressure at the top of the subgrade and temperatures at various depths throughout the cross-section (Figure 1.3). The strain and pressure measurements were made on a weekly basis during the two-year test cycle while the temperature measurements were made minute-by-minute, from which hourly averages were determined. Extensive falling weight deflectometer (FWD) testing was conducted at the twelve locations, noted in Figure 1.4, several times per month to document effects of pavement temperature, aging and potential pavement damage on backcalculated AC moduli during the two-year cycle. Full details regarding the instrumentation and FWD testing have been previously documented (Timm et al., 2011).

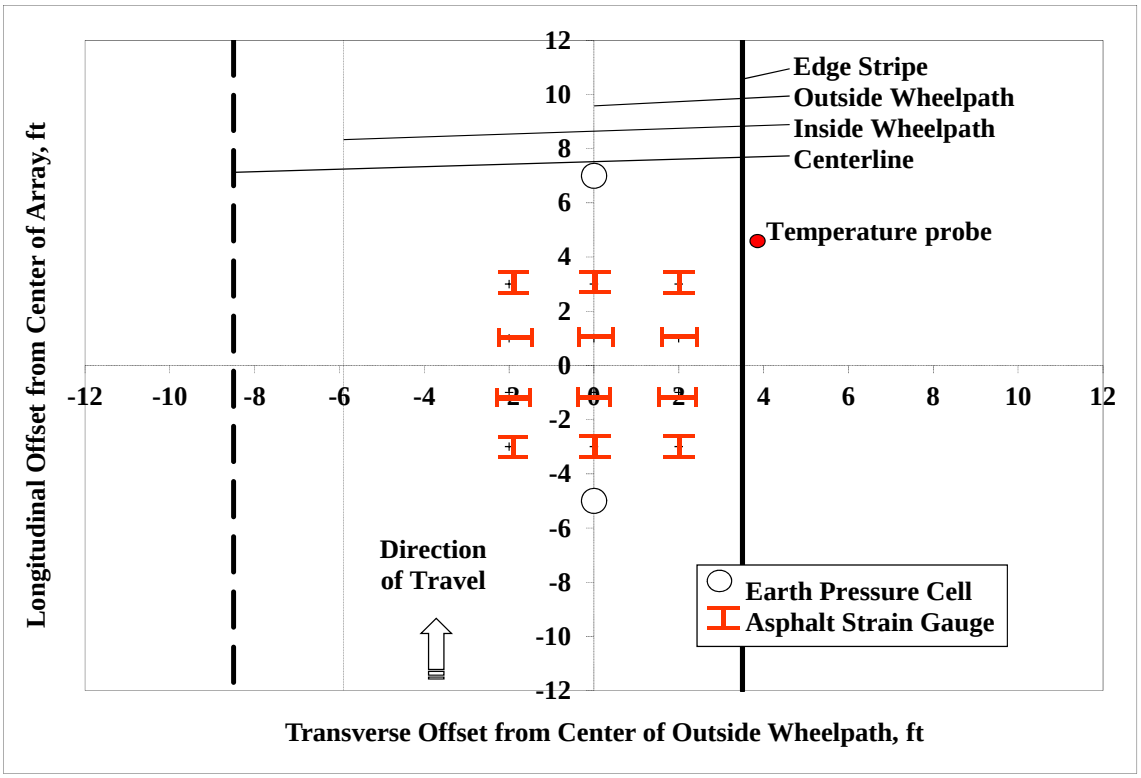

Figure 1.3 Gauge Array

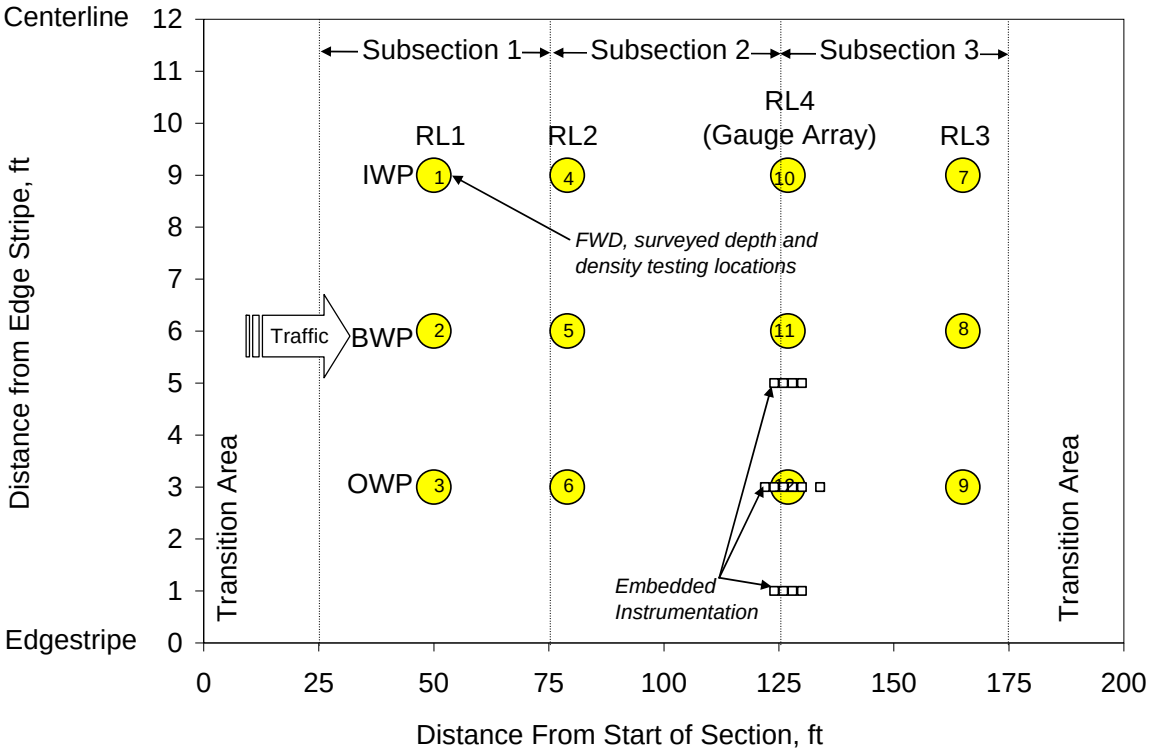

Figure 1.4 Random Location and Instrumentation Schematic

At the time of construction, plant-produced mixtures were sampled for extensive laboratory testing. The previous, interim, report (Timm et al., 2011) documented the sampling, fabrication of specimens and results for the following tests:

- Binder performance grading
- Multiple stress creep recovery (MSCR)
- Dynamic modulus (|E*|)
- Beam fatigue at three strain levels with two beams per strain level
- Asphalt pavement analyzer (APA)

Since the completion of the interim report, these remaining tests have been completed and are documented in this report:

- Hamburg wheel tracking test (HWTT)
- Flow number (F_n)
- Additional beam fatigue testing to have three beams per strain level
- Tensile strength ratio (TSR)
- Uniaxial fatigue (S-VECD)
- Low Temperature Cracking (IDT)

The sections were opened to traffic on August 28, 2009. At that time, weekly pavement response and regular FWD testing began. Weekly performance monitoring, in terms of rutting, ride quality and visual inspection for cracking, also commenced at that time. Trafficking ended on September 28, 2011 after the application of 10.14 million equivalent single axle loads (ESALs). On February 15, 2012, at the direction of the sponsor, two trenches were cut in N5, the 9-inch Thiopave test section, to further investigate rutting within the AC sublayers.

1.2 Objectives and Scope of Work

As mentioned previously, an interim report documenting findings after one year of testing was previously published (Timm et al., 2011). The objective of this report is to document findings from the laboratory testing not previously published and present the entire two-year pavement response and performance history. This report relies upon the one-year report (Timm et al., 2011) as a reference document. The overall goal of this work was to evaluate the Thiopave materials, with respect to laboratory and field performance, as an alternative to conventional asphalt mixtures.

2. LABORATORY TESTING ON PLANT PRODUCED MIXTURES

As described in the previous report (Timm et al., 2011), samples of asphalt binder and plant-produced mix were obtained at the Test Track during construction for characterization in the laboratory. The previous report detailed the sampling process, specimen fabrication and presented results from the tests noted above. Since the completion of the previous report (Timm et al. 2011), additional testing was conducted at the direction of the research sponsor as detailed in the subsections below. It should again be noted that the mixtures were sampled during production and that the target Thiopave contents were not as designed. For simplicity, and to be consistent with the previous report (Timm et al., 2011), the mixtures are referred to in the subsequent sections according to their design values of 30% and 40%, respectively. However, recall that the 30% design was produced at 22% and the 40% design was between 33 and 39%.

2.1 Hamburg Wheel Tracking Test (HWTT)

The Hamburg wheel-track testing (HWTT), shown in Figure 2.1, was performed to determine the rutting and stripping susceptibility of both Thiopave mixtures as well as the control base mixture. Testing was performed and specimens were prepared in accordance with AASHTO T 324. For each mix, three replicates were tested. The specimens were originally compacted to a diameter of 150 mm and a height of 115 mm. These specimens were then trimmed so that two specimens, with a height between 38 mm and 50 mm, were cut from the top and bottom of each gyratory-compacted specimen. The air voids on these cut specimens were 7 ± 2%.

The specimens were tested under a 158 ± 1 lbs wheel load for 10,000 cycles (20,000 passes) while submerged in a water bath which was maintained at a temperature of 50^{o}C. During testing, rut depths were measured by an LVDT which recorded the relative vertical position of the load wheel after each load cycle. After testing, these data were used to determine the point at which stripping occurred in the mixture under loading and the relative rutting susceptibility of those mixtures. Figure 2.2 illustrates typical data output from the Hamburg device. These data show the progression of rut depth with number of cycles. From this curve two tangents are evident, the steady-state rutting portion of the curve and the portion of the curve after stripping. The intersection of these two curve tangents defines the stripping inflection point of the mixture. The slope of the steady-state portion of the curve is also quantified and multiplied by the number of cycles per hour (2,520) to determine the rutting rate per hour. Comparing the stripping inflection points and rutting rates of the five different mixtures gives a measure of the relative moisture and deformation susceptibility of these mixtures.

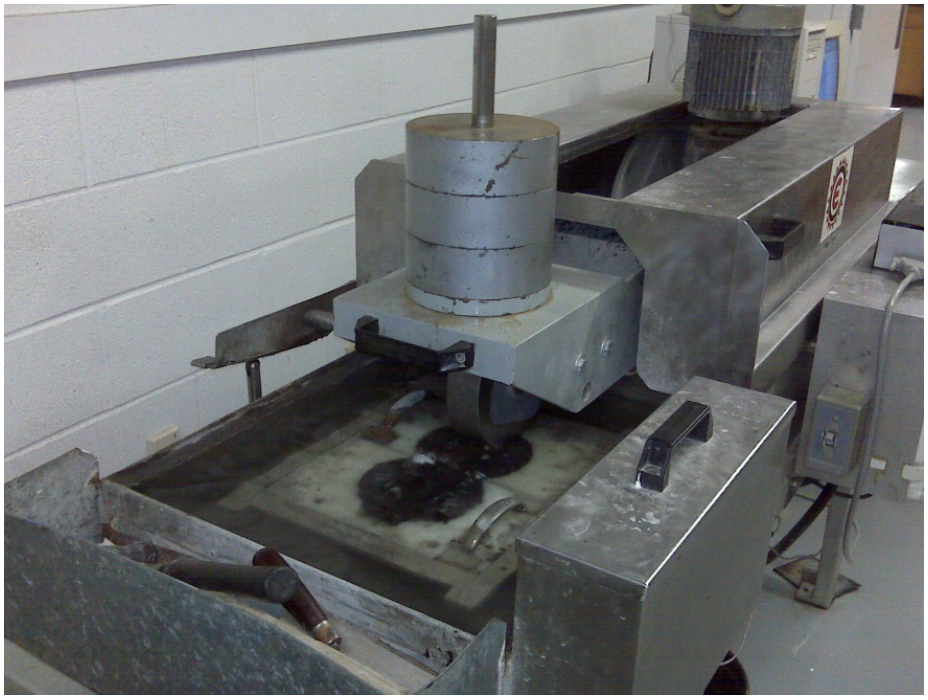

Figure 2.1 Hamburg Wheel-Tracking Device

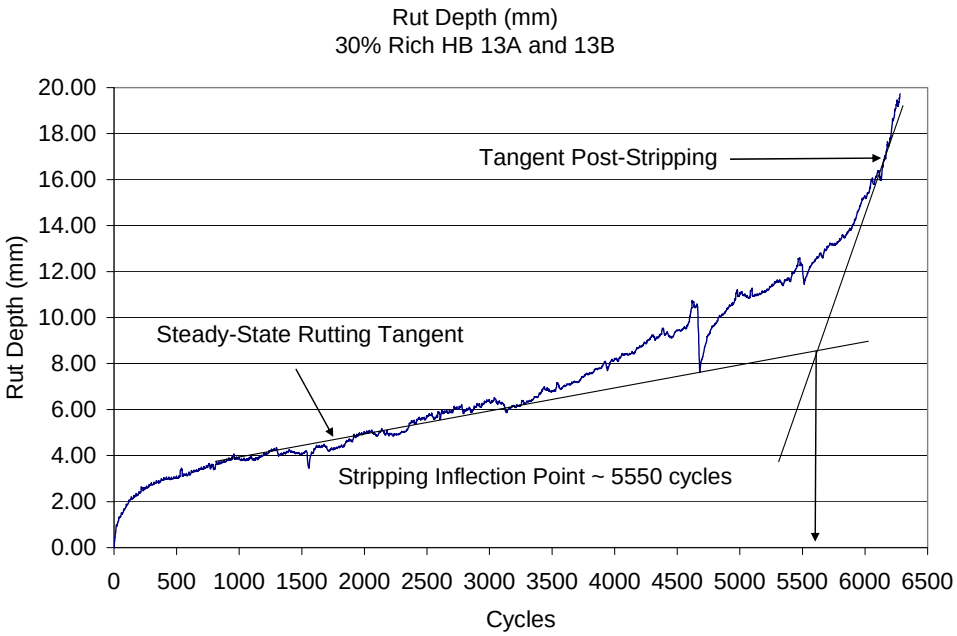

Figure 2.2 Example of Hamburg Raw Data Output

The average stripping inflection points for the three mixtures are shown in Figure 2.3. The error bars represent the ± one standard deviation of the three test results. Numerically, the 30% Thiopave mixture had the largest stripping inflection point. However, an ANOVA ($\alpha = 0.05$) showed no statistical difference between the three mixtures in terms of moisture susceptibility performance in the HWTT (p-value = 0.156).

While there are no nationally recognized specification standards for minimum stripping inflection points, 5,000 cycles is commonly used as a minimum threshold for mixtures resistant to moisture susceptibility (Brown et al., 2001). All three mixtures have average stripping inflection points greater than this minimum threshold.

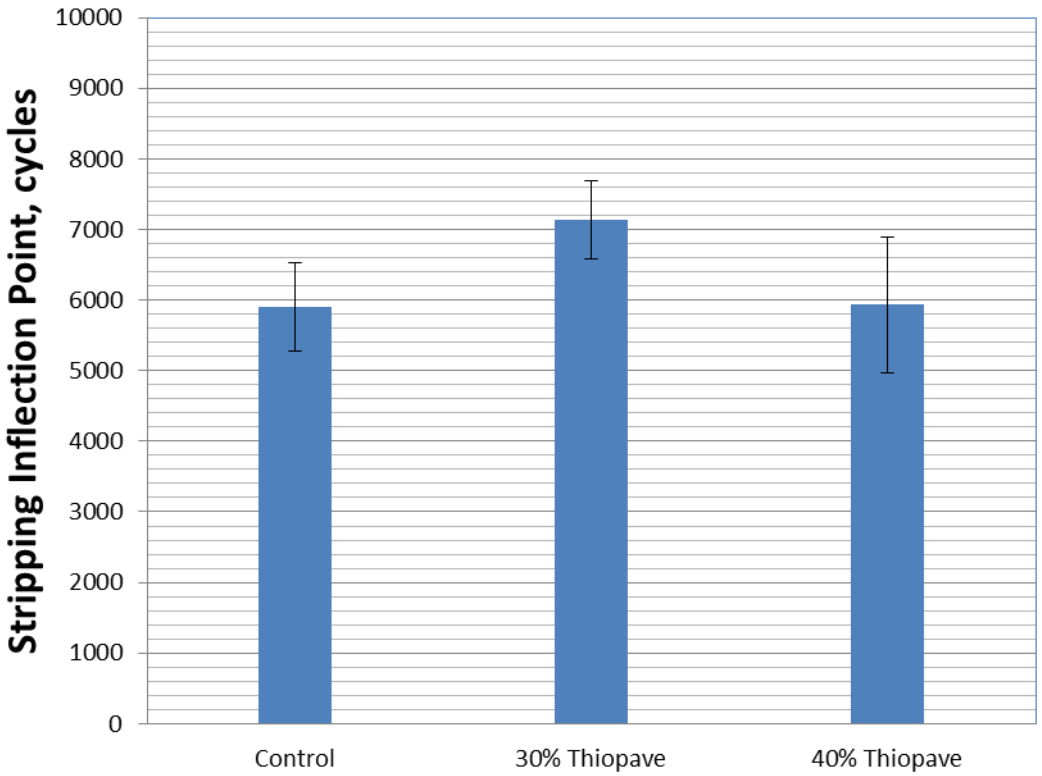

Figure 2.3 Average Stripping Inflection Points

HWTT characterizes an asphalt mixture's resistance to rutting as well as moisture susceptibility through measured rut depths in the HWTT test and rutting rates. However, there is not a national consensus in terms of maximum allowable rut depth or rutting rate for this testing methodology. The average rutting rates and total rut depths for the three mixtures are shown in Figure 2.4. The lower the rutting rates and rut depths, the more resistant the mixture should be in the field. An ANOVA ($\alpha = 0.05$) showed no statistical difference between the three mixtures in terms of either rutting rate (p-value = 0.118) or total rut depth (p-value = 0.118). If the HWTT results accurately characterize the behavior of the mix in the field, the three mixtures should have equivalent performance in terms of rutting.

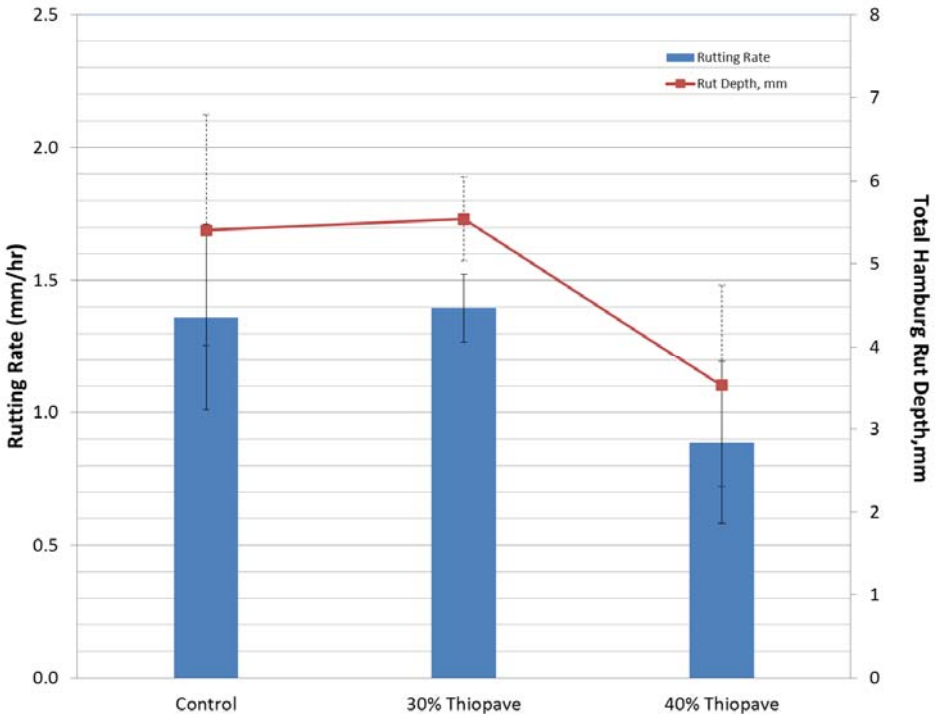

Figure 2.4 Average Hamburg Rutting Results

2.2 Flow Number (F_n)

The determination of the Flow Number (F_n) for the Thiopave and the control 19.0 mm mixtures was performed using an Asphalt Mixture Performance Tester (AMPT) to evaluate rutting potential. Flow number testing was conducted on new specimens, which had not been tested for dynamic modulus. The specimens were fabricated as described in the previous report (Timm et al., 2011). F_n tests were performed at 59.5°C, which is the LTPPBind (version 3.1) 50% reliability temperature at the Test Track at 20 mm below the surface of the pavement. Additionally, the specimens were tested using a deviator stress of 87 psi without the use of confinement. The tests were terminated when the samples reached 10% axial strain. The Francken model (Biligiri et al., 2007) shown in Equation 2.1 was used to determine tertiary flow. Non-linear regression analysis was used to fit the model to the test data.

$$\varepsilon_p(N) = aN^b + c(e^{dN} - 1) \quad (2.1)$$

where:

ε_p (N) = permanent strain at 'N' cycles
N = number of cycles
a, b, c, d = regression coefficients

Figure 2.5 compares the average flow number values for the two Thiopave mixtures as well as the control mixtures placed as the binder and base layer in section S9. Numerically, the 40% Thiopave intermediate mixture using a PG 67-22 base binder had the greatest flow number followed by the control intermediate mixture which used a PG 76-22 binder. However, the mixture which had the poorest numerical performance was the 30% Thiopave base mixture with the PG 67-22 binder, which is expected since this base mixture was designed with higher binder content at only 2 percent air voids. The mixture with 40% Thiopave had six times the resistance to rutting when compared to the 30% Thiopave mixture.

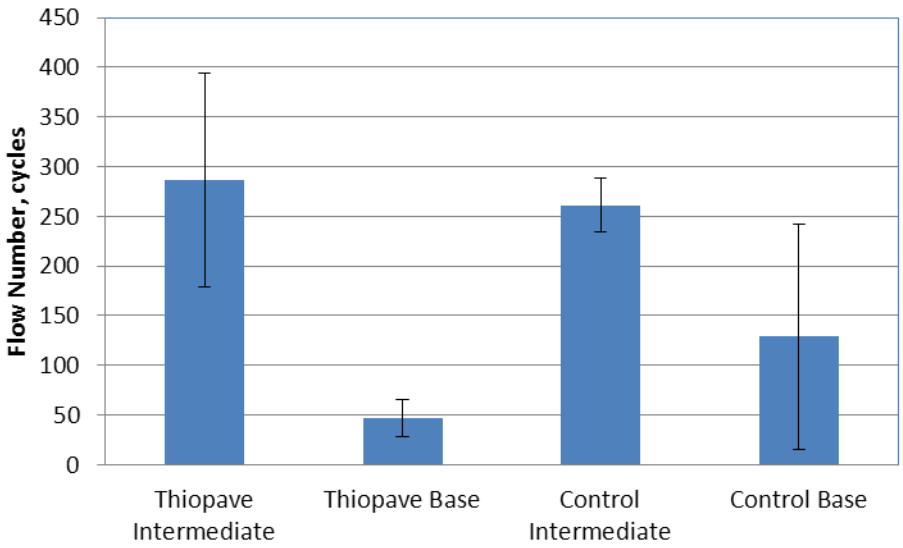

Figure 2.5 Flow Number Test Results

An ANOVA ($\alpha = 0.05$) conducted on the test results showed statistical differences ($p = 0.004$) between the performance of the four mixtures. A Tukey-Kramer analysis ($\alpha = 0.05$) was conducted to group the mixtures based on flow number performance. The Tukey-Kramer test is similar to the more commonly used ANOVA technique, but is able to determine statistical groupings. The 40% Thiopave mixture had equivalent resistance to rutting compared to both control mixtures. While the 30% Thiopave mixture was not as resistant to rutting as the 40% Thiopave mixture and the intermediate control mixture, it did have equivalent performance to the control base mixture. These results are likely due to the high variability in the control base and 40% Thiopave mixtures' flow number results. The COVs for these mixtures were higher than the recommended COV of 20% in AASHTO TP 79-09. However, inspection of the data set for the three specimens yielded no significant outliers that would enable removal of specific data points.

Recent recommendations have been developed for allowable flow numbers for both HMA and WMA mixtures (Table 2.1) when tested in the unconfined condition. Since Thiopave is considered a WMA technology, a reduction in flow number performance is expected compared to HMA mixtures. Since the average flow number for the 40% Thiopave mixture was 286 cycles, it is expected to be able to withstand 10 to 30 million ESALs of trafficking without accumulating significant rutting. Additionally, though the 30% Thiopave mixture only had an average flow number of 47, it still meets the requirements for trafficking of 3 to 10 million ESALs.

Table 2.1 Minimum F_n Requirements (Advanced Asphalt Technologies, 2011; Bonaquist 2011)

Traffic Level, Million ESALs	Minimum Flow Number	
	HMA	*WMA*
< 3	--	--
3 to < 10	53	30
10 to < 30	190	105
≥ 30	740	415

2.3 Beam Fatigue Testing

Bending beam fatigue testing was performed in accordance with AASHTO T 321-07 to determine the fatigue limits of the 19.0 NMAS asphalt mixtures. These were the base mixtures of the Thiopave and control sections. Nine beam specimens were tested for each mix. Each was compacted, per AASHTO T321-07, at 7 ± 1.0% air voids. Within each set of nine, three beams each were tested at 200, 400 and 800 microstrain. The methodology for beam fabrication, testing, and fatigue endurance limit calculations have been previously documented elsewhere (Timm et al, 2011). Data previously reported were based on testing only six beams (two beams at each strain level) as opposed to the nine beams used in this more complete analysis.

A summary of the bending beam fatigue test results for the plant-produced base layers mixtures is presented in Table 2.2. Figure 2.6 compares the fatigue cracking resistance from AASHTO T 321-07 results for the Thiopave and control base mixtures. A power model transfer function ($\varepsilon = \alpha_1 N^{\alpha_2}$) was used to fit the number of cycles to failure (N) to the applied strain level (ε). A summary of the model coefficients and R^2 values is given in Table 2.3. There was a significant difference between the magnitude of the intercept (α_1) and the slope (α_2) between the control mixture and the Thiopave mixtures. These differences were 39 and 21 percent, respectively. The R^2 values for each of the mixtures were above 91%, showing a good model fit for the dataset.

Table 2.2 Bending Beam Fatigue Test Results

Mixture	Microstrain Magnitude	Number of Cycles to Failure
Control Base	800	7,890
		4,260
		17,510
	400	201,060
		216,270
		141,250
	200	6,953,800
		5,994,840
		2,165,480
Thiopave Base	800	8,840
		6,760
		6,410
	400	398,100
		292,860
		82,110
	200	24,700,000*
		54,400,000*
		1,876,430

**Note: Failure point extrapolated based on three-stage Weibull function.*

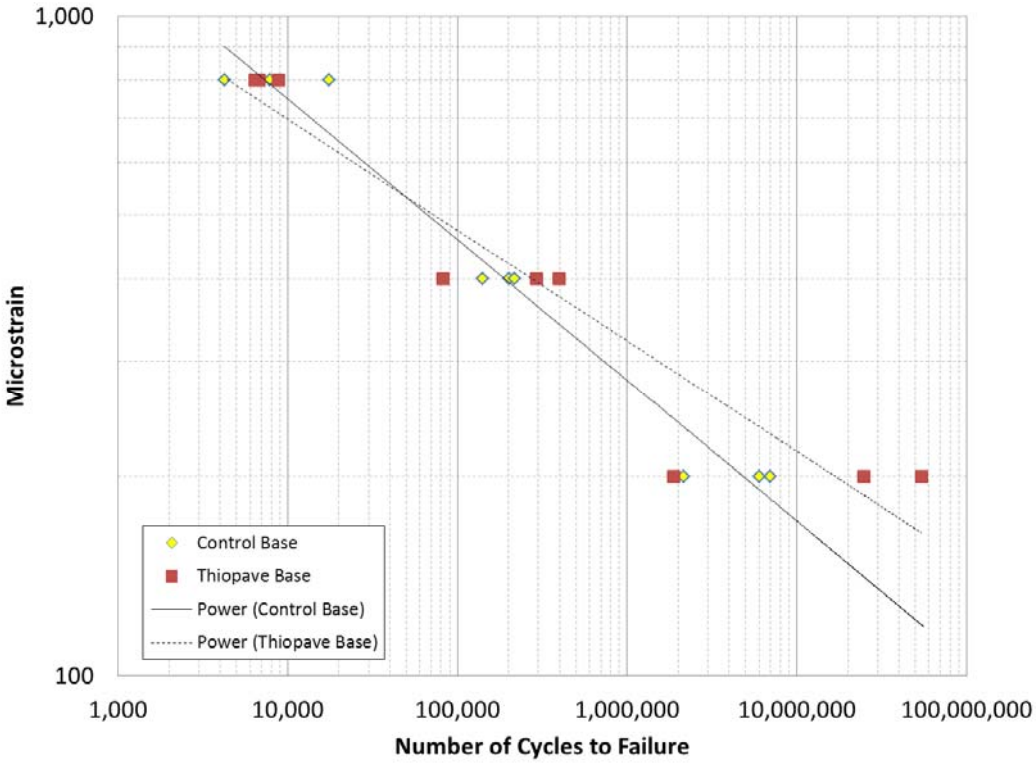

Figure 2.6 Comparison of Fatigue Resistance for Mixtures

Table 2.3 Fatigue Curve Fitting Coefficients (Power Model Form)

Mixture	AASHTO T321		
	α_1	α_2	R^2
Control Base	5374.2	-0.214	0.969
Thiopave Base	3290.7	-0.168	0.914

Table 2.4 shows that the percentage difference between the average fatigue life of the control mixture to that of the Thiopave mixture at the three strain levels tested in this study, using the failure criteria (50% reduction in beam stiffness) defined by AASHTO T 321-07. This information helps evaluate important aspects of the material behavior shown in Figure 2.6 as follows:

- At the highest tested strain (800 με), the base Thiopave mixture exhibited less fatigue life. The average fatigue life of the base Thiopave mixture was 25.6% shorter than that of the base control mixture. These results differ from those previously reported (Timm et al, 2011). While the third Thiopave beam at 800 με had similar fatigue life to the two previously tested beams, the third control mixture beam more than doubled the average fatigue life of the two previous beams.
- At 400 με, the average fatigue life of the base Thiopave mixture designed at 2 percent air voids was 38.4% longer than that of the control mixture.
- At 200 με, the base Thiopave mixture had an average fatigue life 436% longer than the control mixture. This percent increase should be viewed with some caution, however, since two of the Thiopave results were based on extrapolation.

Table 2.4 Percent Change in Cycles to Failure for Thiopave versus Control Mixture

Strain Level	200 με	400 με	800 με
Percent Change in Fatigue Life	436%	38.4%	-25.6%

It should be noted that the trends shown in Figure 2.6 and Table 2.4 were not evident during the preliminary laboratory investigation of these mixtures. This improved trend may be partially due to the lower than the design 30 percent Thiopave addition that was actually achieved during production. Lower Thiopave levels and increased binder content results from lower design air voids apparently achieves much better fatigue performance in the laboratory at moderate and low strain magnitudes.

Table 2.5 shows the 95% one-sided lower prediction of the fatigue endurance limit for the two mixtures tested in this study based on the number of cycles until failure determined in accordance with AASHTO T 321. The procedure for estimating the endurance limit was developed under NCHRP 9-38 (Prowell et al., 2010). Based on the results shown in Table 2.5, the Thiopave base mixture had a fatigue endurance limit 19.8% higher than the control mixture. Again, this may be attributed to the lower-than-expected amounts of Thiopave in this mixture combined with increased asphalt content. The lower Thiopave and higher asphalt contents also resulted in lower moduli than expected, so this demonstrates the tradeoff between modulus and fatigue resistance/tolerance that is possible with the Thiopave mixtures when evaluating these options in mixture design.

It should be noted that the fatigue endurance limit of the Thiopave mixture is approximately 30% lower than the previously reported endurance limit of 157 (Timm et al., 2011). This reduction occurred due to the performance of the third beams tested at 400 and 200 microstrain. At both strain magnitudes, a reduction in the cycles until failure was noticed compared to the first and second beams.

Table 2.5 Predicted Endurance Limits

Mixture	% Virgin Binder*	% Thiopave*	% Total Binder*	Endurance Limit (microstrain)
Control Base	4.7	0.0	4.7	91
Thiopave Base	4.8	1.4	6.2	109

**Note that percentages are of total mixture.*

2.4 Tensile Strength Ratio (TSR)

The moisture susceptibility of the two Thiopave mixtures and control base mixture was determined using AASHTO T 283-07. Six specimens of each mix were compacted to a height of 95 mm and an air void level of 7 ± 0.5%. Three conditioned specimens were vacuum saturated to the point at which 70 to 80% of the interval voids were filled with water. These specimens underwent a freeze-thaw cycle as specified by AASHTO T 283-07.

The indirect tensile strength was determined using a Pine Instruments® Marshall Stability press which loads the specimens at a rate of 2 in/min. The IDT strength was then calculated based on the failure loading and measured specimen dimensions. AASHTO M 323-07 recommends a tensile-strength ratio (TSR) value of 0.8 and above for moisture resistant mixtures.

Table 2.6 gives a summary of the results from the TSR testing of the three mixtures. The TSR values for the control base mixture and the 30% Thiopave mixture exceeded the suggested 0.80 lower limit. Only the 40% Thiopave mixture failed to meet this criterion. Thus, based on the AASHTO recommendation, the 40% Thiopave mixture would not pass for moisture susceptibility.

Table 2.6 also shows the average splitting tensile strengths for both control and Thiopave mixtures. While numerically the strengths of the Thiopave mixtures look less than those of the control mixture, the Tukey-Kramer statistical tests ($\alpha = 0.05$) showed equivalent performance for the control base mixture and the 40% Thiopave mixture. Only the 30% Thiopave mixture had lower conditioned and unconditioned splitting tensile strengths.

Table 2.6 Summary of TSR Testing

Mixture	Treatment	Average Splitting Tensile Strength (psi)	Standard Deviation (psi)	TSR
Control – Base	Conditioned	116.2	13.3	0.86
	Unconditioned	134.6	5.93	
30% Thiopave	Conditioned	78.2	6.30	0.84
	Unconditioned	92.6	10.5	
40% Thiopave	Conditioned	103.3	4.40	0.66
	Unconditioned	156.4	12.2	

2.5 Uniaxial Fatigue (S-VECD)

Uniaxial fatigue testing based on continuum damage mechanics has been studied and conducted in universal servo-hydraulic load frames to characterize the fatigue characteristics of asphalt mixtures. The theoretical background of this method has been presented in several publications (Kim et al., 1997; Daniel and Kim, 2002; Underwood et al., 2006; Hou et al., 2010). However, the recent draft test procedure by Dr. Richard Kim at North Carolina State University allows the uniaxial fatigue test (known as the S-VECD test) to be conducted in the AMPT.

To characterize the fatigue characteristics of a mixture using the S-VECD model, two tests are performed in the AMPT. First, the dynamic modulus of the mixture is determined according to the AASHTO TP 79-10 test protocol to quantify the linear viscoelastic (LVE) characteristics of the mix. Second, a controlled crosshead (CX) cyclic fatigue test is performed using the fatigue testing software in the AMPT to acquire the necessary fatigue data. The test protocol this software utilizes is discussed by Hou et al. (Hou et al., 2010). To conduct this test, an AMPT sample is glued with a steel epoxy to two end platens. The test specimen and end platens are then attached with screws to the actuator and reaction frame of the AMPT, prior to installing on-specimen LVDTs. A photo of this test setup is shown in Figure 2.7.

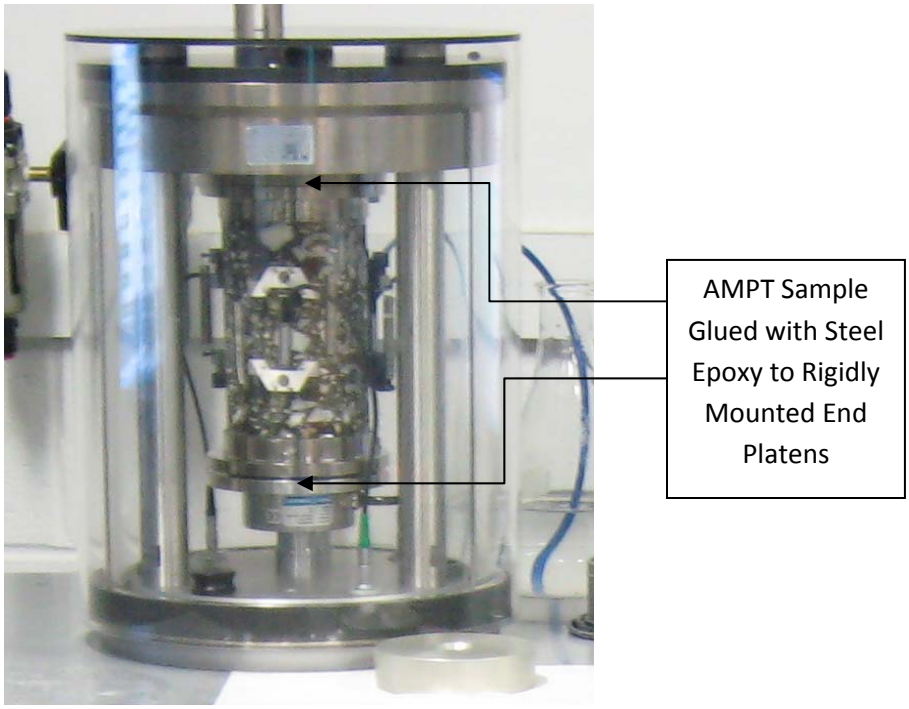

Figure 2.7 Photo of AMPT S-VECD Fatigue Test Setup

The CX test was performed at 20°C with a frequency of 10 Hz. Testing consisted of two phases. First, a small strain (50 to 75 on-specimen με) test was performed to determine the fingerprint dynamic modulus of the specimen. This was done to determine the ratio of the fingerprint dynamic modulus ($|E^*|_{Fingerprint}$) of the testing specimen to the dynamic modulus determined from AMPT dynamic modulus testing ($|E^*|_{LVE}$). This value is known as the dynamic modulus ratio (DMR) and is expected to be between 0.9 and 1.1 (Equation 2.2) (Hou et al., 2010). This

ratio is used for controlling the quality of the fatigue testing and is incorporated into the S-VECD fatigue model (Hou et al., 2010).

Second, the specimen was subjected to a fatigue test in which the AMPT actuator was programmed to reach a constant peak displacement with each loading cycle. During this test, the dynamic modulus and phase angle of the sample were recorded. Failure of the specimen was defined as the point at which the phase angle peaks and then dropped off (Hou et al., 2010). This concept is demonstrated graphically in Figure 2.8.

$$DMR = \frac{|E^*|_{Fingerprint}}{|E^*|_{LVE}} \tag{2.2}$$

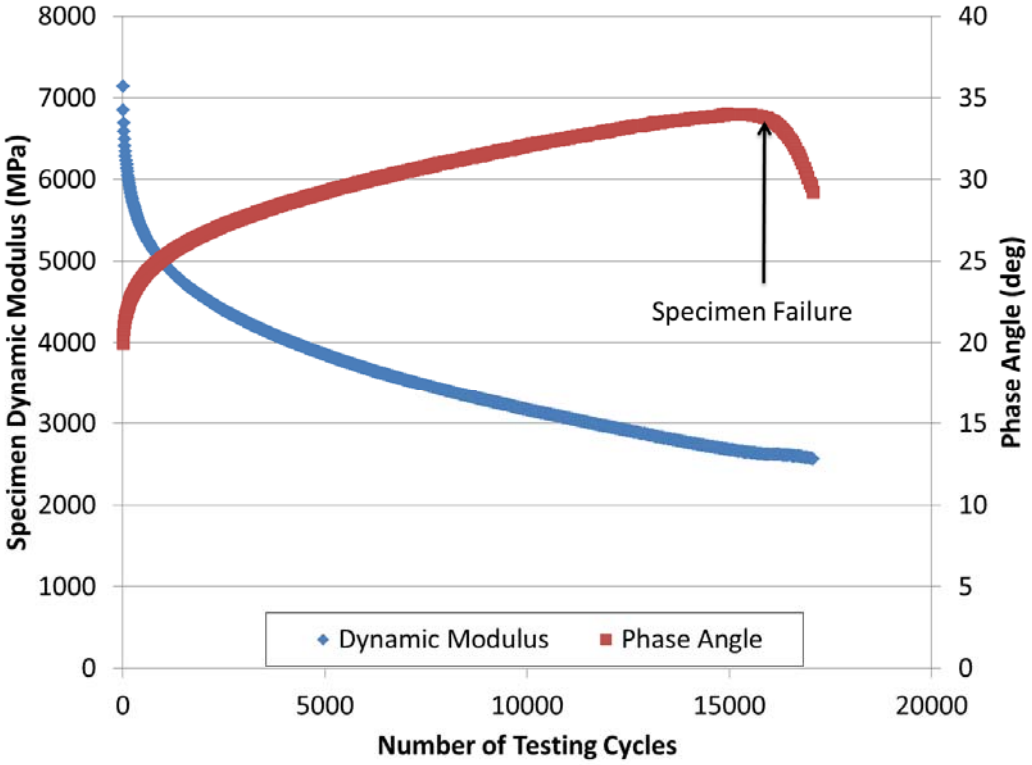

Figure 2.8 Determination of Cycles to Failure for S-VECD Fatigue Test

The initial target peak-to-peak on-specimen strain was specified in the software prior to the start of the test. It was desired that four fatigue specimens be tested with two replicates at two different strain levels. These strain levels were selected empirically so that the cycles to failure of the mix at the two strain levels were approximately an order of magnitude apart (i.e. 1,000 cycles to failure for one strain level versus 10,000 cycles to failure for another strain level). However, past research has shown that sufficient S-VECD fatigue predictions can be made with only two specimens (Hou et al., 2010). Both the dynamic modulus test and controlled crosshead cyclic test were performed using samples prepared in accordance with AASHTO PP 60-09. All samples were prepared to 7 ± 0.5% air voids. Typically, three specimens of mix were required for dynamic modulus testing and four to six specimens were needed to get sufficient fatigue data.

The S-VECD fatigue data analysis was performed using an analysis package developed at North Carolina State University. This software has been used for S-VECD fatigue testing on servo-hydraulic load frames in the past, but was updated to process the data generated by the fatigue testing software in the AMPT. Five primary steps were needed for the data processing:

1. The number of testing cycles to failure was determined for each specimen based on the phase angle curve (see Figure 2.8).
2. The AMPT dynamic modulus data were entered into the fatigue analysis software. The software utilized these data to compute the Prony series coefficients for creep compliance and relaxation modulus of the mixture (Hou et al., 2010). The dynamic modulus data were also used to determine the dynamic modulus mastercurve and the DMR value as discussed earlier.
3. The individual fatigue data files were individually analyzed to determine the C (pseudo-stiffness) versus S (damage parameter) curve. During this step, the individual files were examined to determine the value of C that corresponded to the 'failure' cycle for each mix.
4. The combined C versus S curve for the mix was then determined based on the individual C versus S curves. The composite C versus S curve was fit using a power law, shown as Equation 2.3 (where C_{11} and C_{12} are the regression coefficients) (Hou et al., 2010). These curves are fit to the point of failure (defined by C at failure) for each mix.
   $$C = 1 - C_{11} S^{C_{12}} \tag{2.3}$$
5. Finally, a fatigue prediction was made using the S-VECD model. Fatigue predictions for this study were made using the controlled-strain assumption based on the formula in Equation 2.4 (Hou et al., 2010). These fatigue simulations can be performed in the fatigue analysis software package. However, for this project these simulations were performed in an EXCEL® spreadsheet using the parameters developed by the fatigue analysis software for each mix.

$$Nf = \frac{(f_R)(2^{S\alpha})S_f^{\alpha-\alpha\cdot C_{12}+1}}{(\alpha-\alpha\cdot C_{12}+1)(C_{11}\cdot C_{12})^{\alpha}\left[(\beta+1)(\varepsilon_{0,pp})(|E^*|_{LVE})\right]^{2\alpha}K_1} \tag{2.4}$$

Where:
N_f = number of cycles until fatigue failure
C = pseudo-stiffness
S = damage parameter
f_R = reduced frequency for dynamic modulus shift factor at fatigue simulation temperature and loading frequency
α = damage evolution rate for S-VECD model
$\varepsilon_{0,pp}$ = peak-to-peak strain for fatigue simulation
$|E^*|_{LVE}$ = dynamic modulus of mix from dynamic modulus mastercurve at the fatigue simulation temperature and loading frequency
C_{11}, C_{12} = power law coefficients from C vs S regression
β = mean strain condition (assumed to be zero for this project)
K_1 = adjustment factor based on time history of loading – function of α and β

Simulations were performed on the control base mixture and the 30% Thiopave mixtures at constant-strain levels of 200, 400, and 800 με at a frequency of 10 Hz and a temperature of 20°C to match the beam fatigue testing parameters.

Figure 2.9 exhibits the pseudo-stiffness (C) versus damage parameter (S) curves for the two mixtures tested. These curves were modeled using the power model shown in Equation 2.3 and were generated by the fatigue analysis software. The curves are plotted to the average C at which the samples for that mix failed. It is noted that the curves of the two mixtures look similar in shape; however, the control base mixture had a higher C at failure than the Thiopave mixture. While it is difficult to look at the C-S curve and estimate mixture performance, when used in conjunction with modeling software, the expected mixture performance in either controlled strain or controlled stress can be estimated.

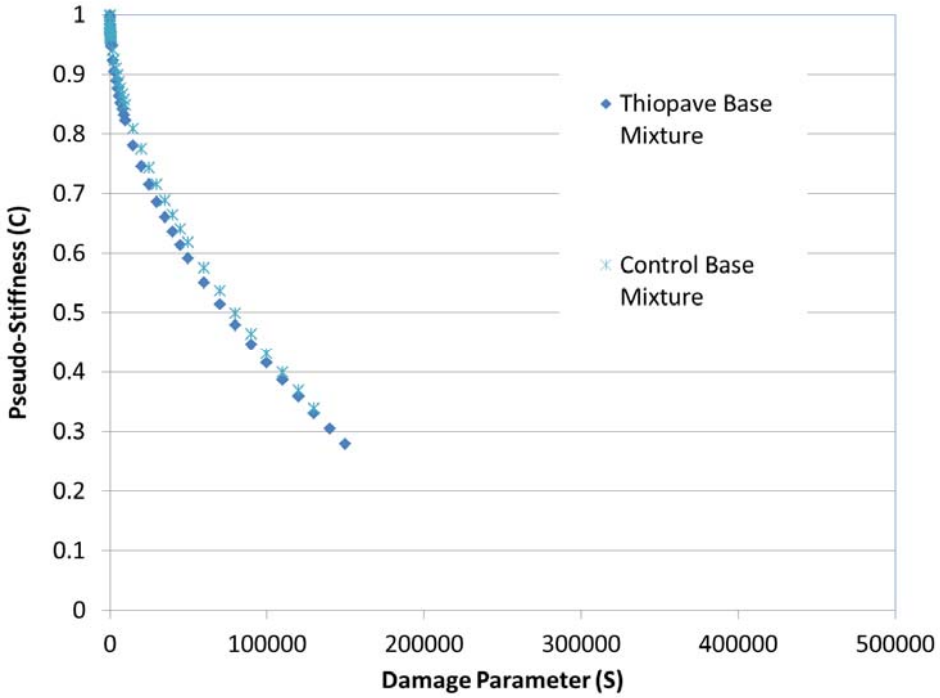

Figure 2.9 Pseudo-Stiffness (C) versus Damage Parameter (S) Curves

The damage characteristic curves generated from the S-VECD model were then combined with the material's modulus to fully evaluate the fatigue resistance of the mixtures. Figure 2.10 shows the predicted number of cycles to failure for both mixtures at various strain levels using the beam fatigue testing parameters. As can be seen, at higher strain magnitudes, the performance of the Thiopave and base mixtures was expected to be practically the same; however, at lower strain magnitudes, the Thiopave mixture was predicted to outperform the control base mixture.

A paired *t*-test ($\alpha = 0.05$) was used to determine if the predicted cycles to failure for the two mixtures were statistically equivalent. While there were numerical differences in the performance of the mixtures, there was not a statistical difference between the predicted cycles to failure ($p = 0.390$).

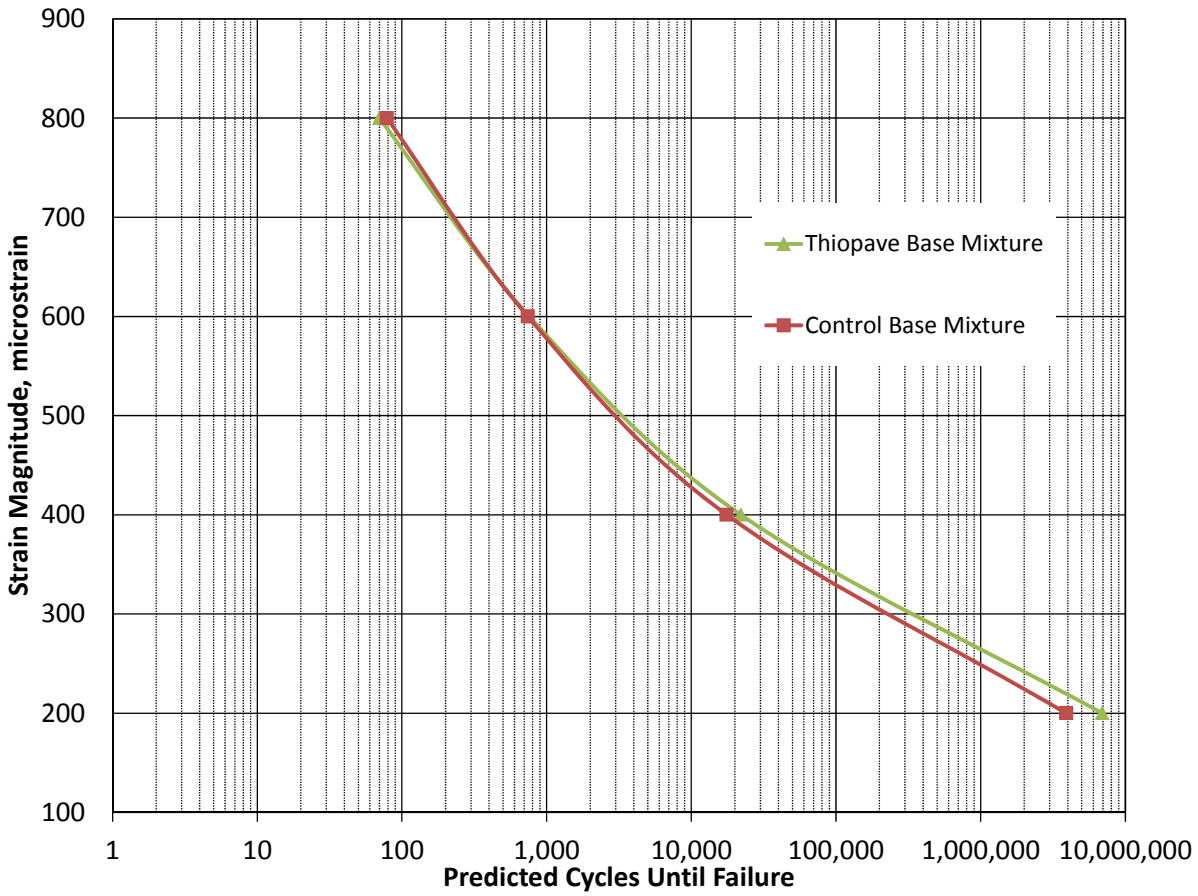

Figure 2.10 Predicted Cycles Until Failure

2.6 Indirect Tension and Strength Testing (IDT)

The critical cracking temperature where the estimated thermal stress exceeds the tested indirect tensile strength of a mixture is used to characterize the low temperature cracking performance of asphalt mixtures. This type of analysis could be referred to as a 'critical temperature analysis.' The lower a mixture's critical cracking temperature, the more resistant that mixture should be to thermal cracking. Both the control and Thiopave mixtures were evaluated using a critical temperature analysis for this study. To estimate the thermal stress and measure the tensile strength at failure, the indirect tensile creep compliance and strength tests (IDT) were conducted for three replicates of each mix as specified in AASHTO T 322-07. A thermal coefficient of contraction for each mixture was estimated based on its volumetric properties and typical values for the thermal coefficient of asphalt and aggregate. This computation is explained in more detail below.

While thermal cracking is not of concern for pavements at the Test Track due to the relatively warm climate, this evaluation was conducted to determine if the Thiopave mixes had equivalent low-temperature cracking performance to that of the control AC. Previous research has indicated this to be the case, albeit using a different laboratory test (thermal stress-restrained specimen

testing or TSRST) (Timm, et al. 2009). Additional research of Thiopave sections paved at NCAT during the WMA Certification program indicated that the addition of Thiopave did not reduce the critical cracking temperature enough to alter the low PG grade of the base binder (Powell and Taylor, 2012).

The IDT system (Figure 2.11), which has been used to predict thermal stress development and low temperature cracking in asphalt mixtures, was used to collect the necessary data for the critical cracking temperature analysis. The testing was conducted using an MTS load frame equipped with an environmental chamber capable of maintaining the low temperatures required for this test. Creep compliance at 0°C, -10°C and -20°C and tensile strength at -10°C in accordance with AASHTO T 322-07 were measured. These temperatures are specified as a function of the low temperature PG grade of the binder in AASHTO T 322-07. The creep test applies a constant load to the asphalt specimen for 100 seconds while the horizontal and vertical strains are measured on each face of the specimen using on-specimen instrumentation.

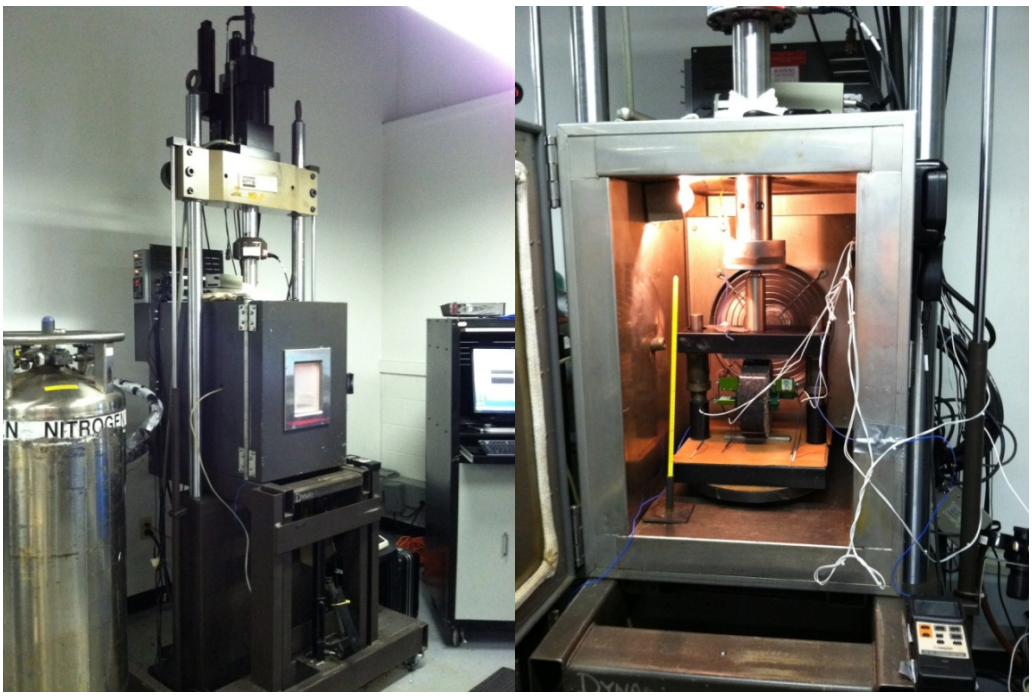

Figure 2.11 MTS® Testing Device used for IDT Testing

Four specimens were prepared for each mix. The first sample was used to find a suitable creep load for that particular mix at each testing temperature. The remaining three specimens were tested at this load for the tested data set. Specimens used for the creep and strength tests were 38 to 50 mm thick and 150 mm in diameter. Specimens were prepared to 7 ± 0.5% air voids. The analyzed creep compliance data and the individual splitting tensile strength values for these mixes are provided in Appendix B.

A complete summary of the methodology used to determine the critical cracking temperature is documented elsewhere (Powell and Taylor 2012). Two primary results are generated by the critical temperature analysis. First, a plot of thermal stress developed in the mixture as a function of time is developed. Secondly, the critical cracking temperature of the asphalt mixture is determined. This temperature represents the temperature at which the predicted thermal tensile stress (generated from the creep compliance data) exceeds the measured indirect tensile strength.

Figure 2.12 shows thermal stress development as a function of a reduction in temperature. Table 2.7 shows the critical temperature and time to failure determined at the point where thermal stress exceeds the tensile strength. Table 2.7 also shows the low-temperature PG grade of the mix as determined by the critical cracking temperature. The final critical temperature is based on an aggregate data set which has been processed into a singular point. Therefore, statistical analyses cannot be completed on the data.

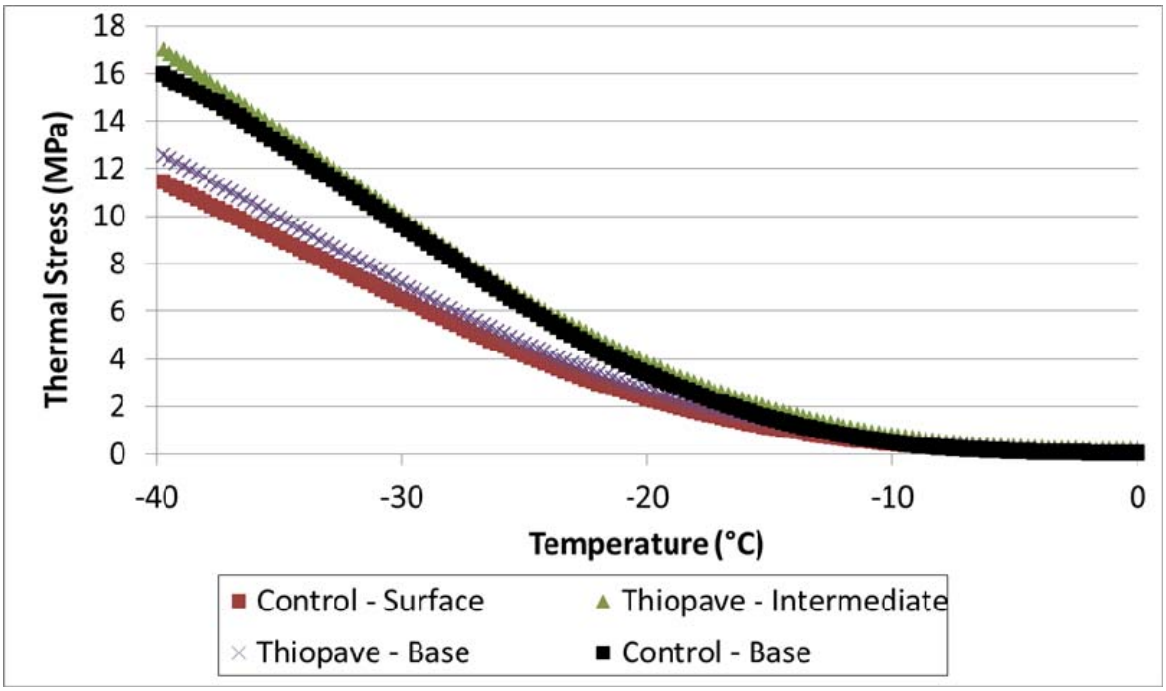

Figure 2.12 Thermal Stress versus Temperature – AASHTO T 322-07 Testing

Table 2.7 Critical Temperature Summary – AASHTO T 322-07

Data	Control – Surface	Control- Base	Thiopave - Intermediate	Thiopave - Base
Failure Time (hour)	4.64	4.14	4.08	4.36
Failure Temperature (deg C)	-26.4	-21.4	-20.8	-23.6
NMAS (mm)	9.5	19	19	19

Based on the results in Figure 2.12, at temperatures below -15°C the control base and Thiopave intermediate mixtures appear to develop thermal stress at a faster rate than that of the Thiopave base and control surface mixtures. The data in Table 2.7 show all of the mixtures have critical cracking temperatures within a 6°C range, with the control surface mixture having the lowest critical temperature (-26.4°C) and the Thiopave intermediate mix having the highest critical temperature (-20.8°C). Therefore, all mixtures had critical temperatures within one PG grade of each other. All of the mixtures used a PG XX-22 base binder grade. From the data in Table 2.7, two of the mixes (control base and Thiopave intermediate) had critical cracking temperatures below the virgin binder grade, performing below expectations. When looking at 19mm NMAS mixes only, all three mixtures had critical cracking temperatures within 3°C of each other. For the 19mm NMAS mixtures, the Thiopave intermediate mixture and Thiopave base mixture had the highest and lowest critical temperatures, respectively. Therefore, there is no clear trend showing the addition of Thiopave having a negative impact on the low temperature cracking performance of these mixtures.

The results of the IDT testing and critical temperature analysis show the addition of the Thiopave material does not negatively impact the low temperature cracking behavior of the asphalt mixes placed during the 2009 NCAT Test Track. These results agree with previous research performed on this material.

3. FALLING WEIGHT DEFLECTOMETER TESTING AND BACKCALCULATION

Falling weight deflectometer (FWD) testing was conducted several Mondays per month to monitor changes in modulus due to environmental effects, seasonal changes, and potential changes due to pavement damage.

The FWD device used was a Dynatest Model 8000 FWD (Figure 3.1) with nine sensors, as listed in Table 3.1 and a 5.91 in. (150 mm) radius split plate. Three replicates at four drop heights, listed in Table 3.2, were applied at each test location on every testing day. Within each section, the twelve locations (inside, outside and between wheelpaths at four random locations) noted in Figure 3.2 were tested with three replicates at four drop heights. The data presented below represent the results measured at the 9,000 lb (40 kN) load level. The test data range from August 28, 2009 through September 19, 2011.

Figure 3.1 Dynatest Model 8000 FWD (Timm et al., 2011)

Table 3.1 FWD Sensor Spacing

Sensor Number	1	2	3	4	5	6	7	8	9
Offset, in.	0	8	12	18	24	36	48	60	72

Table 3.2 FWD Drop Heights and Approximate Weights

Drop Height	Approximate Weight, lb	Replicates
1	6,000	3
2	9,000	3
3	12,000	3
4	16,000	3

Backcalculation of the measured deflection basins was conducted using EVERCALC 5.0. This backcalculation program had been used successfully in previous research cycles at the Test Track (Timm and Priest, 2006; Taylor and Timm, 2009). Based on results from previous backcalculation exercises (Timm and Priest, 2006; Taylor and Timm, 2009), using similar unbound aggregate base and subgrade materials, a three-layer system was established consisting of the entire depth of AC, over the aggregate base on top of the subgrade. The backcalculated moduli presented below represent those results where the root-mean-square of the error (RMSE) in backcalculation between measured and calculated deflections was less than 3%.

Figures 3.2, 3.3 and 3.4 summarize the backcalculated results for the AC, granular base and subgrade, respectively. Data points within each plot represent the average backcalculated modulus across the entire test section at the 9,000 lb (40 kN) load level (drop height 2). The seasonal effects of temperature on AC modulus are clearly evident in Figure 3.2 while the unbound materials exhibited relatively minor changes due to seasonal temperature changes

(Figures 3.3 and 3.4). These results are consistent with previous findings at the Test Track (Timm and Priest, 2006; Taylor and Timm, 2009).

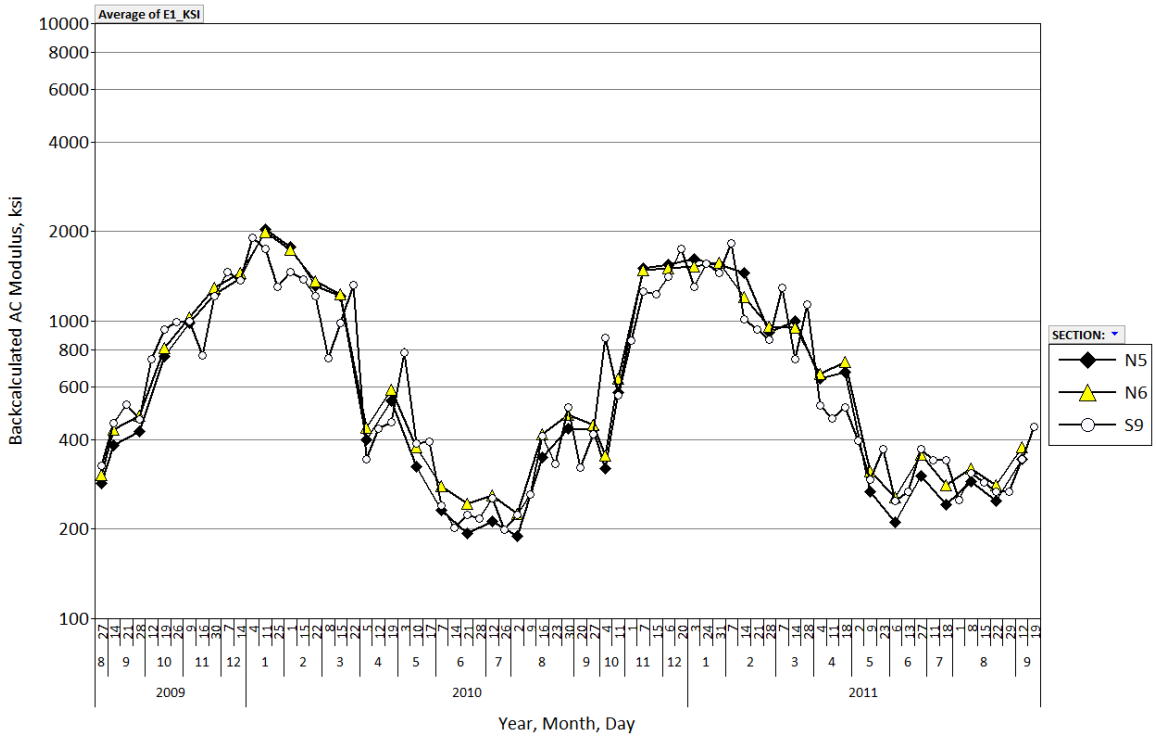

Figure 3.2 Backcalculated AC Modulus vs. Date

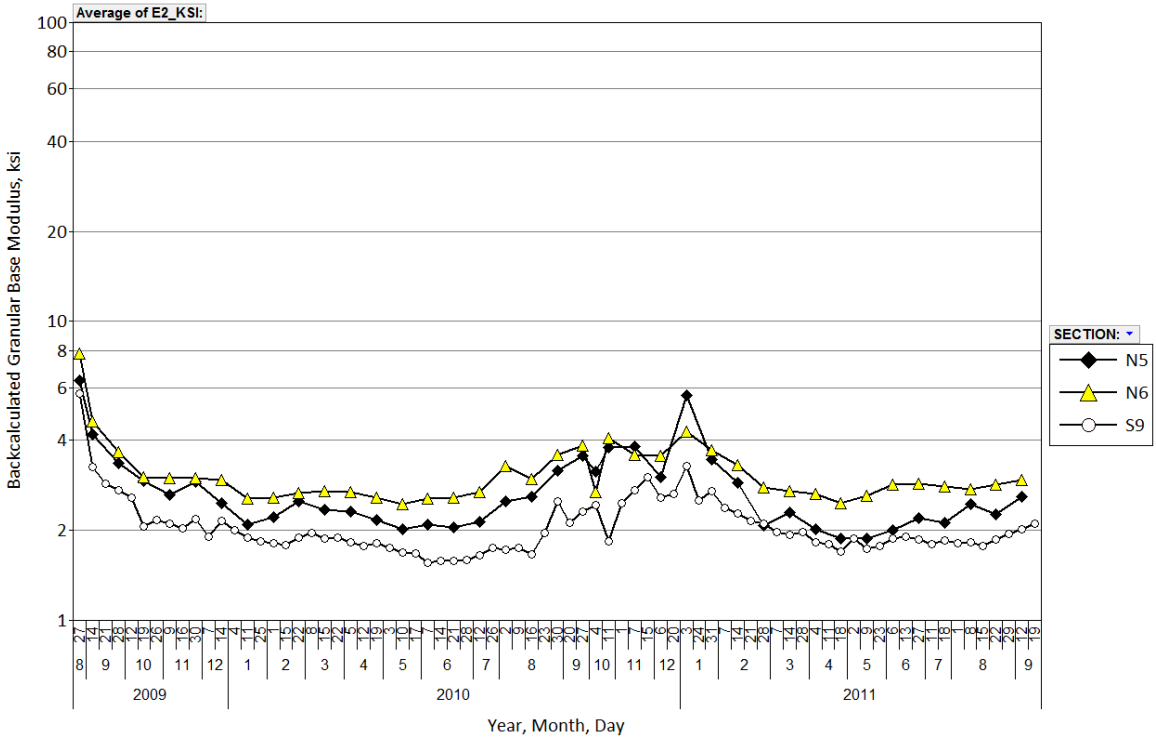

Figure 3.3 Backcalculated Granular Base Modulus vs. Date

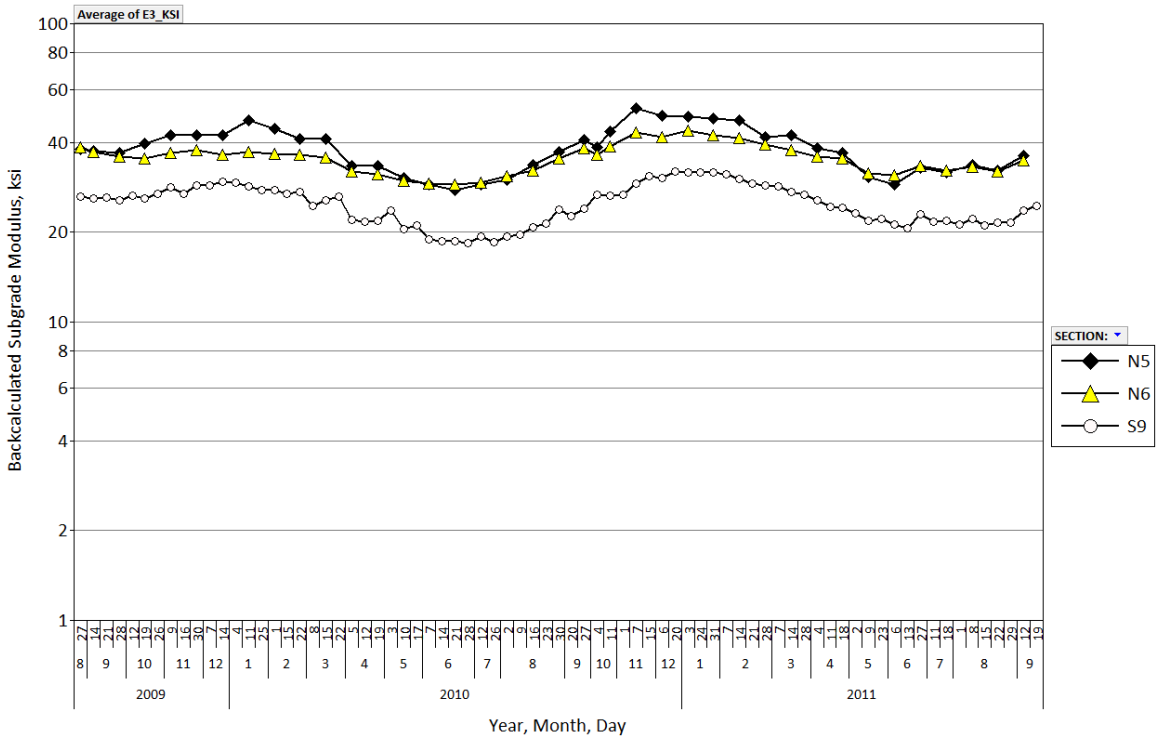

Figure 3.4 Backcalculated Subgrade Soil Modulus vs. Date

Figure 3.3 shows relatively low granular base moduli in each of the test sections. Though these values may seem artificially low, these are consistent with findings from previous laboratory triaxial resilient modulus testing and values obtained from FWD evaluation at the Test Track on this crushed granite material (Timm and Priest, 2006; Taylor and Timm, 2009).

Figure 3.4 indicates good consistency in subgrade soil modulus between the two Thiopave sections on the north tangent while the soil on the south tangent control section was somewhat lower. As explained previously (Timm et al., 2011), this difference likely resulted from the construction history of the respective sections. Sections N5 and N6 were placed in test cells used previously for structural evaluations with relatively thin cross-sections. Therefore, in preparation for paving, N5 and N6 only required milling through the previous AC and granular base leaving the subgrade largely intact. This subgrade had been quarried and placed in 2003 from the lower cut of the West curve at the Test Track. Section S9 was placed in a cell that required deep milling (26 inches) of the AC followed by placement and compaction of newly quarried material from the upper hill area of the West curve at the Test Track. Slight differences in materials and duration of consolidation could be responsible for the differences in the subgrade moduli. With respect to structural modeling, the fact that they are different is not as critical as accurately quantifying the difference.

At the time of each FWD test, the mid-depth temperatures were recorded by embedded temperature probes in each section. Figure 3.5 plots the backcalculated AC modulus versus mid-depth temperature for each section in addition to best-fit exponential functions with the form:

$$E = \alpha_1 e^{\alpha_2 T} \quad (3.1)$$

where:

E = dynamic AC modulus, ksi
T = test temperature, F
α_1, α_2 = best-fit regression constants

Equation 3.1 has been used in previous Test Track research cycles to characterize the modulus-temperature relationship for both laboratory and field-determined moduli (Timm and Priest, 2006; Taylor and Timm, 2009). A temperature-corrected AC modulus (E_{Tref}) was determined from Equation 3.1 at a given reference temperature (T_{ref}) by dividing Equation 3.1 at T_{ref} by the same equation at the measured temperature (T_{meas}). After canceling terms and solving for E_{Tref}, the following equation was determined:

$$E_{T_{ref}} = E_{T_{meas}} e^{\alpha_2 \left(T_{ref} - T_{meas}\right)} \quad (3.2)$$

Equation 3.2 illustrates that the key variable in performing the temperature correction is the exponential regression coefficient, α_2.

Each data point in Figure 3.5 represents the AC modulus determined from the backcalculation of a deflection basin at the 9,000 lb (40 kN) load level, of which there were three replicates, resulting in three data points for each temperature. Therefore, there is more scatter in the data than that shown previously in Figure 3.2. Despite the increased scatter, the change in AC modulus was well explained by change in mid-depth temperature ($R^2 \geq 0.96$). As found previously (Timm et al., 2011), the three regression lines cross at approximately 70°F. At cooler temperatures, the Thiopave sections appear to have higher moduli, while at warmer temperatures, the control section has the highest modulus. It should be pointed out that AC modulus determined through |E*| on individual mixtures did not necessarily show this same trend. However, it is important to keep in mind that some significant differences exist between laboratory |E*| testing and backcalculation of dynamic modulus. First, backcalculation considers the entire depth of AC that includes all the AC lifts in each section while |E*| testing considers each lift separately. Second, |E*| tests are conducted at uniform temperatures throughout the specimen while there are thermal gradients throughout the depth of AC in the field. Third, |E*| tests are conducted at fixed frequencies throughout the specimen. FWD tests in the field are actually tested under a frequency gradient that is derived from a mixture's proximity to the surface. Given these significant testing differences, one could expect to see differences between laboratory and field data.

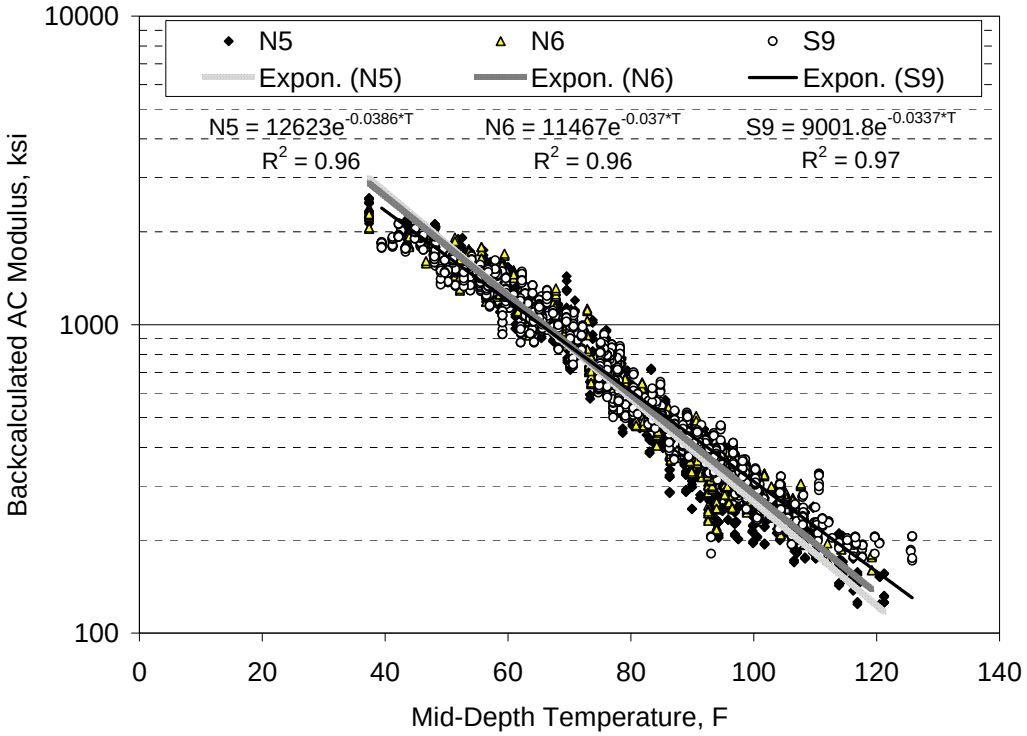

Figure 3.5 Backcalculated AC Modulus vs. Mid-Depth Temperature

To examine the differences between sections in backcalculated AC moduli over a range of temperatures, the moduli were temperature-corrected using the coefficients from Figure 3.5 in equation 3.2. Three reference temperatures were selected (50, 68 and 110°F) (10, 20 and 43ºC) that represented the range of FWD test temperatures. The results are summarized in Figure 3.6 according to average, standard deviation and coefficient of variation. In each case, the COV was less than or equal to 15% which is half of a common benchmark (30%) for backcalculated AC modulus variability (Allen and Graves, 1994; Noureldin, 1994; Timm et al., 1999). Therefore, the AC moduli appear exceptionally consistent within each section.

Statistical testing was conducted using the Tukey-Kramer approach ($\alpha = 0.05$) to detect differences and sectional groupings with respect to AC modulus at each reference temperature. At 50°F (10ºC), all sections were statistically different with N5 having the highest modulus followed by N6 and S9. At 68°F (20ºC), the average moduli between N5 and the others was not statistically distinguishable though N6 and S9 were found to be different. At 110°F (43ºC), the differences in means were enough to distinguish between each section; N5 had the lowest modulus, followed by N6 and S9. These findings were consistent with the one-year analysis (Timm et al., 2011).

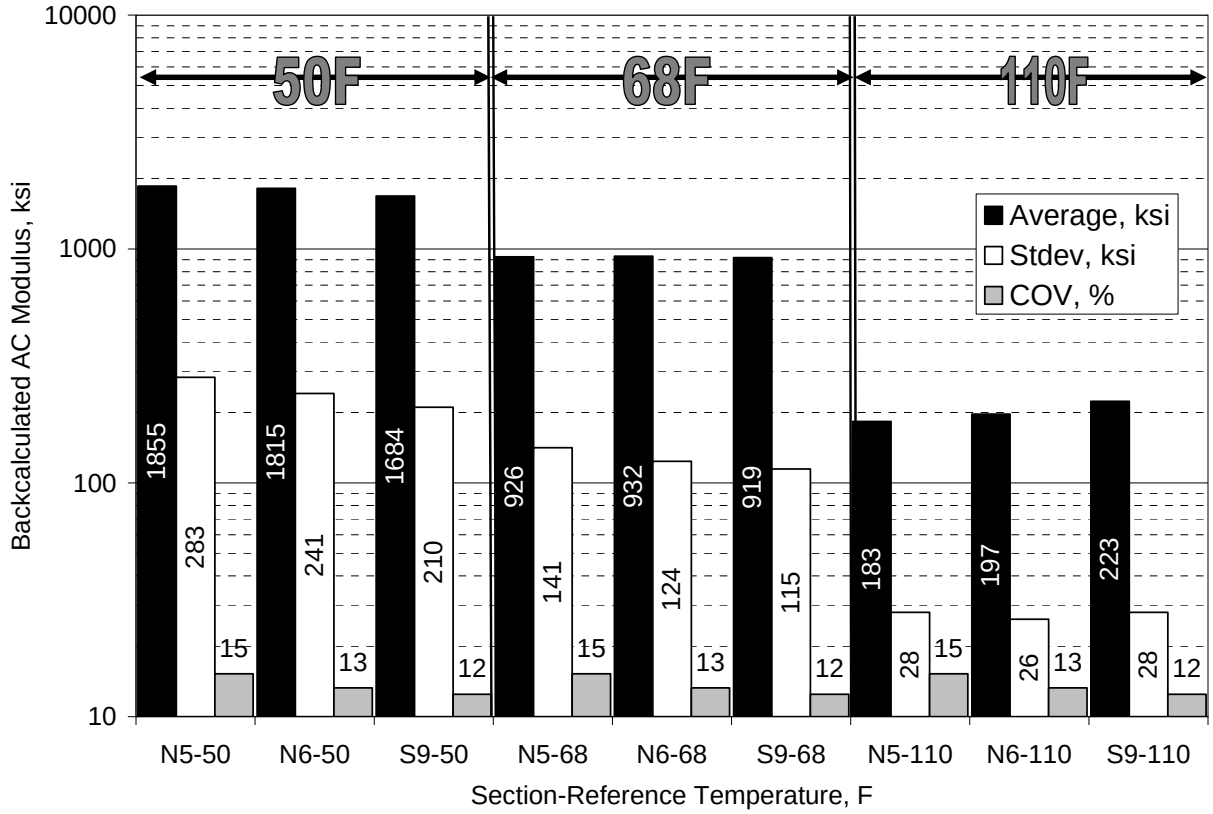

Figure 3.6 Backcalculated AC Modulus Corrected to Reference Temperatures

A final step in this analysis was to plot backcalculated AC modulus at 68°F (20ºC) versus date to look for dramatic changes in AC modulus that would indicate possible pavement distress. Figure 3.7 shows relatively little change in modulus over time through the entire experimental cycle. Linear regression lines were fit to each data set which suggested very little correlation ($R^2 <$ 0.09) between AC modulus and test date. The slight upward trend (positive slope) may indicate very slight aging over time, but is relatively insignificant relative to the overall magnitude of the moduli.

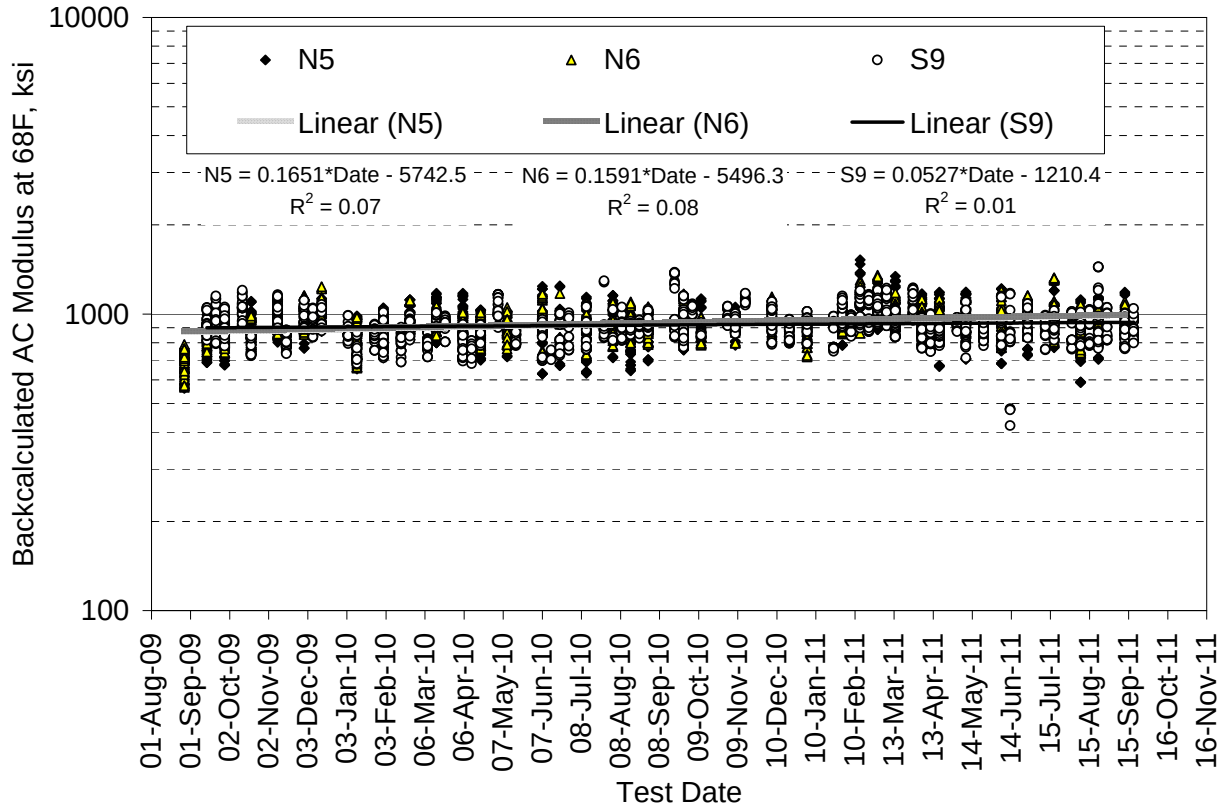

Figure 3.7 Backcalculated AC Modulus vs. Date at 68°F

4. PAVEMENT RESPONSE MEASUREMENTS

During the entire 2-year research cycle, weekly pavement response measurements were made using the embedded asphalt strain gauges and earth pressure cells in the granular base and subgrade soil. Weekly data collection consisted of collecting approximately fifteen truck passes (three passes of five trucks) in each section. The frequency of testing and number of trucks collected were consistent with previous data collection efforts at the Test Track which were shown to be sufficient to capture daily variability, seasonal variability and wheel wander effects (Timm and Priest, 2004; Priest and Timm, 2006). The response data in this report were gathered between August 28, 2009 and September 28, 2011.

The previous report (Timm et al., 2011) detailed the data collection, processing and storage procedure for the dynamic pavement response measurements and is omitted here for brevity. After collecting, processing and archiving the data, there were a number of analyses conducted. The following subsections examine seasonal trends in pavement response, temperature effects on pavement response, responses normalized to particular reference temperatures and responses over time at a normalized temperature.

4.1 Seasonal Trends in Pavement Response

There were four primary measured pavement responses: longitudinal strain in the AC, transverse strain in the AC, vertical pressure in the aggregate base and vertical pressure in the subgrade soil. Figures 4.1 through 4.4 show plots of these responses versus test date for the single axle loadings

only, though similar trends were observed with the other axle types. Each data point in each plot represents the "best-hit" on that particular test date. The seemingly large fluctuation between consecutive test dates is a product of alternating collection times between morning and afternoon on a week-to-week basis. This ensured that a fuller range of temperatures was sampled during a particular season.

In each plot, the seasonal trends are clearly evident with lower responses during the cooler months and increased responses during warmer months. Though there are section-to-section differences, each exhibits a similar trend with respect to seasonal changes. On any particular date, Section N5 (9 in. (229 mm) Thiopave) typically had the lowest pavement responses which resulted primarily from the 2-in. (51 mm) thickness advantage over the other two sections. Sections N6 (7 in. (178 mm) Thiopave) and S9 (control), built to approximately the same AC thickness had more similar pavement responses. These trends, also observed in the one-year report (Timm et al., 2011) are more evident when responses are examined relative to temperature as shown in the next subsection.

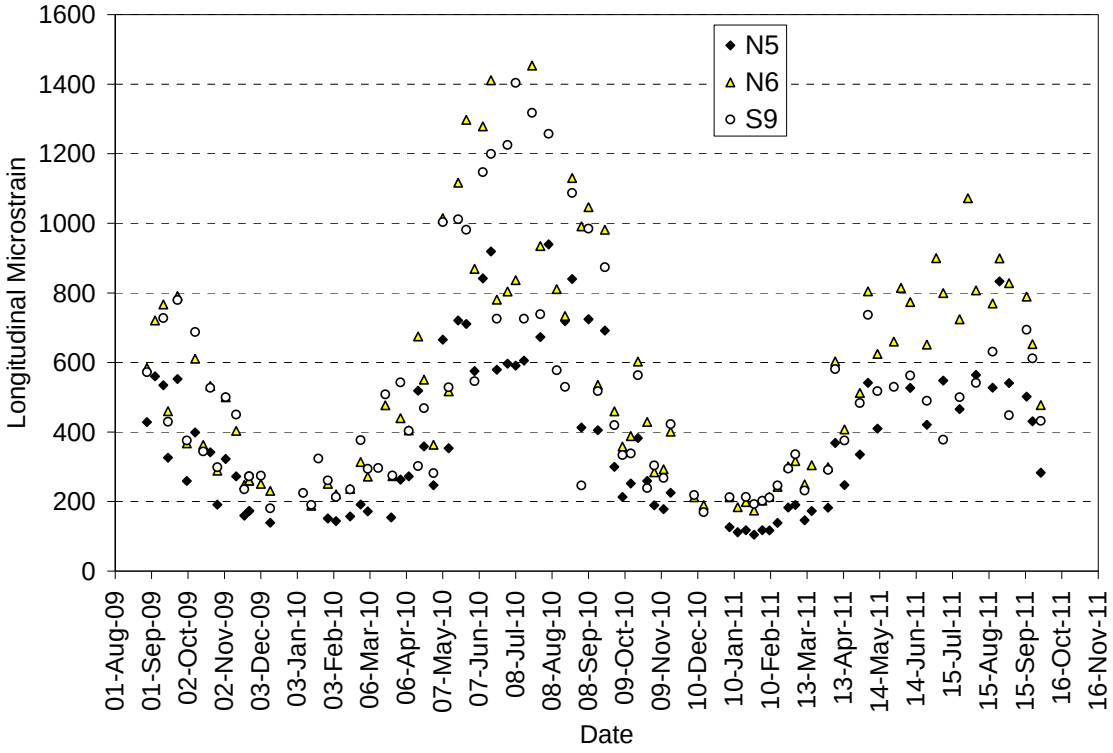

Figure 4.1 Longitudinal Microstrain Under Single Axles

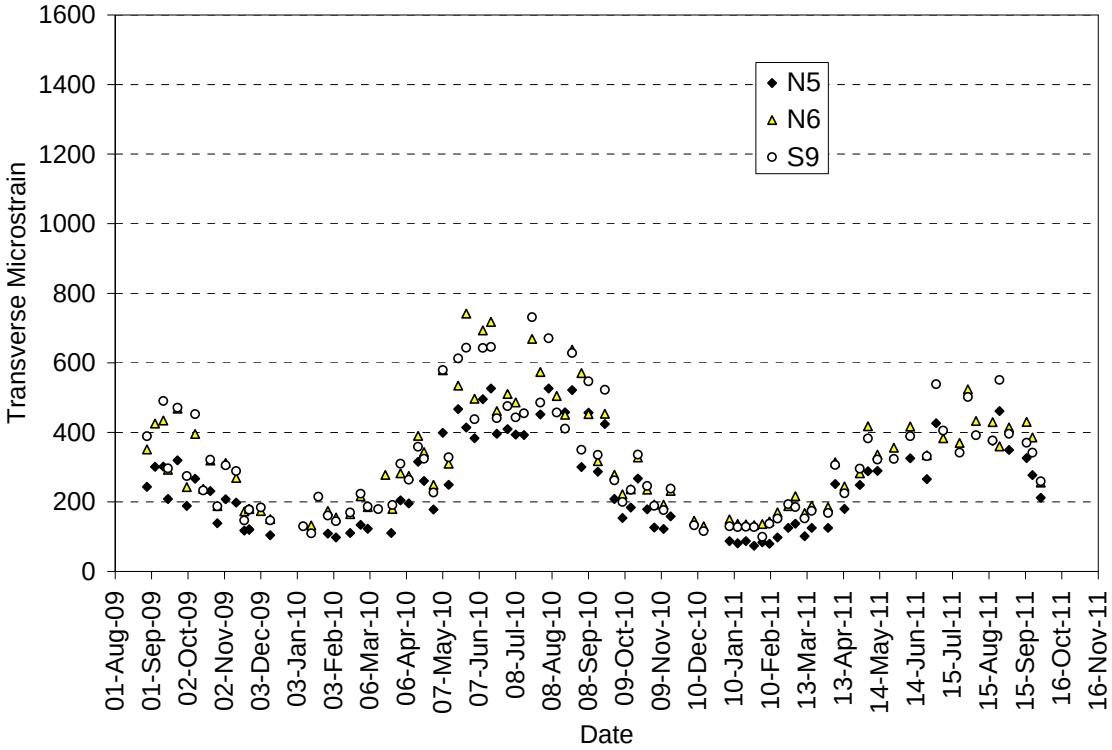

Figure 4.2 Transverse Microstrain Under Single Axles

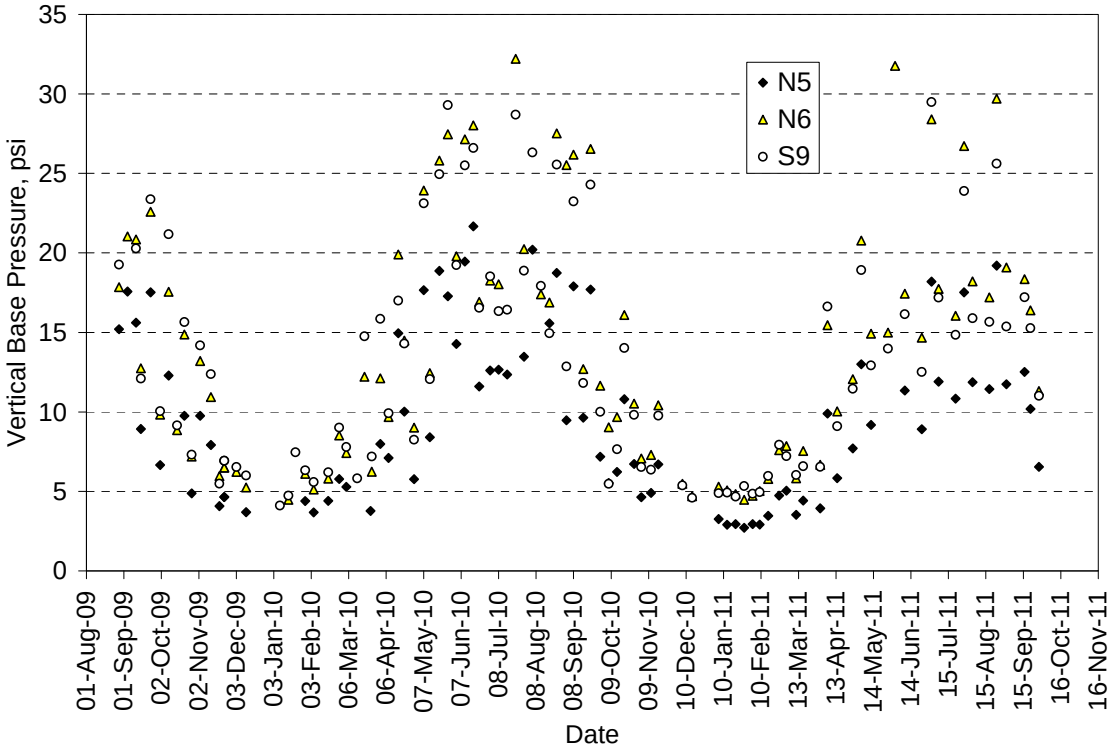

Figure 4.3 Aggregate Base Pressure Under Single Axles

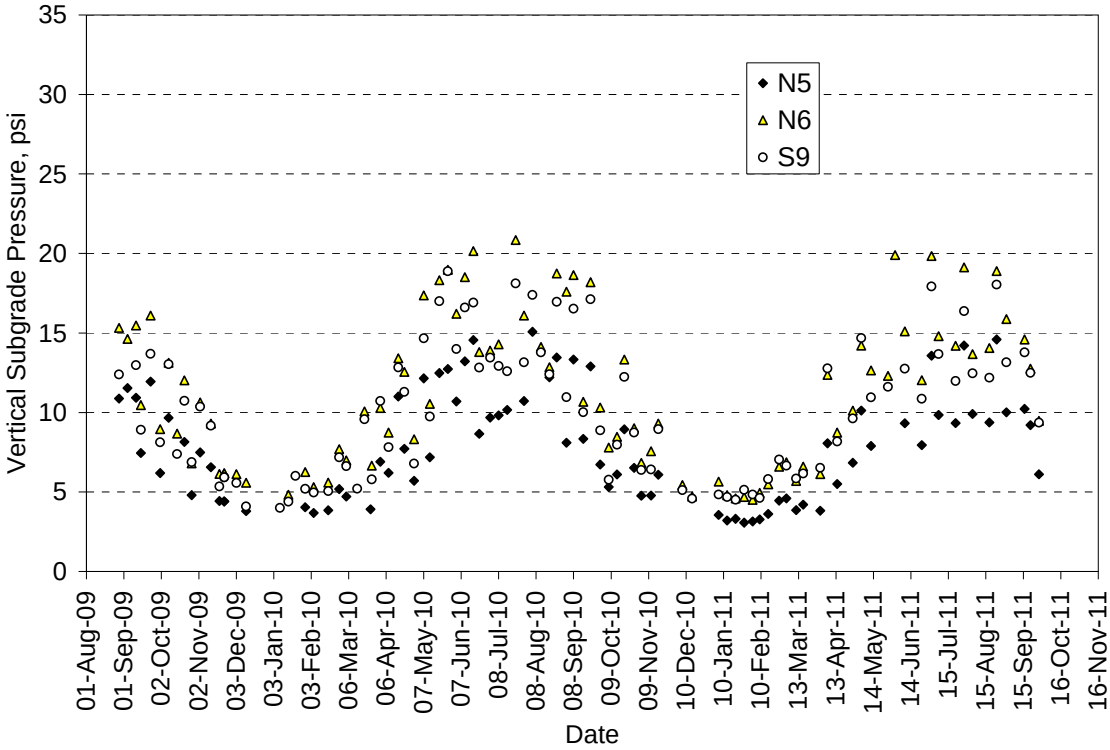

Figure 4.4 Subgrade Pressure Under Single Axles

4.2 Pavement Response vs. Temperature

The data presented in Figures 4.1 through 4.4 were the best-hit pavement responses on a particular test date. These data were replotted in Figures 4.5 through 4.8 against their corresponding mid-depth pavement temperature. Exponential regression equations, much like those determined for the backcalculated AC moduli, were best-fit to each data set in Figures 4.5 through 4.8 representing single axles. Additional equations were developed for each of the axle types, the results of which are presented in Table 4.1. In total, 36 sets of regression parameters were determined (3 sections∗4 responses∗3 axle types = 36). In 27 of 36 equations, the R^2 exceeded 90%. Eight of the remaining nine equations had R^2 exceeding 80%. The poorest fit was for the aggregate base pressure in S9 under steer axle loading (R^2 = 76%). Clearly, mid-depth temperature is a strong predictor of each of the measured pavement responses. It should be noted that very similar trends were reported in the one-year analysis (Timm et al., 2011). Differences in the regression results stem primarily from having approximately twice the number of data points available for this analysis.

It is important to note that the sections followed similar exponential trends which indicates similar responses under dynamic axle loading such that the materials (control vs. Thiopave) can be modeled in a similar fashion. S9 (Control) and N6 (Thiopave), having approximately the same thickness, yielded very similar responses across the temperature spectrum. The exception was the vertical pressures measured in the subgrade which were consistently higher for N6 relative to S9. It was previously documented (Timm et al., 2011) that the aggregate base thickness in N6 was on average approximately 0.8 inches (20 mm) thinner than the base in S9. Therefore, it is reasonable and expected that N6 would have slightly greater subgrade stresses.

The notable distinction between the thinner sections (N6, S9) and N5 is due primarily to the 2 inch (51 mm) thickness advantage of this section.

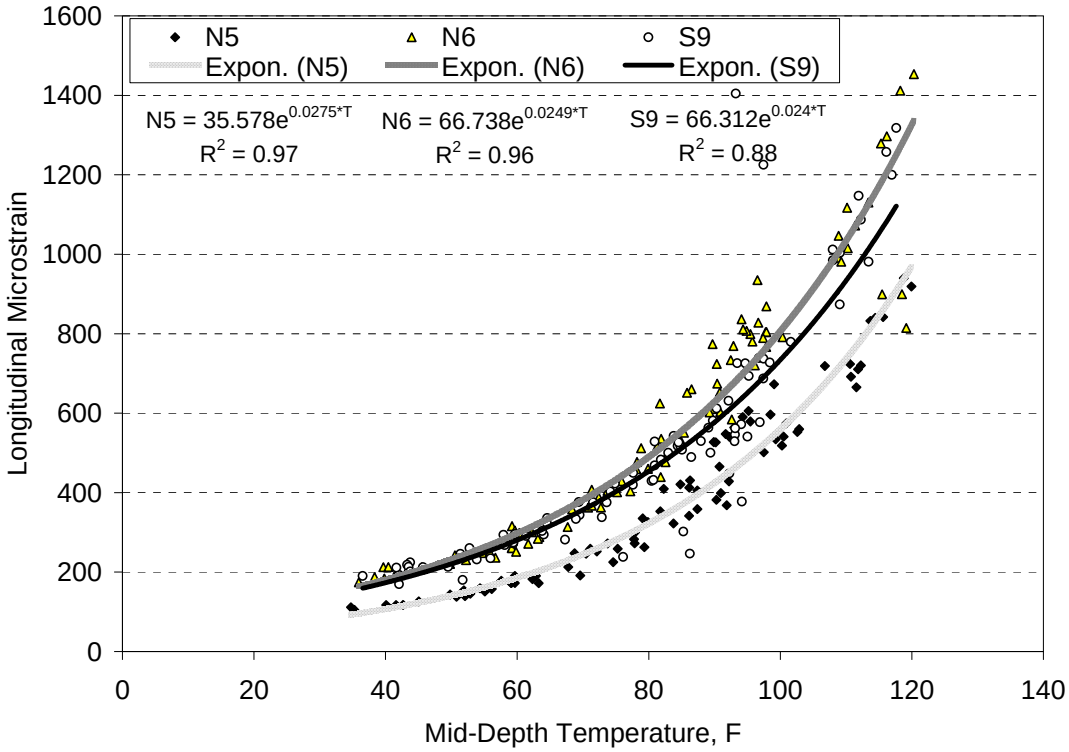

Figure 4.5 Longitudinal Strain vs. Mid-Depth Temperature Under Single Axles

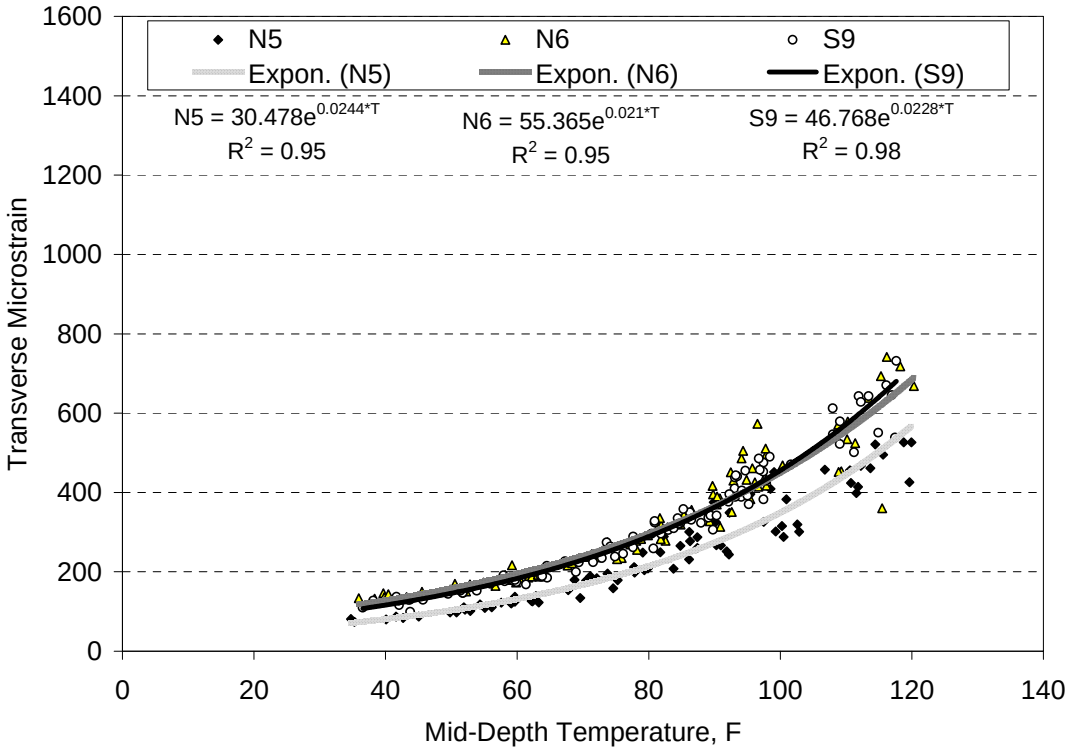

Figure 4.6 Transverse Strain vs. Mid-Depth Temperature Under Single Axles

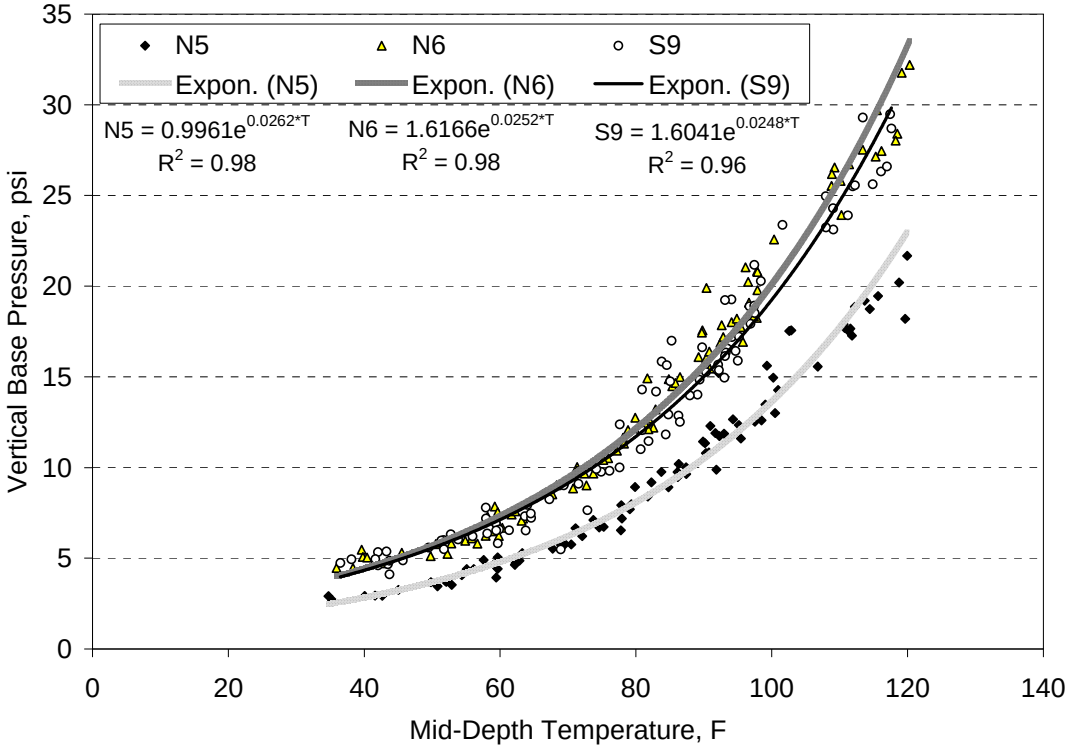

Figure 4.7 Base Pressure vs. Mid-Depth Temperature Under Single Axles

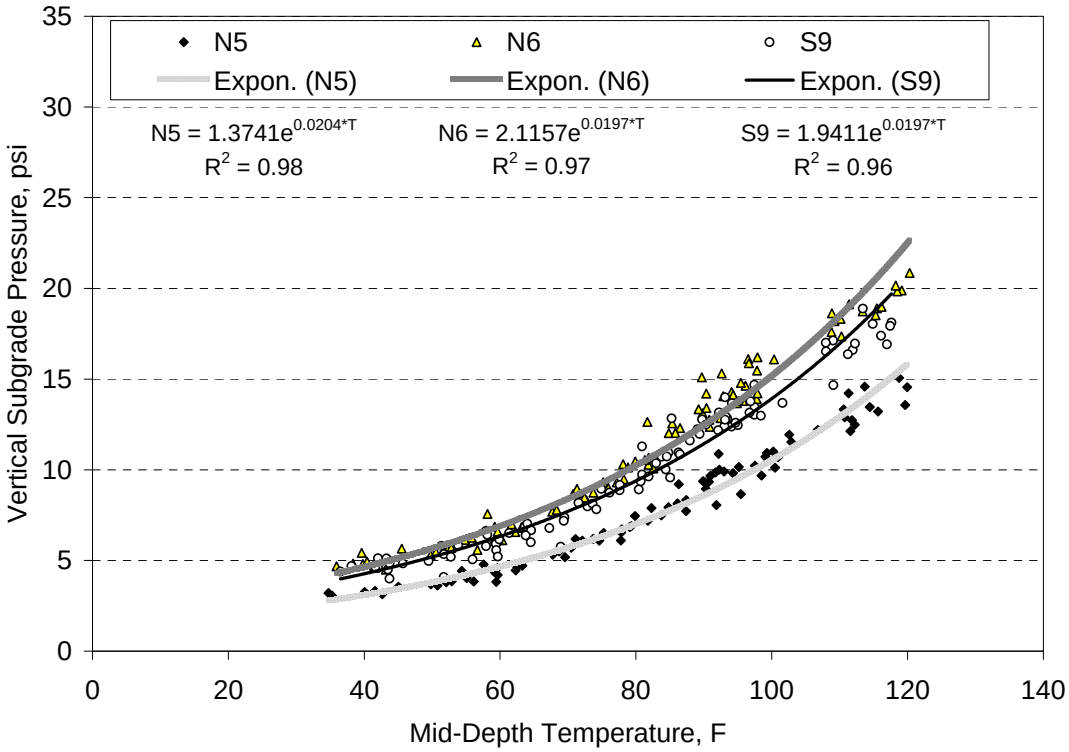

Figure 4.8 Subgrade Pressure vs. Mid-Depth Temperature Under Single Axles

Table 4.1 Pavement Response vs. Temperature Regression Terms

		Longitudinal Strain			Transverse Strain			Base Pressure			Subgrade Pressure		
Section	Axle	k_1	k_2	R^2	k_1	k_2	R^2	k_1	k_2	R^2	k_1	k_2	R^2
N5	Steer	15.472	0.031	0.97	19.167	0.029	0.88	0.378	0.030	0.97	0.538	0.024	0.97
	Single	35.578	0.028	0.97	30.478	0.024	0.95	0.996	0.026	0.98	1.374	0.020	0.98
	Tandem	25.962	0.031	0.97	34.265	0.023	0.94	1.234	0.025	0.98	1.786	0.018	0.97
N6	Steer	33.555	0.028	0.88	31.169	0.028	0.88	0.578	0.031	0.96	0.777	0.024	0.96
	Single	66.738	0.025	0.96	55.365	0.021	0.95	1.617	0.025	0.98	2.116	0.020	0.97
	Tandem	58.415	0.026	0.95	63.978	0.018	0.86	2.012	0.023	0.98	2.565	0.018	0.97
S9	Steer	28.336	0.028	0.81	26.118	0.030	0.94	0.783	0.024	0.76	0.867	0.021	0.83
	Single	66.312	0.024	0.88	46.768	0.023	0.98	1.604	0.025	0.96	1.941	0.020	0.96
	Tandem	49.332	0.027	0.88	47.276	0.022	0.97	1.997	0.023	0.95	2.482	0.017	0.95

4.3 Pavement Responses Normalized to Reference Temperatures

To characterize statistical differences in pavement response between sections, temperature corrections were applied to each data set (longitudinal strain, transverse strain, base pressure, subgrade pressure) at 50, 68 and 110°F (10, 20 and 43ºC). Temperature-corrected responses were determined according to:

$$response_{T_{ref}} = response_{T_{meas}} e^{k_2\left(T_{ref} - T_{meas}\right)} \quad (4.1)$$

Where:
$response_{Tref}$ = response at T_{ref}
$response_{Tmeas}$ = response at T_{meas}
T_{ref} = mid-depth reference temperature (50, 68, 110°F (10, 20 and 43ºC))
T_{meas} = mid-depth measured temperature, F
k_2 = section, axle and response-specific regression constant from Table 4.1

The average, standard deviation and coefficient of variation were determined at each reference temperature. Tukey-Kramer statistical tests (α=0.05) were conducted on each data set to establish groupings with the results discussed below. Only results for the single axles are presented here, though similar trends were noted amongst the other axles.

4.3.1 Longitudinal Strain Responses

Figure 4.9 summarizes the temperature-corrected longitudinal strain measurements under single axles. The data indicate relative consistency with COV's less than 21%. Tukey-Kramer testing found N5 (9 in. (229 mm) -Thiopave) to be lower than the other two sections at each temperature which was expected due to its 2" (51 mm) thickness advantage.

At 50°F (10ºC), there was no statistical difference between the control (S9 at 7 in. (178 mm)) and N6 (7 in. (178 mm) Thiopave) despite statistically-significant lower modulus in the control section (see Figure 3.6). This could be explained by the slight thickness advantage of S9 relative to N6. Also, there is a theoretical inverse exponential relationship between strain and modulus. This means that differences at cold temperatures (high moduli) have less of an impact on strain than at warmer temperatures (low moduli). Therefore, though the Thiopave section (N6) may have higher modulus at 50°F (10ºC) than the control, it was not high enough to differentiate the strain response.

At 68°F (20ºC), there were significant differences detected between the control (S9 at 7 in. (178 mm)) and N6 (7 in. (178 mm) Thiopave). However, one could argue whether 20 με is practically significant. Previous studies had set a benchmark strain level of 30 με for between gauge precision (Willis and Timm, 2009). At 110°F (43ºC), the difference observed between the control (S9 at 7 in. (178 mm)) and N6 (7 in. (178 mm) Thiopave) sections was statistically significant and at 90 με is also considered practically significant. Evidently, the slight thickness advantage and higher modulus of S9 at 110°F (43ºC) resulted in lower strain levels.

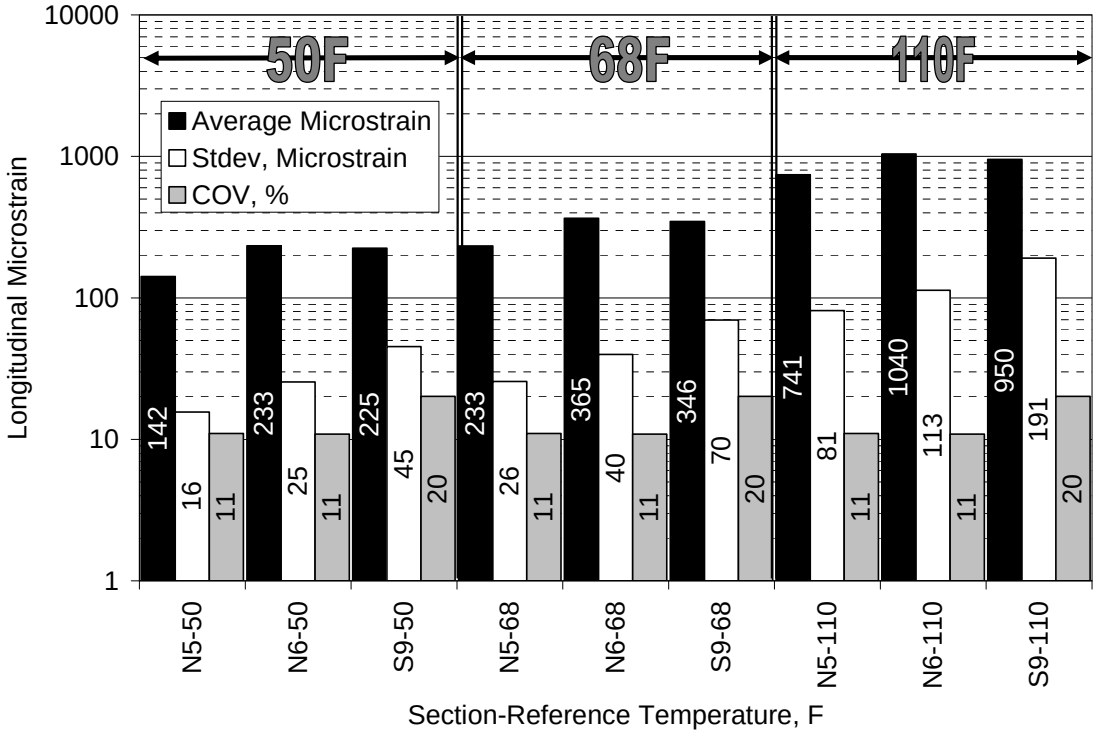

Figure 4.9 Longitudinal Strain Under Single Axles at Three Reference Temperatures

At the conclusion of testing, there was no cracking evident in any of the three sections. However, fatigue performance estimates can be made for comparison purposes to evaluate relative performance estimates using the strain data in Figure 4.9 with the fatigue transfer functions presented in Section 2.3. Table 4.2 lists the measured average strain at 68°F (20ºC) (from Figure 4.9) and the corresponding predicted fatigue life using the transfer functions presented in Table 2.3. It is important to note that despite N6 and S9 having practically equivalent strain levels at 68°F (20ºC), the fatigue characteristics of the Thiopave-modified base mixture yields an improvement of approximately 1.24 times in the predicted fatigue life over the control section. The improved fatigue characteristics combined with increased thickness in section N5 increases the predicted fatigue life by a factor of 14.2 over the control section.

Table 4.2 Predicted Fatigue Life at 68°F

Section	Average Microstrain at 68°F	Predicted Fatigue Life – Cycles to Failure at 68°F
N5	233	5,206,041
N6	365	453,767
S9	346	367,064

4.3.2 Transverse Strain Responses

Figure 4.10 summarizes the transverse strains under single axle loadings. As found in previous studies (Timm and Priest, 2008; Timm et al., 2011), the transverse strains were generally lower than their longitudinal counterparts. Also, the transverse strains were somewhat more consistent than longitudinal with COV's below 14%. The Tukey-Kramer statistical testing found N5 (9 in. (229 mm) Thiopave) to be lower than the other sections at each temperature, as expected from the increased thickness of N5. Differences between N6 and S9 were statistically-significant at 50 and 68°F (10 and 20ºC), though one could again argue the practical significance of 12 to 13 με differences. At 110°F (43ºC), N6 and S9 were statistically the same in the transverse direction.

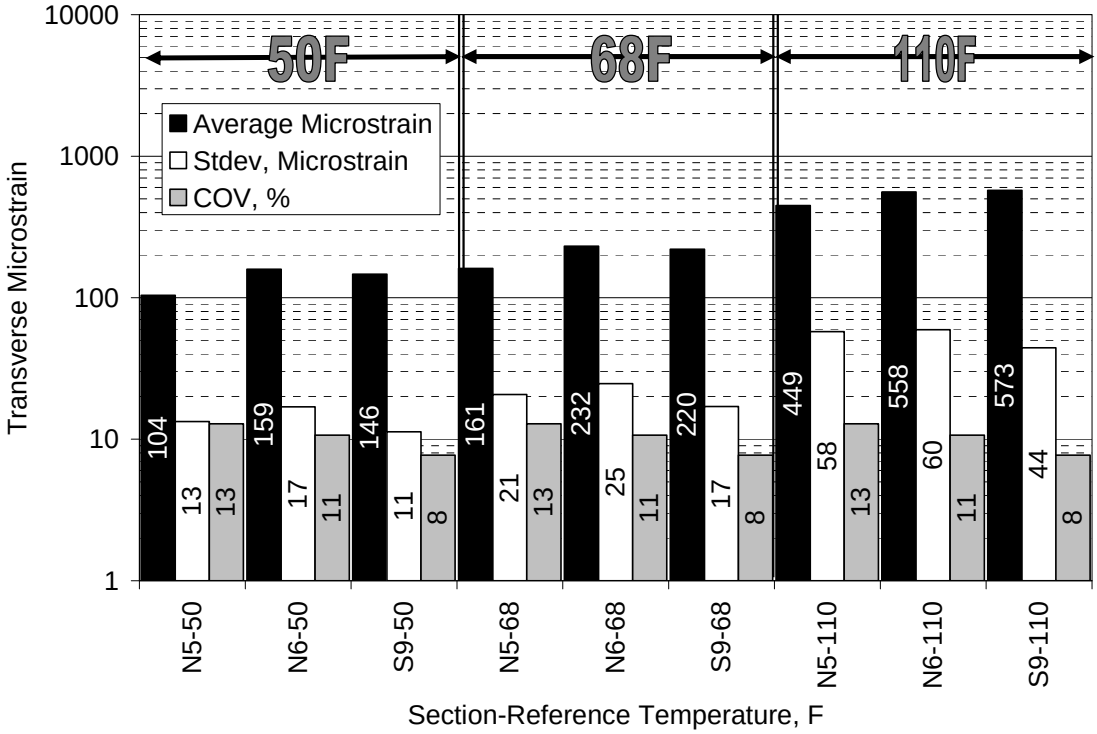

Figure 4.10 Transverse Strain Under Single Axles at Three Reference Temperatures

4.3.3 Aggregate Base Vertical Pressure Responses

Figure 4.11 summarizes the vertical pressures in the aggregate base under single axle loadings. These data are even less variable than the strain measurements with COV's below 11%. Again, Tukey-Kramer testing (α=0.05) found the thicker Thiopave section to experience lower pressure at all temperatures, as expected. The high degree of precision in the data, however, enabled

statistical differences to be detected at 68°F and 110°F (20 and 43ºC) between the control (S9 at 7 in. (178 mm)) and N6 (7 in. (178 mm) Thiopave). These differences, however, were not practical at 1 psi (7 kPa) or less.

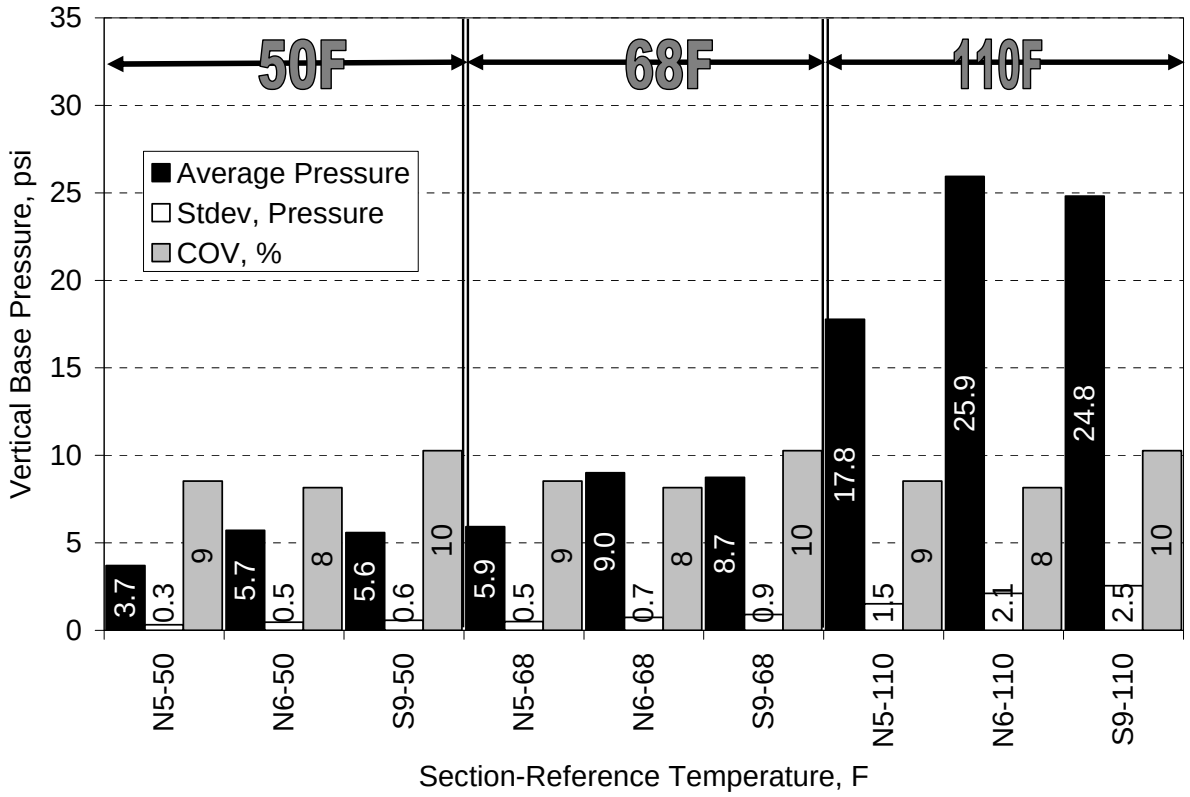

Figure 4.11 Base Pressure Under Single Axles at Three Reference Temperatures

4.3.4 Subgrade Vertical Pressure Responses

The temperature-corrected vertical pressures in the subgrade are plotted in Figure 4.12. These measurements were highly consistent with all COV's less than 9%. This level of precision enabled differences to be detected at all temperatures between all sections using the Tukey-Kramer (α=0.05) approach. As noted previously, the aggregate base in S9 is slightly thicker than N6, so one would expect lower stresses in the subgrade. Though statistically different, one could again argue the practical significance of less than 2 psi (14 kPa) difference between S9 and N6.

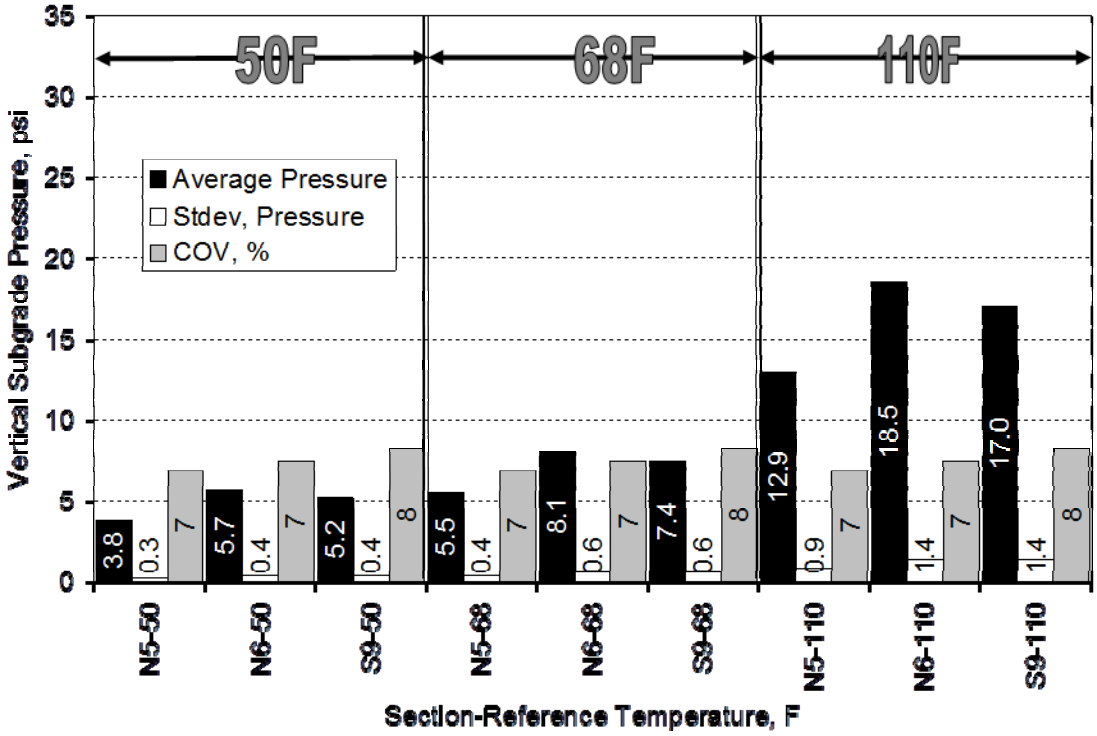

Figure 4.12 Subgrade Pressure Under Single Axles at Three Reference Temperatures

4.4 Pavement Response Over Time at 68°F (20°C)

Responses corrected to 68°F (20ºC) were plotted against test date, as was done with the backcalculated AC moduli data, to look for signs of distress in the response measurements. Figures 4.13 through 4.16 show relatively constant measurements over time, which is consistent with the AC moduli versus time, presented earlier (Figure 3.7). Both data sets indicate no structural cracking in the sections. The two outliers seen in Figure 4.13 were further investigated. No justification could be found, other than their non-conformance to the general trend, to remove them from the data set so they were left in-place.

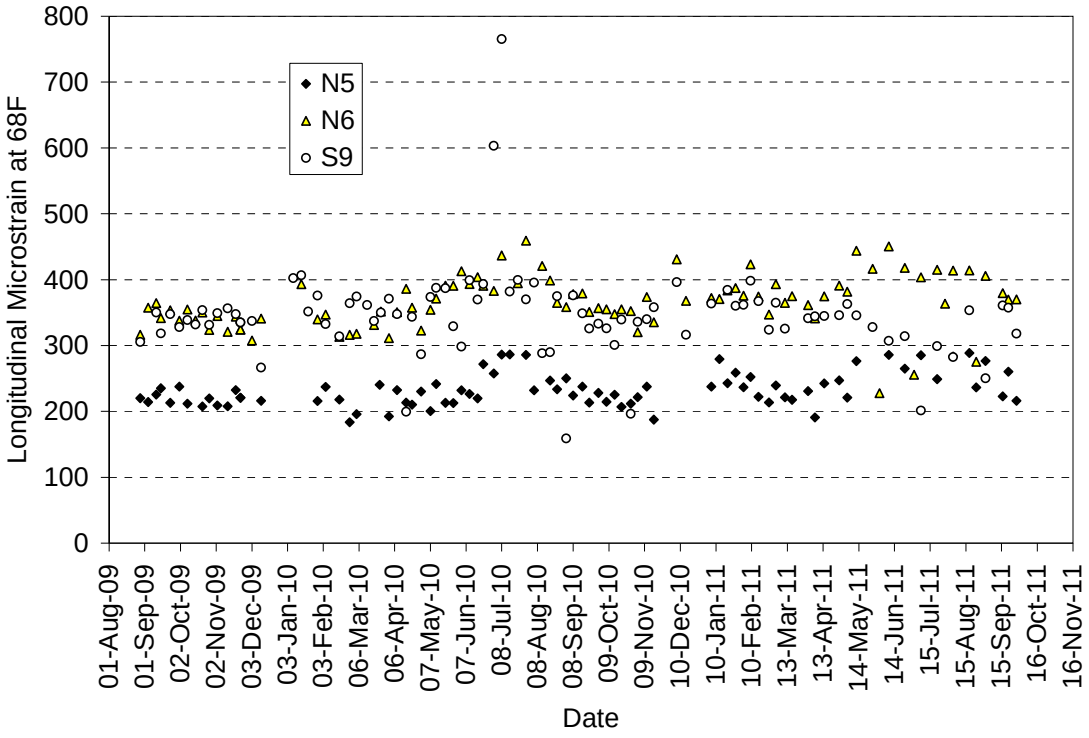

Figure 4.13 Longitudinal Microstrain Under Single Axles vs. Date at 68°F

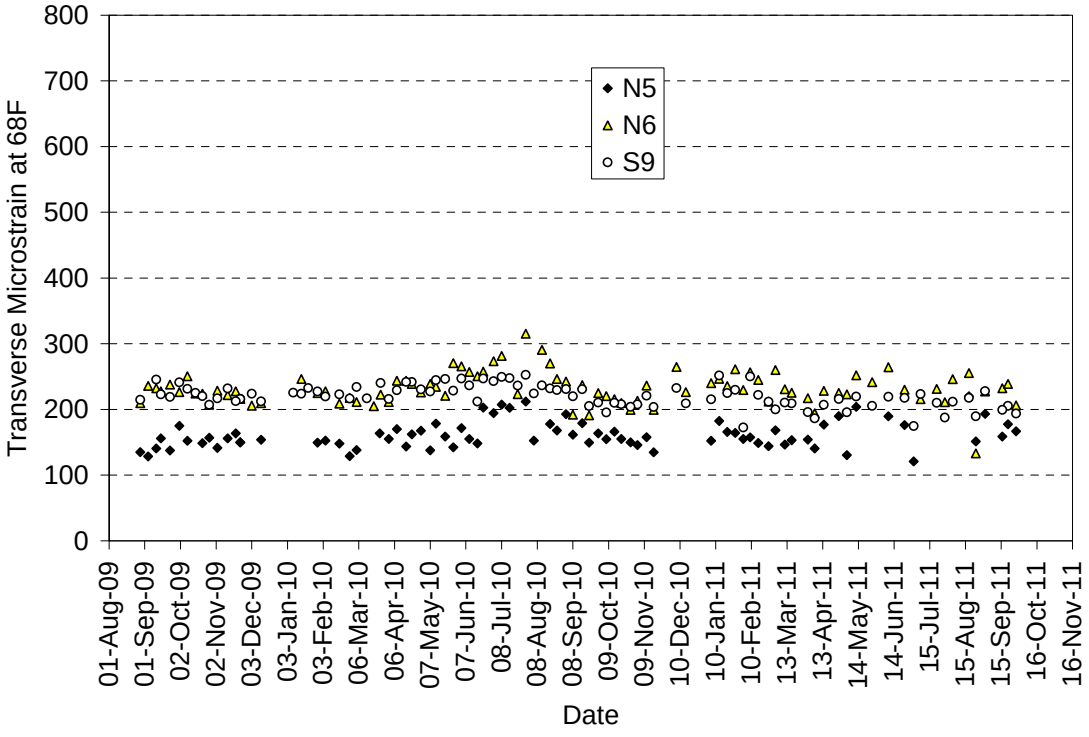

Figure 4.14 Transverse Microstrain Under Single Axles vs. Date at 68°F

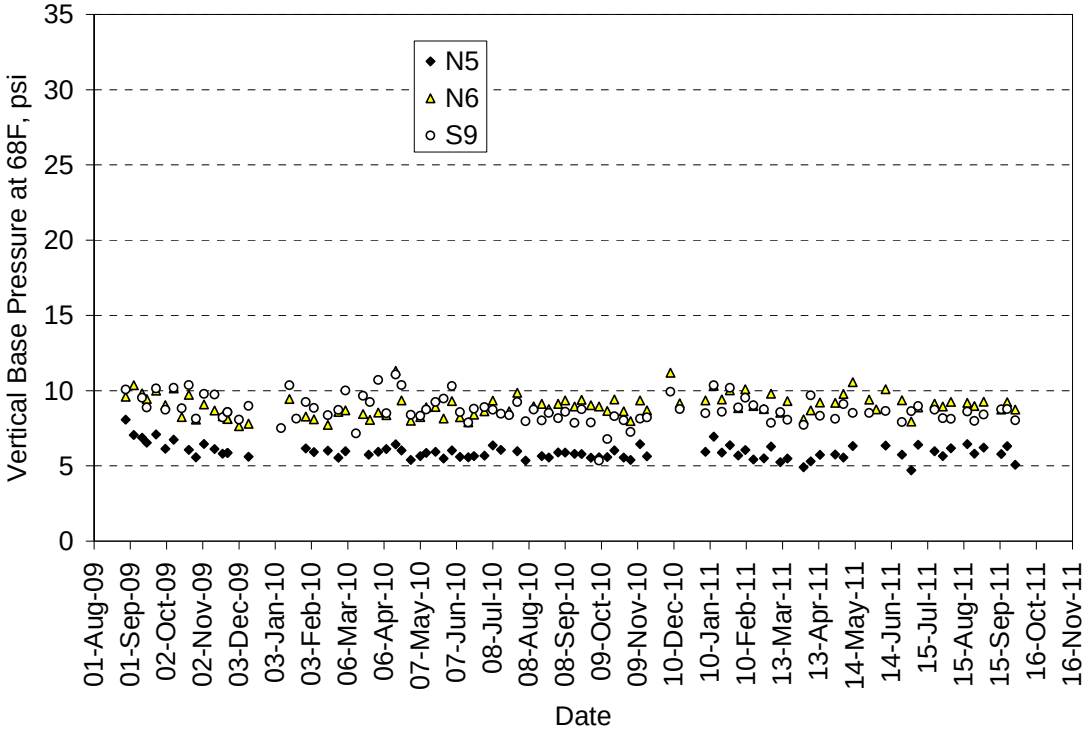

Figure 4.15 Base Pressure Under Single Axles vs. Date at 68°F

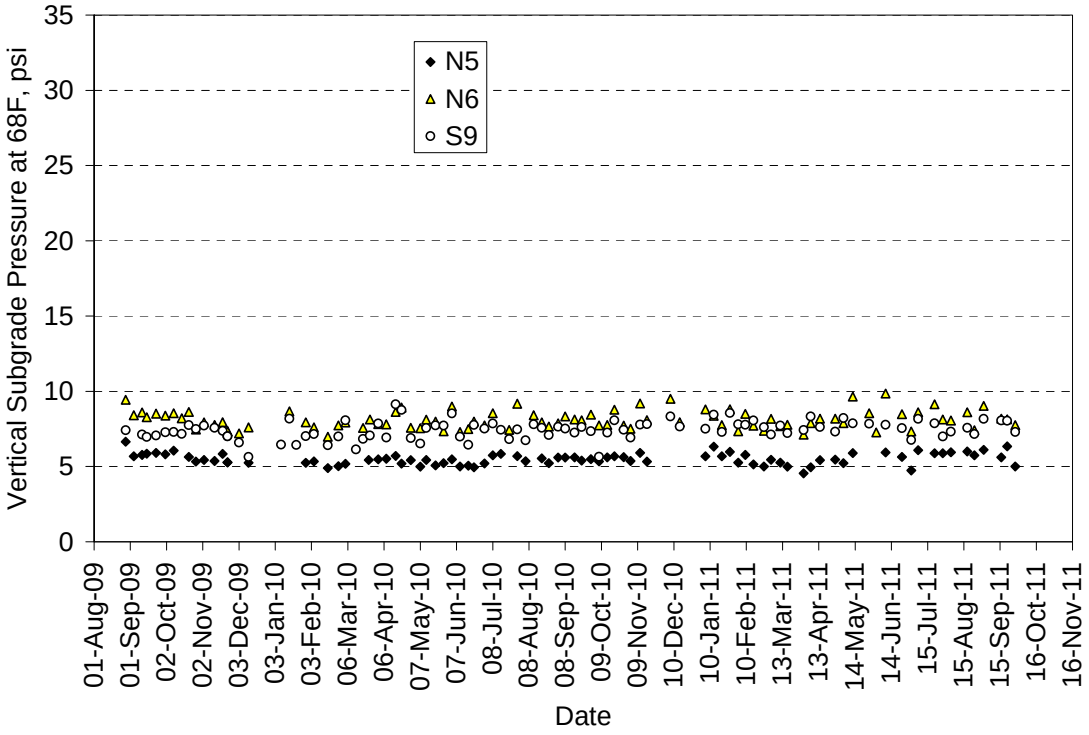

Figure 4.16 Subgrade Pressure Under Single Axles vs. Date at 68°F

5. PAVEMENT PERFORMANCE

At the conclusion of traffic, 10.14 million ESALs had been applied to the sections. At that time, no cracking was evident on any of the sections. During the two-year test cycle, measurements of rutting and roughness (International Roughness Index (IRI)) were made using a Roadware ARAN van. Figure 5.1 illustrates the average rutting progression (both wheelpaths) in each section with a three-point moving average fit to each series. As seen in previous research cycles (Timm et al., 2006; Willis et al., 2009), rutting tended to increase during summer months and level off during colder months. It appears from Figure 5.1 that N5 had slightly more rutting than N6 with the control section having the least, though all are below a commonly-accepted threshold for failure of 12.5 mm (0.5 in.).

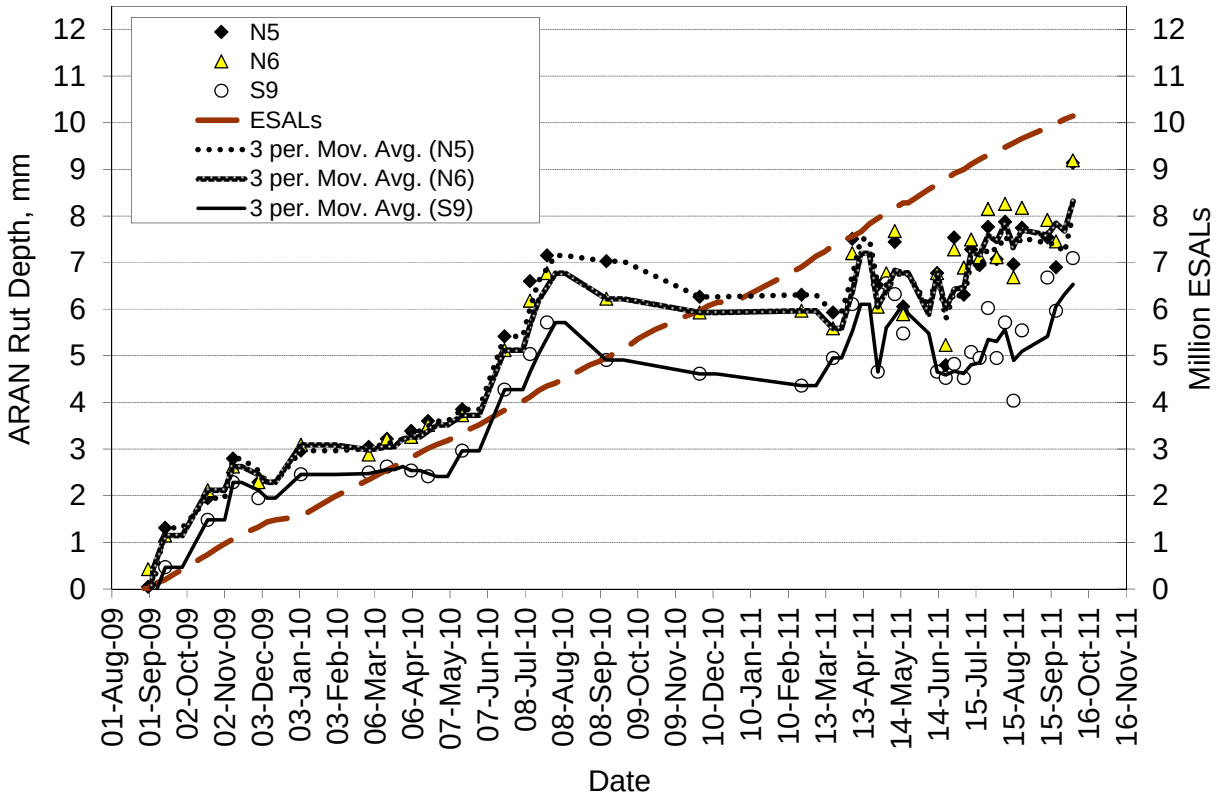

Figure 5.1 ARAN-Measured Rutting vs. Date

A statistical comparison of rutting between sections was conducted using final wire-line measurements made at the conclusion of traffic. Wire-line rutting measurement determines the rut depth from a straight line extending across the lane, parallel to the cross-slope, at the pavement surface and does not include any upward surface distortion that may be present. Using ten measurements per section, the average and standard deviation of rut depth in the outside (most severe) wheelpath were determined. Figure 5.2 shows these data and two-tailed t-testing (α=0.05) between sections. The two-tailed t-tests indicated no differences between the Thiopave sections while the control was statistically lower, though the difference was only 3 to 4 mm. This result makes sense in the context of the backcalculated AC moduli (Figure 3.6) which showed the control section had higher modulus at warmer temperatures when the mixtures were more susceptible to rutting.

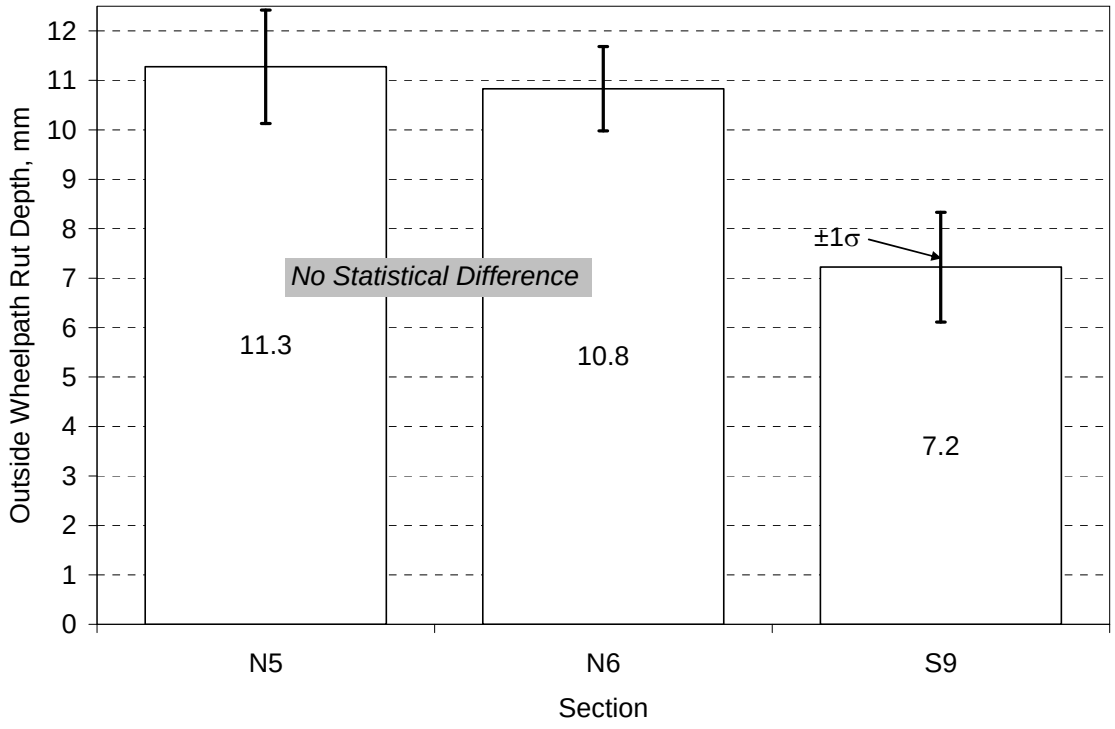

Figure 5.2 Final Outside Wheelpath Rut Depths – Measured by Wire-line

To further investigate the nature and extent of rutting, it was decided to cut two trenches in Section N5 which had the highest numerical, if not statistically significant rutting. Trenching was conducted on February 15, 2012 with one trench at the location of maximum rutting in the section (Trench 1) and the other trench at the center of the gauge array (Trench 2).

The trench locations were first marked as indicated in Figure 5.3. The trench extended from just inside the centerline to the edge of pavement as was wide enough to accommodate a backhoe bucket that was used to lift the slabs from the trenches. Figure 5.4 shows the cutting operation, executed by a third-party contractor. Figure 5.5 shows that the rut depths downstream of Trench 2 were sufficient to channelize water from the cutting saw.

Figure 5.3 Marking Trench 1

a) Trench 1 **b) Trench 2**

Figure 5.4 Cutting Operations

Figure 5.5 Water Pooling in Ruts (Trench 2)

Once the slabs were cut, a backhoe was used to lift each slab from the pavement as shown in Figures 5.6 and 5.7. Careful attention was paid to the lift interfaces during extraction to see if there was any debonding or slippage as the slabs were removed. Neither slab showed any evidence of debonding as had been seen with previous slab removal activity (Peters and Timm, 2009).

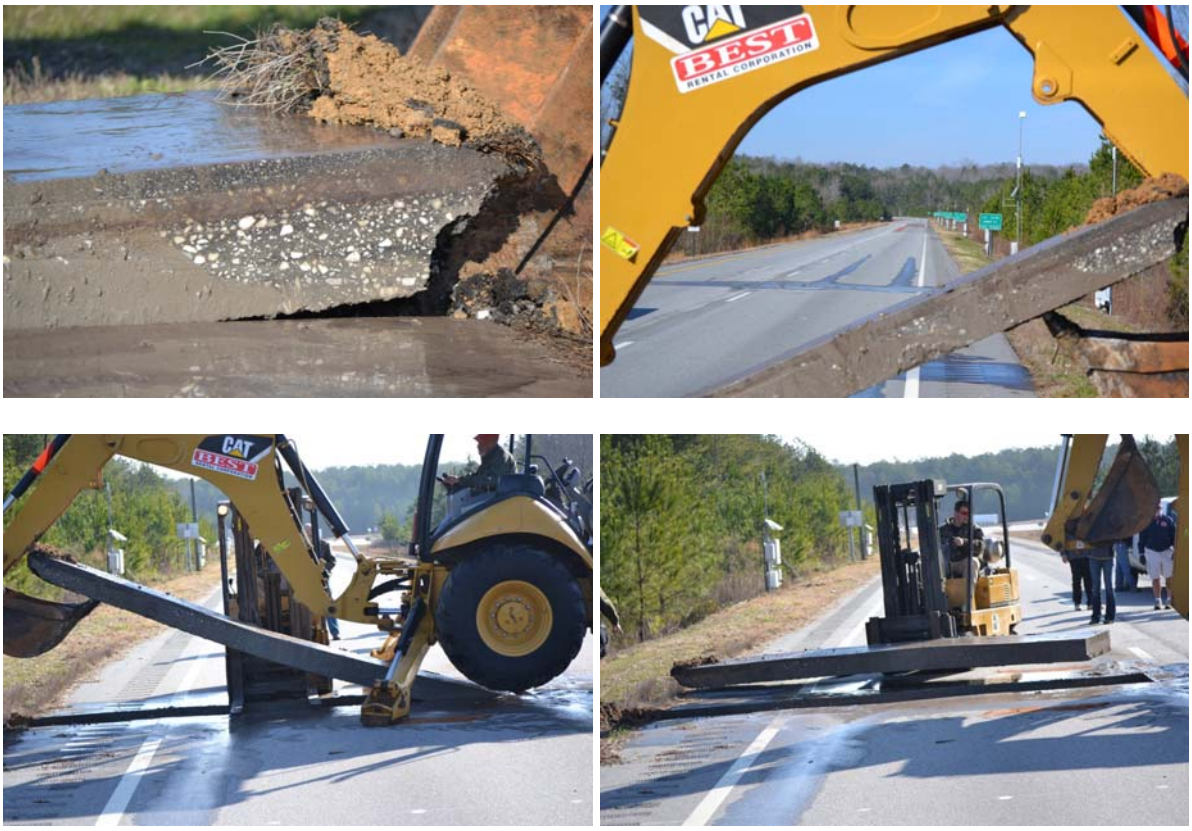

Figure 5.6 Lifting and Extracting Slab from Trench 1

Figure 5.7 Lifting and Extracting Slab from Trench 2

The slab taken from Trench 2, and Trench 2 itself, were also visually inspected for quality of gauge installation. Figure 5.8 (a) shows the end of an asphalt strain gauge locked into the AC. No voids were visible around the gauge that would indicate slippage between the gauge and AC. Figure 5.8 (b) clearly shows two metal flanges belonging to a single gauge embedded in slightly finer mix placed during installation. Again, the gauge appears to be well-compacted within the AC. These observations lend greater confidence to the measured strain data previously presented.

a) Embedded Gauge in Slab from Trench 2

b) Gauge Flanges in Trench 2 Wall

Figure 5.8 Embedded Gauges

After the slabs had been removed, the trench edges and faces were cleaned. A walking dipstick (Figure 5.9) was used to measure the surface profile on each side of the trench and an average surface profile for each trench was determined. The device measures differential elevation over a 9.5 inch (241 mm) horizontal interval. The as-built cross slope (approximately 2.5%) was subtracted out of the transverse profiles to better quantify the depth of rutting. A carpenters square, placed square to the pavement surface at each dipstick measurement, was then used to establish the depth to each lift interface (Figure 5.10). This was done on each trench face and averages, per trench, were again determined.

Figure 5.9 Walking Dipstick at Surface

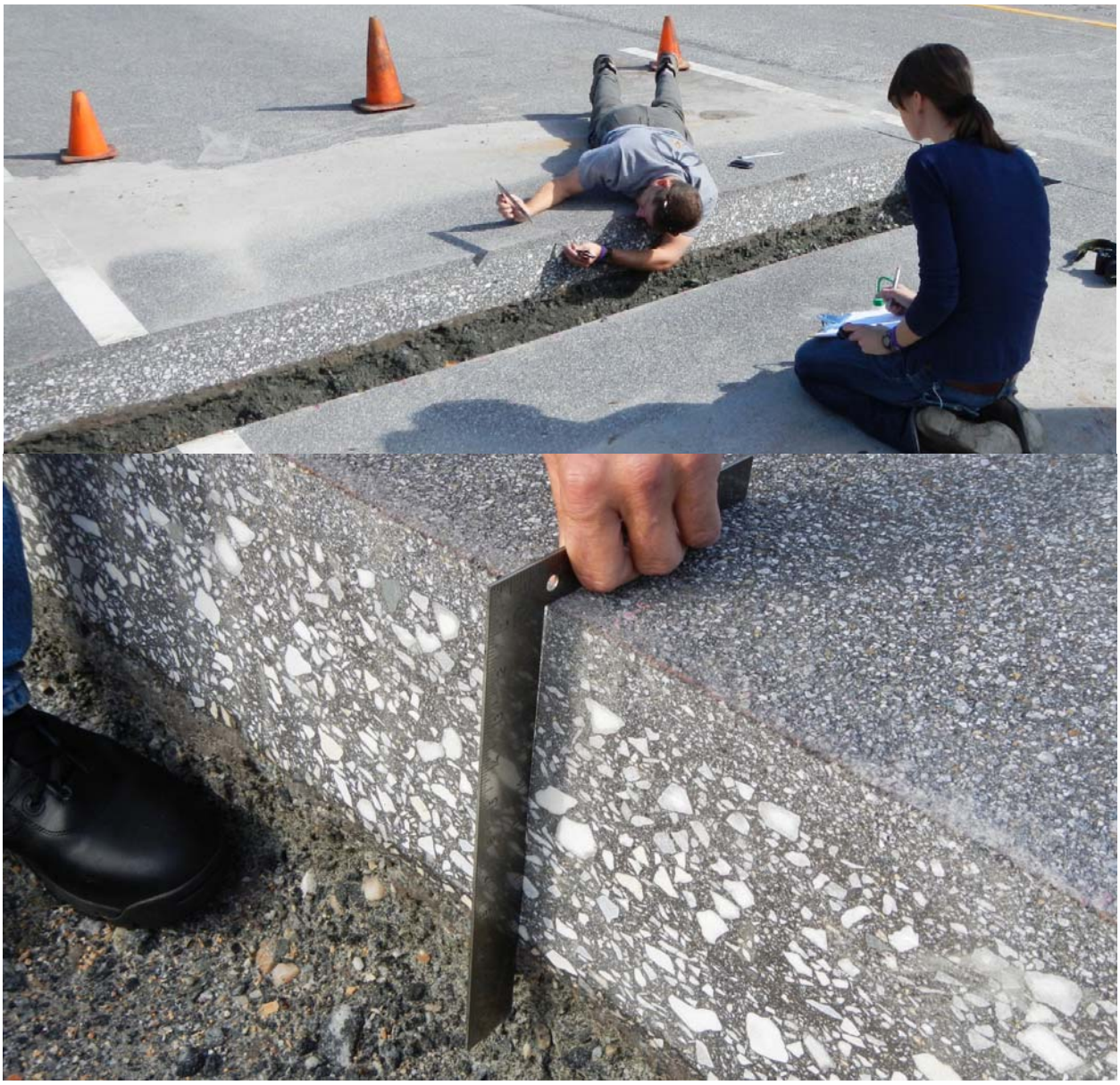

Figure 5.10 Measuring Subsurface Profile

Figures 5.11 and 5.12 show the average transverse profiles of the surface and each sublayer lift interface for Trench 1 and Trench 2, respectively. In each figure, traffic is moving into the page with the rut depths only reported for the outside wheelpath. Furthermore, the reported rut depths represent peak to trough at transverse offsets corresponding to the maximum peak and trough of the surface. This method results in higher reported rut depths than those represented by wire-line measurements previously presented (Figure 5.2). The reason for reporting rutting in this fashion was to capture the full extent of distortion, both upward and downward in the sublayers.

Most notable in these figures was the percentage each sublayer contributed to the total rut depth. The percentages were computed by subtracting rut depths in adjacent lifts and dividing by the total surface-measured rutting. For example, in Figure 5.11, the surface layer contributed (0.73”-0.47”)/0.73” = 35% of the total rutting. Looking at both figures, the surface layer (non-Thiopave

mixture) combined with the aggregate base/subgrade layer contributed at least 61% of the total rut depth. Where the rutting was more severe in Trench 1, 55% of the rutting occurred in the top two lifts with very little occurring in the two underlying Thiopave layers. In Trench 2, rutting of the Thiopave layers was more evenly distributed (13%, 17% and 9% respectively).

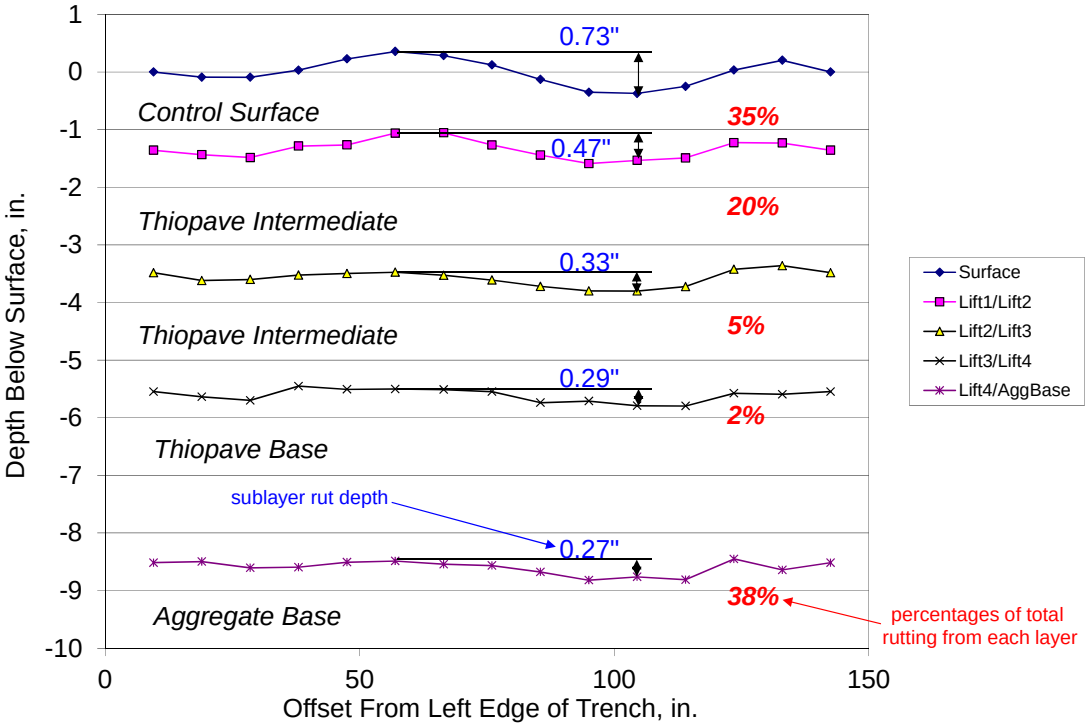

Figure 5.11 Trench 1 Rutting Profile

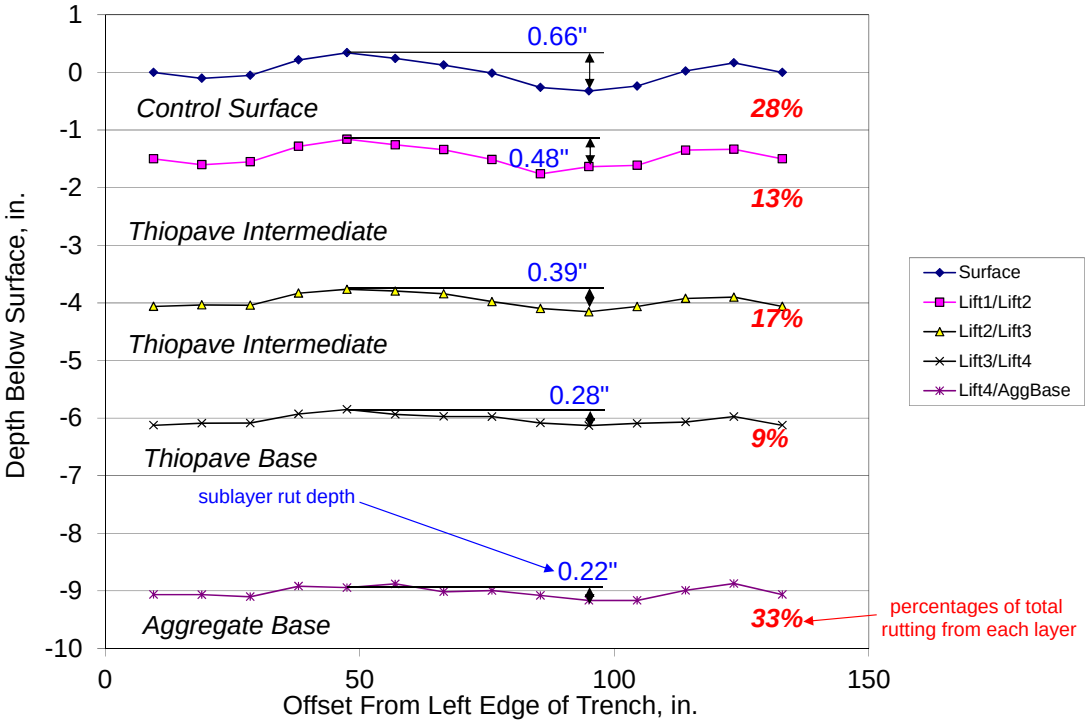

Figure 5.12 Trench 2 Rutting Profile

Weekly ride quality measurements, quantified by the International Roughness Index (IRI), are shown in Figure 5.13 for each section. Sections N6 (7 in. (178 mm) Thiopave) and S9 (7 in. (178 mm) control) were nearly indistinguishable. Neither section exhibited significant changes in IRI versus time or ESALs. The R^2 for trendlines fitting IRI versus test date were relatively low ($R^2 \leq 0.3$) with very low fitted slopes for both sections. Interestingly, N5 showed a reasonable correlation ($R^2 = 0.72$) between IRI and test date. However, at a maximum of approximately 85 in/mile, this section also performed very well and was well below a commonly accepted threshold of 170 in/mile that would trigger some sort of rehabilitation. This 170 in/mile value, as reported by Shafizadeh and Mannering (2003), was recommended by the FHWA for "acceptable ride quality," in its 1998 National Strategic Plan for the National Highway System (NHS).

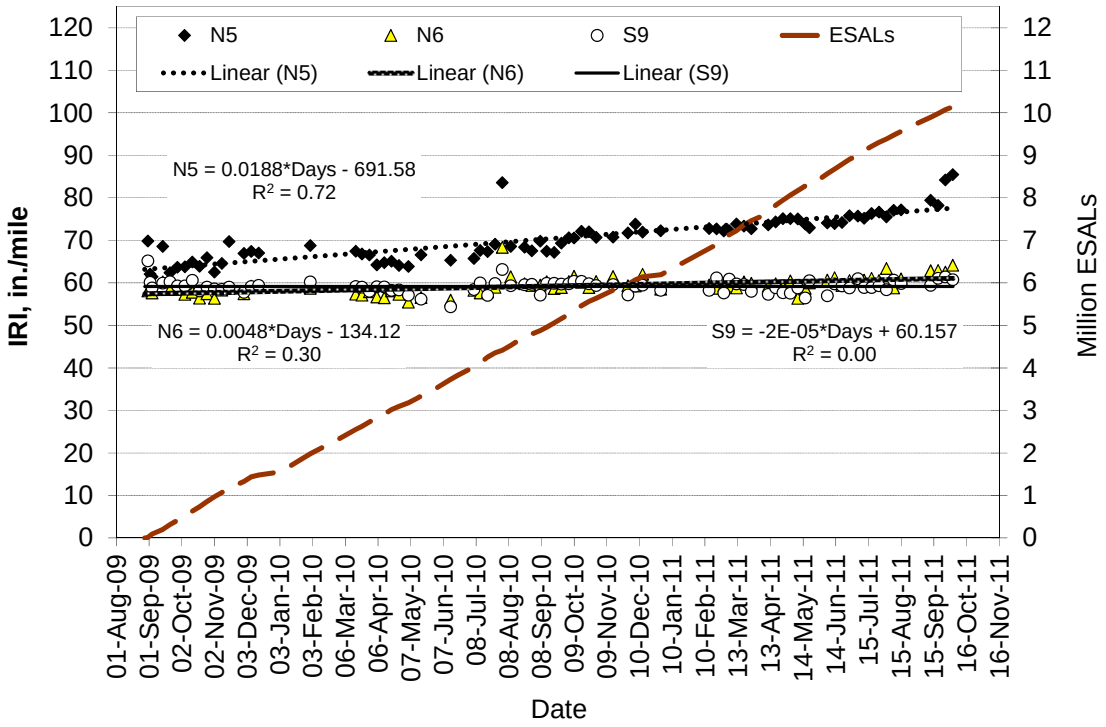

Figure 5.13 IRI & ESALs vs Date

To further examine the IRI trend, IRI was plotted against cumulative ESALs rather than test date as shown in Figure 5.14. This, of course, again shows no significant change in N6 and S9. However, the slope of the N5 trendline is very informative. It indicates that the IRI increased approximately 1.4 inches per mile for every one million ESALs applied. This trend is not likely to continue as the pavement begins to exhibit cracking, however.

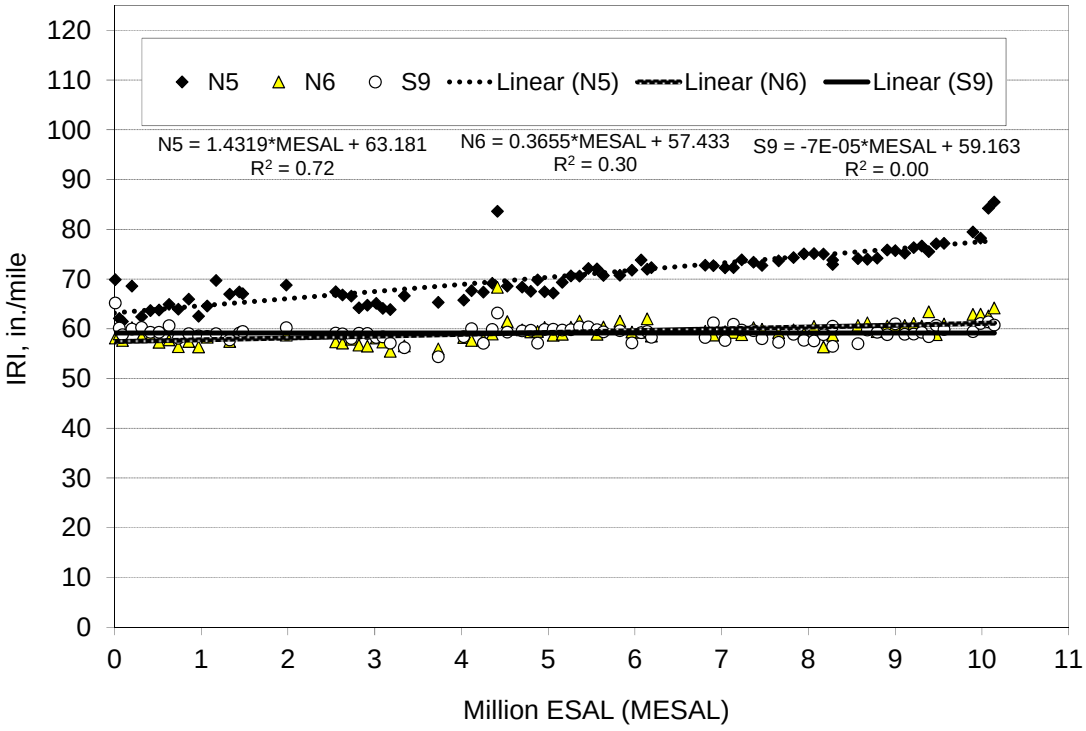

Figure 5.14 IRI vs. ESALs

6. KEY FINDINGS, CONCLUSIONS AND RECOMMENDATIONS

This report was intended to document additional lab testing and field performance of the Thiopave and control sections under the full two-year, 10.14 million ESAL, research cycle at the NCAT Test Track. Based on the data presented herein the following key findings, conclusions and recommendations can be made:

6.1 Laboratory Characterization

1. The moisture resistance of the Thiopave and control mixtures was evaluated based on the stripping inflection point and tensile strength ratio determined using the Hamburg wheel-tracking device (AASHTO T 324-04) and modified Lottman (AASHTO T 283-07) tests, respectively.
   a. While the Thiopave base mix had the highest average stripping inflection point, it was not significantly different from those of the Thiopave intermediate mix and the control base mixture, based on an ANOVA ($\alpha = 0.05$). All of the average stripping inflection points were greater than 5,000 cycles, which is commonly used as a minimum threshold for moisture resistance mixtures (Brown et al., 2001).
   b. However, based on the modified Lottman test results, the Thiopave base mix (TSR = 0.66) failed to meet the minimum TSR criterion of 0.8, as recommended in AASHTO M 323-07 for moisture resistant mixtures. The other two mixtures—Thiopave intermediate and control base mixtures—had similar TSR values, which were both greater than 0.8. A further statistical analysis of the splitting tensile strengths showed a different trend. The Thiopave intermediate and control base mixtures had equivalent conditioned and unconditioned splitting tensile strengths, which were statistically higher than those of the Thiopave base mix.
2. In addition to the APA test, whose results were presented in the previous report (Timm et al., 2011), the Hamburg wheel-tracking and flow number tests were also used to evaluate the mixture resistance to permanent deformation as follows:
   a. In the Hamburg test, while the control base and Thiopave base mixtures had higher average rut depths and rutting rates than the Thiopave intermediate mix, the differences were not statistically significant based on an ANOVA ($\alpha = 0.05$).
   b. In the flow number test, the Thiopave base mixture, designed for a higher binder content at 2 percent air voids, had the lowest average flow number, followed by the control base mix and then the control intermediate mix. The Thiopave intermediate mix showed the highest flow number. Based on a statistical grouping analysis, the Thiopave base and control base mixes were grouped with lower flow numbers, and the Thiopave intermediate, control intermediate and control base mixtures were grouped with higher flow numbers. Based on the recently recommended flow number criteria for HMA and WMA (AAT, 2011; Bonaquist, 2011), the Thiopave and control intermediate mixtures would withstand 10 to 30 million ESALs, and the Thiopave and control base mixtures would meet the criteria for trafficking of 3 to 10 million ESALs.
3. In addition to the test results based on two replicate beams reported in the previous report (Timm et al., 2011), a third replicate beam was tested at each of the three strain levels—200, 400 and 800 microstrain—in the bending beam fatigue testing for the control and Thiopave base mixtures. The final results were different from those previously reported (Timm et al., 2011), and a summary of the analysis follows:

   a. Based on the analysis using a power-model transfer function presented in the previous report, the Thiopave mixture exhibited longer fatigue life than the control base at all the strain levels. However, based on the complete data set, the Thiopave mixture showed 436% and 38.4% longer fatigue life at 200 and 400 microstrain, respectively, but it had 25.6% less fatigue life at 800 microstrain.
   b. The predicted endurance limits based on the complete dataset for the control and Thiopave base mixes were 91 and 109 microstrain, respectively, instead of 89 and 157 microstrain as previously reported. This reduction occurred due to a noticeable reduction in the numbers of cycles to failure of the third beams tested at 400 and 200 microstrain, compared to the first and second beams.
4. The resistance of the two base mixtures was also evaluated using a uniaxial fatigue test in the AMPT based on the simplified viscoelastic continuum damage approach (S-VECD). The analysis also suggested that the Thiopave base mixture would have longer fatigue life at 200 and 400 microstrain and slightly shorter fatigue life at 800 microstrain.
5. The resistance to low temperature cracking was evaluated using the indirect tension and strength (IDT) testing methodology. A critical cracking temperature for low temperature cracking was developed from these results. The results of the investigation indicated no clear effect of the addition of Thiopave on the low temperature cracking behavior of the mixes tested. These results were consistent with previous findings.

6.2 Structural Response and Characterization

1. Strong correlations between backcalculated composite AC moduli and mid-depth pavement temperature were determined for each test section. It was found that the Thiopave sections were influenced more by temperature than the control section. At colder temperatures (50^oF), the thickest Thiopave section (N5) had the statistically highest AC modulus, followed by the thinner Thiopave section (N6) and the control section (S9). At intermediate temperatures (68^oF), the average backcalculated AC moduli between N5 and the other sections was not distinguishable, though N6 was statistically higher than S9. At warmer temperatures (110^oF), N5 was the softest followed by N6 and S9.
2. Plots of temperature-corrected backcalculated AC moduli versus time did not show appreciable changes due to aging or pavement damage. With respect to AC modulus, each section appears structurally healthy after 10 million ESALs.
3. Pavement response was found to be strongly correlated to mid-depth pavement temperature for each axle type (single, tandem and steer) in each section. An exponential function was used to characterize the relationship between temperature and pavement response. Pavement responses were normalized to three reference temperatures to determine the statistical significance of differences between sections in terms of pavement response.
   a. In all cases, section N5 (9 in. (229 mm) Thiopave) was found to have statistically lower pavement responses which was expected since it had a 2 inch (51 mm) thickness advantage over the other two sections.
   b. Some statistical differences were noted between the control and the 7 in. (178 mm) Thiopave section, though they often were not practically different (i.e., less than 30 με or less than 2 psi). At 110^oF (43ºC), however, longitudinal strain in the control section was statistically and practically lower than N6 (7 in. (178 mm) Thiopave). This finding was expected since it was slightly thicker and was found to have a higher average AC modulus at this temperature.

4. Since no cracking had been observed in any section, estimates of cracking performance were made by combining laboratory-derived fatigue cracking equations with measured strain levels at 68°F (20ºC). Section N5 (9 in. (229 mm) Thiopave) is expected to have 14.2 times the fatigue life of the control due primarily to its thickness advantage. Section N6 (7 in. (178 mm) Thiopave) has a predicted 1.24 times longer fatigue expectation relative to the control.
5. Plots of temperature-normalized pavement response versus time demonstrated relatively consistent data, which was consistent with relatively stable backcalculated AC moduli and is an indicator of sound structural integrity.

6.3 Performance

1. At the conclusion of traffic, no cracking was evident in any of the three test sections. It is recommended to leave the two 7 inch (178 mm) sections in place for further trafficking to fully evaluate differences in field cracking performance.
2. No statistical differences in final wire-line rutting were found between the two Thiopave sections which had 10-11 mm of rutting. The control section was statistically lower with approximately 7 mm. All three sections were below the 12.5 mm (1/2 inch) rutting failure threshold used at the Test Track.
3. Forensic trenching conducted in Section N5 (9 in. (229 mm) Thiopave) determined that at least 60% of the total rutting measured at the pavement surface came from the conventional surface lift and aggregate base, combined. The remaining rutting was attributed to the Thiopave lifts.
4. Ride quality in each section was deemed excellent. The control (7 in.) and 7 in. (178 mm) Thiopave had no appreciable change in roughness during the entire two year cycle. The 9 in. (229 mm) Thiopave section did have a steady increase in roughness over time, but was still well below a typical trigger value that would prompt rehabilitation treatments.

REFERENCES

1. Advanced Asphalt Technologies, LLC. *A Manual for Design of Hot Mix Asphalt with Commentary*. NCHRP Report 673, National Academies of Sciences, Transportation Research Board, 2011.
2. Allen, D.L. and R.C. Graves. Variability in Measurement of In-Situ Material Properties. *Proceedings, Fourth International Conference on the Bearing Capacity of Roads and Airfields*, Vol. 2, 1994, pp. 989-1005.
3. Biligiri, K.P. K.E. Kaloush, M.W. Mamlouk, and M.W. Witczak. Rational Modeling of Tertiary Flow of Asphalt Mixtures, *Transportation Research Record No. 2001*, Washington, D.C., 2007, pp. 63-72.
4. Bonaquist, R. *Mix Design Practices for Warm Mix Asphalt*. NCHRP Report 691, National Academies of Sciences, Transportation Research Board, 2011.
5. Brown, E.R., P.S. Kandhal, and J. Zhang. *Performance Testing for Hot Mix Asphalt*. Report 01-05, National Center for Asphalt Technology, Auburn University, November 2001.
6. Daniel, Jo Sias, and Y. Richard Kim. Development of a Simplified Fatigue Test and Analysis Procedure Using a Viscoelastic, Continuum Damage Model. *Journal of Association of Asphalt Paving Technologists*, 2002.
7. Hou, Tian, B. Shane Underwood, and Y. Richard Kim. Fatigue Performance Prediction of North Carolina Mixtures Using the Simplified Viscoelastic Contiuum Damage Model. *Journal of Association of Asphalt Paving Technologists*, 2010.
8. Kim, Y. R., Hyon-Jong Lee, and D.N. Little. Fatigue Characterization of Asphalt Concrete Using Viscoelasticity and Continuum Damage Theory. *Journal of Association of Asphalt Paving Technologists*, 1997, pp. 520-569.
9. Noureldin, A.S. Influence of Stress Levels and Seasonal Variations on In Situ Pavement Layer Properties. *Transportation Research Record No. 1448*, Washington, D.C., 1994, pp. 16-24.
10. Peters-Davis, K. and D.H. Timm. *Recalibration of the Asphalt Layer Coefficient*. Report 09-03, National Center for Asphalt Technology, Auburn University, 2009.
11. Powell, R. Buzz, and Adam J. Taylor. *Design, Construction, and Performance of Sulfur-Modified Mix in the WMA Certification Program at the NCAT Pavement Test Track - Final Report*. Report 12-01, National Center for Asphalt Technology, Auburn University, 2012.
12. Priest, A.L. and D.H. Timm. *Methodology and Calibration of Fatigue Transfer Functions for Mechanistic-Empirical Flexible Pavement Design*. Report 06-03, National Center for Asphalt Technology, Auburn University, 2006.
13. Prowell, B.D., E.R. Brown, R.M. Anderson, J. Sias-Daniel, H. Von Quintus, S. Shen, S.H. Carpenter, S. Bhattacharjee and S. Maghsoodloo. *Validating the Fatigue Endurance Limit for Hot Mix Asphalt*. NCHRP Report 646, Transportation Research Board, Washington, D.C., 2010.
14. Shafizadeh, K. and F. Mannering. Acceptability of Pavement Roughness on Urban Highways by Driving Public. *Transportation Research Record No. 1860*, Washington, D.C., 2003, pp. 187-193.
15. Taylor, A.J. and D.H. Timm. *Mechanistic Characterization of Resilient Moduli for Unbound Pavement Layer Materials*. Report 09-06, National Center for Asphalt Technology, Auburn University, 2009.

16. Timm, D.H., M.M. Robbins, J.R. Willis, N. Tran and A.J. Taylor. *Evaluation of Mixture Performance and Structural Capacity of Pavements Using Shell Thiopave: Phase II - Construction, Laboratory Evaluation, and Full-Scale Testing of Thiopave Test Sections - One Year Report*. Report 11-03, National Center for Asphalt Technology, Auburn University, 2011.
17. Timm, D.H. *Design, Construction, and Instrumentation of the 2006 Test Track Structural Study*. Report 09-01, National Center for Asphalt Technology, Auburn University, 2009.
18. Timm, D.H., N.H. Tran, A.J. Taylor, M.M. Robbins and R. Powell. *Evaluation of Mixture Performance and Structural Capacity of Pavements Using Shell Thiopave®*. Report 09-05, National Center for Asphalt Technology, Auburn University, 2009.
19. Timm, D.H. and A.L. Priest. Flexible Pavement Fatigue Cracking and Measured Strain Response at the NCAT Test Track. *Proceedings of the 87th Annual Transportation Research Board*, Washington, D.C., 2008.
20. Timm, D.H. and A.L. Priest. *Material Properties of the 2003 NCAT Test Track Structural Study*. Report 06-01, National Center for Asphalt Technology, Auburn University, 2006.
21. Timm, D.H., R. West, A.L. Priest, S.S. Immanuel, J. Zhang and E.R. Brown. *Phase II NCAT Test Track Results*. Report 06-05, National Center for Asphalt Technology, Auburn University, 2006.
22. Timm, D.H., D.E. Newcomb and B. Birgisson. *Mechanistic-Empirical Flexible Pavement Thickness Design: The Minnesota Method*. Staff Paper, MN/RC-P99-10, Minnesota Department of Transportation, St. Paul, MN, 1999.
23. Underwood, B. Shane, Y. Richard Kim, and Murthy Guddati. Characterization and Performance Prediciton of ALF Mixtures Using a Viscoelastoplastic Contiuum Damage Model. *Journal of Association of Asphalt Paving Technologists*, 2006.
24. Willis, J.R. and D.H. Timm. Repeatability of Asphalt Strain Gauges. Report No. 09-07, National Center for Asphalt Technology, Auburn University, 2009.
25. Willis, J.R., D.H. Timm, R.C. West, R. Powell, M.M. Robbins, A.J. Taylor, A. Smit, N. Tran, M. Heitzman and A. Bianchini. *Phase III NCAT Test Track Findings*. Report 09-08, National Center for Asphalt Technology, Auburn University, 2009.

APPENDIX A – MIX DESIGN AND AS-BUILT AC PROPERTIES

Table A.1 Mix Design Gradations and Properties (Timm et al., 2011)

Mixture Type	Control			Thiopave	
Lift	Surface	Intermediate	Base	Intermediate	Base
Sieve Size, mm	**Aggregate Gradation, Percent Passing Sieve Size**				
25	100	100	100	100	100
19	100	93	93	93	93
12.5	100	82	84	82	82
9.5	100	71	73	71	71
4.75	78	52	55	52	52
2.36	60	45	47	45	45
1.18	46	35	36	35	35
0.6	31	24	25	24	24
0.3	16	12	14	12	12
0.15	10	7	8	7	7
0.075	5.8	3.9	4.6	3.9	3.9
Property	**Mix Design Parameters**				
Virgin Asphalt PG Grade	76-22	76-22	67-22	67-22	67-22
Target Thiopave, % of combined binder wt	0	0	0	40	30
Design Air Voids (VTM), %	4	4	4	3.5	2
Virgin Binder, % wt of mix	5.8	4.7	4.6	3.7	4.4
Thiopave and Compaction Aid, % wt of mix	0	0	0	2.5	1.9
Total Combined Binder (P_b), % wt of mix	5.8	4.7	4.6	6.2	6.3
Effective Binder (P_{be}), % wt of mix	5.1	4.1	4.1	5.6	5.8
Total Combined Binder (V_b), % vol of mix	13.4	11.3	11.1	12.2	13.2
Effective Binder (V_{be}), % vol of mix	11.8	10.0	9.9	11.1	12.1
Dust Proportion (DP)	1.1	0.9	1.1	0.7	0.7
Maximum Specific Gravity (G_{mm})	2.483	2.575	2.574	2.581	2.558
Voids in Mineral Aggregate (VMA), %	15.8	13.9	13.9	14.6	14.1
Voids Filled with Asphalt (VFA), %	75	71	71	76	86

Table A.2 As-Built Properties of Asphalt Concrete (Timm et al., 2011)

Section	N5 (Thiopave 9")				N6 (Thiopave 7")			S9 (Control 7")		
Lift	1	2	3	4	1	2	3	1	2	3
NMAS, mm[a]	9.5	19	19	19	9.5	19	19	9.5	19	19
PG Grade (Virgin Binder)[b]	76-22	67-22	67-22	67-22	76-22	67-22	67-22	76-22	76-22	67-22
Delivery Temperature, F[c]	288	243	229	225	282	238	249	275	316	254
% Total Binder[d]	6.1	5.7	5.6	6.2	6.1	5.7	6.1	6.1	4.4	4.7
% Thiopave[e]	0	39	33	22	0	35	22	0	0	0
$\%G_{mm}$[f]	94.1	93.0	92.9	93.6	93.8	92.9	93.7	93.1	92.8	92.6

[a]NMAS: nominal maximum aggregate size
[b]PG Grade (Virgin Binder): asphalt grade without Thiopave modification
[c]Delivery Temperature: surface temperature of mix measured directly behind paver with infrared device
[d]% Total Binder: total gravimetric asphalt content (includes Thiopave material where indicated). Determined by ignition oven.
[e]%Thiopave: percent of total binder percentage that is Thiopave
[f]$\%G_{mm}$: percent of maximum theoretical density

10/5/2009

Quadrant: N
Section: 5 *Mix Type = Surface - Control*
Sublot: 1

Laboratory Diary

General Description of Mix and Materials

Design Method:	Super
Compactive Effort:	80 gyrations
Binder Performance Grade:	76-22
Modifier Type:	SBS
Aggregate Type:	Grn/Sand/Lms
Design Gradation Type:	Fine

Avg. Lab Properties of Plant Produced Mix

Sieve Size	Design	QC
25 mm (1"):	100	100
19 mm (3/4"):	100	100
12.5 mm (1/2"):	100	100
9.5 mm (3/8"):	100	100
4.75 mm (#4):	78	83
2.36 mm (#8):	60	62
1.18 mm (#16):	46	47
0.60 mm (#30):	31	33
0.30 mm (#50):	16	16
0.15 mm (#100):	10	10
0.075 mm (#200):	5.8	6.4
Binder Content (Pb):	5.8	6.1
Eff. Binder Content (Pbe):	5.1	5.4
Dust-to-Binder Ratio:	1.1	1.2
Rice Gravity (Gmm):	2.483	2.472
Avg. Bulk Gravity (Gmb):	2.384	2.380
Avg Air Voids (Va):	4.0	3.7
Agg. Bulk Gravity (Gsb):	2.667	2.671
Avg VMA:	15.8	16.3
Avg. VFA:	75	77

Construction Diary

Relevant Conditions for Construction

Completion Date:	August 3, 2009
24 Hour High Temperature (F):	91
24 Hour Low Temperature (F):	72
24 Hour Rainfall (in):	0.00
Planned Subot Lift Thickness (in):	1.3
Paving Machine:	Roadtec

Plant Configuration and Placement Details

Component	% Setting
Asphalt Content (Plant Setting)	6.2
89 Columbus Granite	36.0
8910 Opelika Limestone Screenings	23.0
M10 Columbus Granite	13.0
Shorter Coarse Sand	28.0

As-Built Sublot Lift Thickness (in):	1.3
Total Thickness of All 2009 Sublots (in):	9.0
Approx. Underlying HMA Thickness (in):	0.0
Type of Tack Coat Utilized:	PG67-22
Target Tack Application Rate (gal/sy):	0.05
Approx. Avg. Temperature at Plant (F):	340
Avg. Measured Mat Compaction:	94.1%

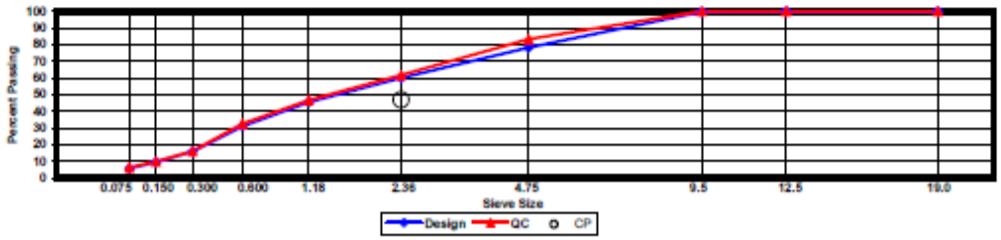

General Notes:
1) Mixes are referenced by quadrant (E=East, N=North, W=West, and S=South), section # (sequential) and sublot (top=1);
3) The total HMA thickness of all structural study sections (N1-N11 and S8-S12) ranges from 5-3/4 to 14 inches by design;
3) All non-structural sections are supprted by a uniform perpetual foundation in order to study surface mix performance;
4) SMA and OGFC refer to stone matrix asphalt and open-graded friction course, respectively; and
5) All liquid asphalt purchased for use in Track reconstruction contained LOF 6500 antistrip additive at a rate of 0.5 percent

10/5/2009

Quadrant: N
Section: 5
Sublot: 2

Mix Type = Intermediate - Thiopave

Laboratory Diary

General Description of Mix and Materials

Design Method:	WMA-T
Compactive Effort:	60 gyrations
Binder Performance Grade:	67-22
Modifier Type:	Thiopave
Aggregate Type:	Lms/Sand/Grn
Design Gradation Type:	Fine

Avg. Lab Properties of Plant Produced Mix

Sieve Size	Design	QC
25 mm (1"):	100	100
19 mm (3/4"):	93	90
12.5 mm (1/2"):	82	81
9.5 mm (3/8"):	71	73
4.75 mm (#4):	52	58
2.36 mm (#8):	45	46
1.18 mm (#16):	35	36
0.60 mm (#30):	24	24
0.30 mm (#50):	12	12
0.15 mm (#100):	7	8
0.075 mm (#200):	3.9	4.7
Binder Content (Pb):	6.2	5.7
Eff. Binder Content (Pbe):	5.6	5.3
Dust-to-Binder Ratio:	0.7	0.9
Rice Gravity (Gmm):	2.581	2.554
Avg. Bulk Gravity (Gmb):	2.491	2.439
Avg Air Voids (Va):	3.5	4.5
Agg. Bulk Gravity (Gsb):	2.737	2.772
Avg VMA:	14.6	17.1
Avg. VFA:	76	74

Construction Diary

Relevant Conditions for Construction

Completion Date:	July 24, 2009
24 Hour High Temperature (F):	90
24 Hour Low Temperature (F):	68
24 Hour Rainfall (in):	0.00
Planned Subot Lift Thickness (in):	2.8
Paving Machine:	Roadtec

Plant Configuration and Placement Details

Component	% Setting
Asphalt Content (Plant Setting)	4.0
78 Opelika Limestone	30.0
57 Opelika Limestone	18.0
M10 Columbus Granite	25.0
Shorter Coarse Sand	27.0
Thiopave	40.0
Compaction Agent	1.0

Actual Thiopave Content = 39%

As-Built Sublot Lift Thickness (in):	2.8
Total Thickness of All 2009 Sublots (in):	9.0
Approx. Underlying HMA Thickness (in):	0.0
Type of Tack Coat Utilized:	NTSS-1HM
Target Tack Application Rate (gal/sy):	0.05
Approx. Avg. Temperature at Plant (F):	275
Avg. Measured Mat Compaction:	93.0%

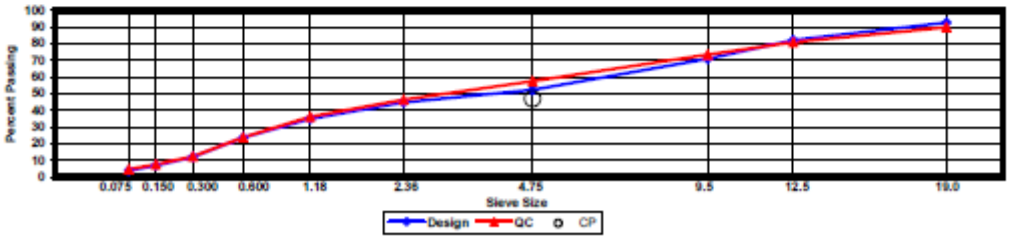

General Notes:

1) Mixes are referenced by quadrant (E=East, N=North, W=West, and S=South), section # (sequential) and sublot (top=1);
3) The total HMA thickness of all structural study sections (N1-N11 and S8-S12) ranges from 5-3/4 to 14 inches by design;
3) All non-structural sections are supprted by a uniform perpetual foundation in order to study surface mix performance;
4) SMA and OGFC refer to stone matrix asphalt and open-graded friction course, respectively; and
5) All liquid asphalt purchased for use in Track reconstruction contained LOF 6500 antistrip additive at a rate of 0.5 percent

10/5/2009

Quadrant: N
Section: 5 *Mix Type = Intermediate - Thiopave*
Sublot: 3

Laboratory Diary

General Desccription of Mix and Materials

Design Method:	WMA-T
Compactive Effort:	60 gyrations
Binder Performance Grade:	67-22
Modifier Type:	Thiopave
Aggregate Type:	Lms/Sand/Grn
Design Gradation Type:	Fine

Avg. Lab Properties of Plant Produced Mix

Sieve Size	Design	QC
25 mm (1"):	100	98
19 mm (3/4"):	93	92
12.5 mm (1/2"):	82	82
9.5 mm (3/8"):	71	72
4.75 mm (#4):	52	54
2.36 mm (#8):	45	44
1.18 mm (#16):	35	34
0.60 mm (#30):	24	23
0.30 mm (#50):	12	12
0.15 mm (#100):	7	8
0.075 mm (#200):	3.9	4.9
Binder Content (Pb):	6.2	5.6
Eff. Binder Content (Pbe):	5.6	5.1
Dust-to-Binder Ratio:	0.7	1.0
Rice Gravity (Gmm):	2.581	2.553
Avg. Bulk Gravity (Gmb):	2.491	2.440
Avg Air Voids (Va):	3.5	4.4
Agg. Bulk Gravity (Gsb):	2.737	2.762
Avg VMA:	14.6	16.6
Avg. VFA:	76	73

Construction Diary

Relevant Conditions for Construction

Completion Date:	July 23, 2009
24 Hour High Temperature (F):	89
24 Hour Low Temperature (F):	74
24 Hour Rainfall (in):	0.00
Planned Subot Lift Thickness (in):	2.3
Paving Machine:	Roadtec

Plant Configuration and Placement Details

Component	% Setting
Asphalt Content (Plant Setting)	4.0
78 Opelika Limestone	30.0
57 Opelika Limestone	18.0
M10 Columbus Granite	25.0
Shorter Coarse Sand	27.0
Thiopave	40.0
Compaction Agent	1.0

Actual Thiopave Content = 33%

As-Built Sublot Lift Thickness (in):	2.0
Total Thickness of All 2009 Sublots (in):	9.0
Approx. Underlying HMA Thickness (in):	0.0
Type of Tack Coat Utilized:	NTSS-1HM
Target Tack Application Rate (gal/sy):	0.07
Approx. Avg. Temperature at Plant (F):	275
Avg. Measured Mat Compaction:	92.9%

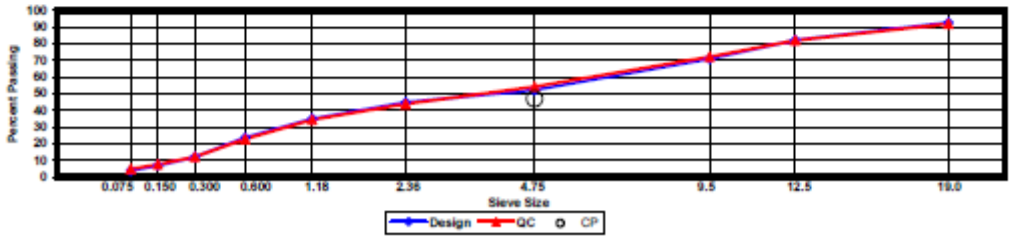

General Notes:
1) Mixes are referenced by quadrant (E=East, N=North, W=West, and S=South), section # (sequential) and sublot (top=1);
3) The total HMA thickness of all structural study sections (N1-N11 and S8-S12) ranges from 5-3/4 to 14 inches by design;
3) All non-structural sections are supprted by a uniform perpetual foundation in order to study surface mix performance;
4) SMA and OGFC refer to stone matrix asphalt and open-graded friction course, respectively; and
5) All liquid asphalt purchased for use in Track reconstruction contained LOF 6500 antistrip additive at a rate of 0.5 percent

10/5/2009

Quadrant: N
Section: 5
Sublot: 4

Mix Type = Base - Thiopave

Laboratory Diary

General Descciption of Mix and Materials

Design Method:	WMA-T
Compactive Effort:	60 gyrations
Binder Performance Grade:	67-22
Modifier Type:	Thiopave
Aggregate Type:	Lms/Sand/Grn
Design Gradation Type:	Fine

Avg. Lab Properties of Plant Produced Mix

Sieve Size	Design	QC
25 mm (1"):	100	100
19 mm (3/4"):	93	93
12.5 mm (1/2"):	82	82
9.5 mm (3/8"):	71	73
4.75 mm (#4):	52	55
2.36 mm (#8):	45	44
1.18 mm (#16):	35	35
0.60 mm (#30):	24	24
0.30 mm (#50):	12	12
0.15 mm (#100):	7	8
0.075 mm (#200):	3.9	4.8
Binder Content (Pb):	6.3	6.2
Eff. Binder Content (Pbe):	5.8	5.8
Dust-to-Binder Ratio:	0.7	0.8
Rice Gravity (Gmm):	2.558	2.518
Avg. Bulk Gravity (Gmb):	2.507	2.459
Avg Air Voids (Va):	2.0	2.3
Agg. Bulk Gravity (Gsb):	2.737	2.749
Avg VMA:	14.1	16.1
Avg. VFA:	86	85

Construction Diary

Relevant Conditions for Construction

Completion Date:	July 23, 2009
24 Hour High Temperature (F):	89
24 Hour Low Temperature (F):	74
24 Hour Rainfall (in):	0.00
Planned Subot Lift Thickness (in):	2.8
Paving Machine:	Roadtec

Plant Configuration and Placement Details

Component	% Setting
Asphalt Content (Plant Setting)	5.1
78 Opelika Limestone	30.0
57 Opelika Limestone	18.0
M10 Columbus Granite	25.0
Shorter Coarse Sand	27.0
Thiopave	30.0
Compaction Agent	1.0

Actual Thiopave Content = 22%

As-Built Sublot Lift Thickness (in):	2.9
Total Thickness of All 2009 Sublots (in):	9.0
Approx. Underlying HMA Thickness (in):	0.0
Type of Tack Coat Utilized:	NA
Target Tack Application Rate (gal/sy):	NA
Approx. Avg. Temperature at Plant (F):	275
Avg. Measured Mat Compaction:	93.6%

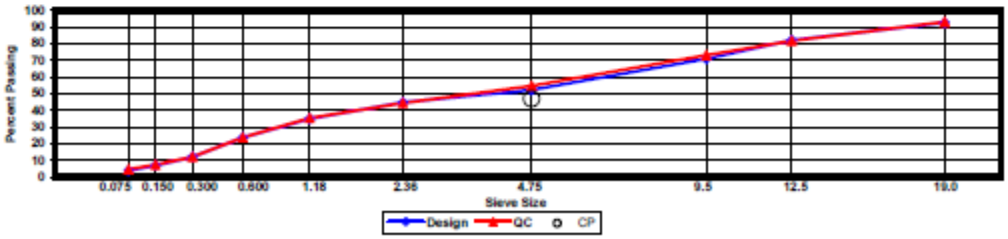

General Notes:

1) Mixes are referenced by quadrant (E=East, N=North, W=West, and S=South), section # (sequential) and sublot (top=1);
3) The total HMA thickness of all structural study sections (N1-N11 and S8-S12) ranges from 5-3/4 to 14 inches by design;
3) All non-structural sections are supprted by a uniform perpetual foundation in order to study surface mix performance;
4) SMA and OGFC refer to stone matrix asphalt and open-graded friction course, respectively; and
5) All liquid asphalt purchased for use in Track reconstruction contained LOF 6500 antistrip additive at a rate of 0.5 percent

10/5/2009

Quadrant: N
Section: 6 *Mix Type = Surface - Control*
Sublot: 1

Laboratory Diary

General Descciption of Mix and Materials

Design Method:	Super
Compactive Effort:	80 gyrations
Binder Performance Grade:	76-22
Modifier Type:	SBS
Aggregate Type:	Grn/Sand/Lms
Design Gradation Type:	Fine

Avg. Lab Properties of Plant Produced Mix

Sieve Size	Design	QC
25 mm (1"):	100	100
19 mm (3/4"):	100	100
12.5 mm (1/2"):	100	100
9.5 mm (3/8"):	100	100
4.75 mm (#4):	78	82
2.36 mm (#8):	60	55
1.18 mm (#16):	46	45
0.60 mm (#30):	31	30
0.30 mm (#50):	16	16
0.15 mm (#100):	10	10
0.075 mm (#200):	5.8	6.4
Binder Content (Pb):	5.8	6.1
Eff. Binder Content (Pbe):	5.1	5.4
Dust-to-Binder Ratio:	1.1	1.2
Rice Gravity (Gmm):	2.483	2.466
Avg. Bulk Gravity (Gmb):	2.384	2.370
Avg Air Voids (Va):	4.0	3.9
Agg. Bulk Gravity (Gsb):	2.667	2.662
Avg VMA:	15.8	16.4
Avg. VFA:	75	76

Construction Diary

Relevant Conditions for Construction

Completion Date:	August 3, 2009
24 Hour High Temperature (F):	91
24 Hour Low Temperature (F):	72
24 Hour Rainfall (in):	0.00
Planned Subot Lift Thickness (in):	1.3
Paving Machine:	Roadtec

Plant Configuration and Placement Details

Component	% Setting
Asphalt Content (Plant Setting)	6.2
89 Columbus Granite	36.0
8910 Opelika Limestone Screenings	23.0
M10 Columbus Granite	13.0
Shorter Coarse Sand	28.0

As-Built Sublot Lift Thickness (in):	1.1
Total Thickness of All 2009 Sublots (in):	6.9
Approx. Underlying HMA Thickness (in):	0.0
Type of Tack Coat Utilized:	PG67-22
Target Tack Application Rate (gal/sy):	0.05
Approx. Avg. Temperature at Plant (F):	340
Avg. Measured Mat Compaction:	93.8%

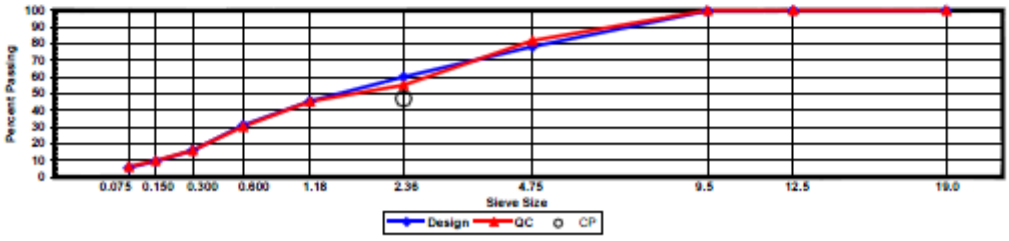

General Notes:
1) Mixes are referenced by quadrant (E=East, N=North, W=West, and S=South), section # (sequential) and sublot (top=1);
3) The total HMA thickness of all structural study sections (N1-N11 and S8-S12) ranges from 5-3/4 to 14 inches by design;
3) All non-structural sections are supprted by a uniform perpetual foundation in order to study surface mix performance;
4) SMA and OGFC refer to stone matrix asphalt and open-graded friction course, respectively; and
5) All liquid asphalt purchased for use in Track reconstruction contained LOF 6500 antistrip additive at a rate of 0.5 percent

10/5/2009

Quadrant: N
Section: 6
Sublot: 2

Mix Type = Intermediate - Thiopave

Laboratory Diary

General Descciption of Mix and Materials

Design Method:	WMA-T
Compactive Effort:	60 gyrations
Binder Performance Grade:	67-22
Modifier Type:	Thiopave
Aggregate Type:	Lms/Sand/Grn
Design Gradation Type:	Fine

Avg. Lab Properties of Plant Produced Mix

Sieve Size	Design	QC
25 mm (1"):	100	100
19 mm (3/4"):	93	89
12.5 mm (1/2"):	82	82
9.5 mm (3/8"):	71	75
4.75 mm (#4):	52	57
2.36 mm (#8):	45	46
1.18 mm (#16):	35	36
0.60 mm (#30):	24	24
0.30 mm (#50):	12	12
0.15 mm (#100):	7	8
0.075 mm (#200):	3.9	4.9
Binder Content (Pb):	6.2	5.7
Eff. Binder Content (Pbe):	5.6	5.2
Dust-to-Binder Ratio:	0.7	0.9
Rice Gravity (Gmm):	2.581	2.554
Avg. Bulk Gravity (Gmb):	2.491	2.440
Avg Air Voids (Va):	3.5	4.5
Agg. Bulk Gravity (Gsb):	2.737	2.768
Avg VMA:	14.6	16.9
Avg. VFA:	76	74

Construction Diary

Relevant Conditions for Construction

Completion Date:	July 24, 2009
24 Hour High Temperature (F):	90
24 Hour Low Temperature (F):	68
24 Hour Rainfall (in):	0.00
Planned Subot Lift Thickness (in):	2.8
Paving Machine:	Roadtec

Plant Configuration and Placement Details

Component	% Setting
Asphalt Content (Plant Setting)	4.0
78 Opelika Limestone	30.0
57 Opelika Limestone	18.0
M10 Columbus Granite	25.0
Shorter Coarse Sand	27.0
Thiopave	40.0
Compaction Agent	1.0

Actual Thiopave Content = 35%

As-Built Sublot Lift Thickness (in):	2.8
Total Thickness of All 2009 Sublots (in):	6.9
Approx. Underlying HMA Thickness (in):	0.0
Type of Tack Coat Utilized:	NTSS-1HM
Target Tack Application Rate (gal/sy):	0.05
Approx. Avg. Temperature at Plant (F):	275
Avg. Measured Mat Compaction:	92.9%

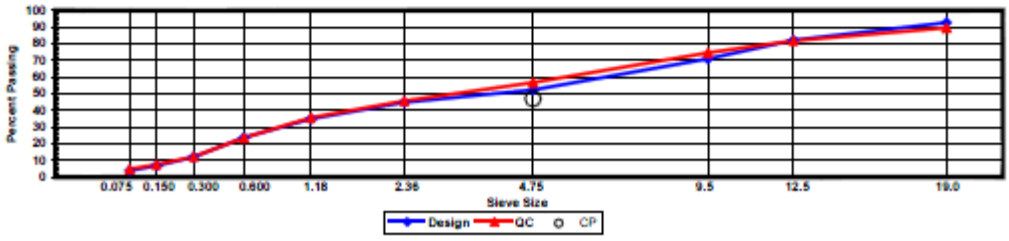

General Notes:

1) Mixes are referenced by quadrant (E=East, N=North, W=West, and S=South), section # (sequential) and sublot (top=1);
3) The total HMA thickness of all structural study sections (N1-N11 and S8-S12) ranges from 5-3/4 to 14 inches by design;
3) All non-structural sections are supprted by a uniform perpetual foundation in order to study surface mix performance;
4) SMA and OGFC refer to stone matrix asphalt and open-graded friction course, respectively; and
5) All liquid asphalt purchased for use in Track reconstruction contained LOF 6500 antistrip additive at a rate of 0.5 percent

10/5/2009

Quadrant: N
Section: 6 *Mix Type = Base - Thiopave*
Sublot: 3

Laboratory Diary

General Descciption of Mix and Materials

Design Method:	WMA-T
Compactive Effort:	60 gyrations
Binder Performance Grade:	67-22
Modifier Type:	Thiopave
Aggregate Type:	Lms/Sand/Grn
Design Gradation Type:	Fine

Avg. Lab Properties of Plant Produced Mix

Sieve Size	Design	QC
25 mm (1"):	100	100
19 mm (3/4"):	93	93
12.5 mm (1/2"):	82	82
9.5 mm (3/8"):	71	74
4.75 mm (#4):	52	55
2.36 mm (#8):	45	45
1.18 mm (#16):	35	35
0.60 mm (#30):	24	24
0.30 mm (#50):	12	12
0.15 mm (#100):	7	8
0.075 mm (#200):	3.9	4.8
Binder Content (Pb):	6.3	6.1
Eff. Binder Content (Pbe):	5.8	5.6
Dust-to-Binder Ratio:	0.7	0.8
Rice Gravity (Gmm):	2.568	2.521
Avg. Bulk Gravity (Gmb):	2.507	2.448
Avg Air Voids (Va):	2.0	2.9
Agg. Bulk Gravity (Gsb):	2.737	2.747
Avg VMA:	14.1	16.3
Avg. VFA:	86	82

Construction Diary

Relevant Conditions for Construction

Completion Date:	July 23, 2009
24 Hour High Temperature (F):	89
24 Hour Low Temperature (F):	74
24 Hour Rainfall (in):	0.00
Planned Subot Lift Thickness (in):	3.0
Paving Machine:	Roadtec

Plant Configuration and Placement Details

Component	% Setting
Asphalt Content (Plant Setting)	5.1
78 Opelika Limestone	30.0
57 Opelika Limestone	18.0
M10 Columbus Granite	25.0
Shorter Coarse Sand	27.0
Thiopave	30.0
Compaction Agent	1.0

Actual Thiopave Content = 22%

As-Built Sublot Lift Thickness (in):	3.1
Total Thickness of All 2009 Sublots (in):	6.9
Approx. Underlying HMA Thickness (in):	0.0
Type of Tack Coat Utilized:	NA
Target Tack Application Rate (gal/sy):	NA
Approx. Avg. Temperature at Plant (F):	275
Avg. Measured Mat Compaction:	93.7%

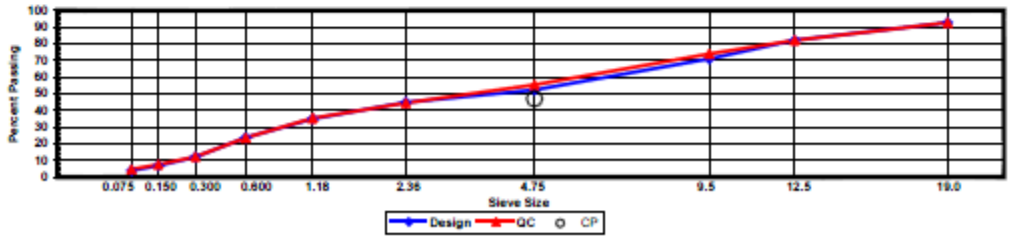

General Notes:
1) Mixes are referenced by quadrant (E=East, N=North, W=West, and S=South), section # (sequential) and sublot (top=1);
3) The total HMA thickness of all structural study sections (N1-N11 and S8-S12) ranges from 5-3/4 to 14 inches by design;
3) All non-structural sections are supprted by a uniform perpetual foundation in order to study surface mix performance;
4) SMA and OGFC refer to stone matrix asphalt and open-graded friction course, respectively; and
5) All liquid asphalt purchased for use in Track reconstruction contained LOF 6500 antistrip additive at a rate of 0.5 percent

10/5/2009

Quadrant: S
Section: 9 *Mix Type = Surface - Control*
Sublot: 1

Laboratory Diary

General Description of Mix and Materials

Design Method:	Super
Compactive Effort:	80 gyrations
Binder Performance Grade:	76-22
Modifier Type:	SBS
Aggregate Type:	Grn/Sand/Lms
Design Gradation Type:	Fine

Avg. Lab Properties of Plant Produced Mix

Sieve Size	Design	QC
25 mm (1"):	100	100
19 mm (3/4"):	100	100
12.5 mm (1/2"):	100	100
9.5 mm (3/8"):	100	100
4.75 mm (#4):	78	81
2.36 mm (#8):	60	59
1.18 mm (#16):	46	46
0.60 mm (#30):	31	31
0.30 mm (#50):	16	16
0.15 mm (#100):	10	9
0.075 mm (#200):	5.8	6.0
Binder Content (Pb):	5.8	6.1
Eff. Binder Content (Pbe):	5.1	5.4
Dust-to-Binder Ratio:	1.1	1.1
Rice Gravity (Gmm):	2.483	2.472
Avg. Bulk Gravity (Gmb):	2.384	2.374
Avg Air Voids (Va):	4.0	4.0
Agg. Bulk Gravity (Gsb):	2.667	2.670
Avg VMA:	15.8	16.5
Avg. VFA:	75	76

Construction Diary

Relevant Conditions for Construction

Completion Date:	July 16, 2009
24 Hour High Temperature (F):	92
24 Hour Low Temperature (F):	74
24 Hour Rainfall (in):	0.00
Planned Subot Lift Thickness (in):	1.3
Paving Machine:	Roadtec

Plant Configuration and Placement Details

Component	% Setting
Asphalt Content (Plant Setting)	6.5
89 Columbus Granite	36.0
8910 Opelika Limestone Screenings	23.0
M10 Columbus Granite	13.0
Shorter Coarse Sand	28.0
As-Built Sublot Lift Thickness (in):	1.2
Total Thickness of All 2009 Sublots (in):	7.0
Approx. Underlying HMA Thickness (in):	0.0
Type of Tack Coat Utilized:	NTSS-1HM
Target Tack Application Rate (gal/sy):	0.04
Approx. Avg. Temperature at Plant (F):	335
Avg. Measured Mat Compaction:	93.1%

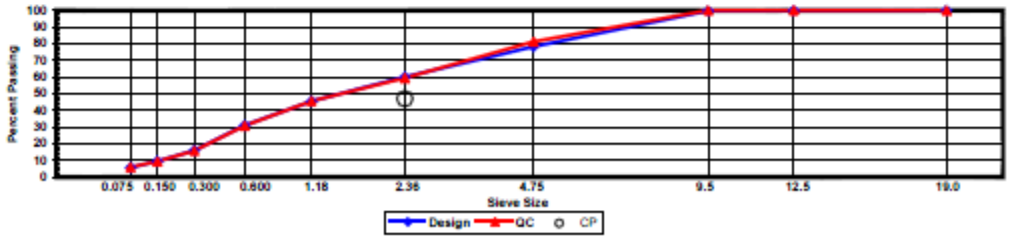

General Notes:

1) Mixes are referenced by quadrant (E=East, N=North, W=West, and S=South), section # (sequential) and sublot (top=1);
3) The total HMA thickness of all structural study sections (N1-N11 and S8-S12) ranges from 5-3/4 to 14 inches by design;
3) All non-structural sections are supprted by a uniform perpetual foundation in order to study surface mix performance;
4) SMA and OGFC refer to stone matrix asphalt and open-graded friction course, respectively; and
5) All liquid asphalt purchased for use in Track reconstruction contained LOF 6500 antistrip additive at a rate of 0.5 percent

10/5/2009

Quadrant: S
Section: 9 *Mix Type = Intermediate - Control*
Sublot: 2

Laboratory Diary

General Desccription of Mix and Materials

Design Method:	Super
Compactive Effort:	80 gyrations
Binder Performance Grade:	76-22
Modifier Type:	SBS
Aggregate Type:	Lms/Sand/Grn
Design Gradation Type:	Fine

Avg. Lab Properties of Plant Produced Mix

Sieve Size	Design	QC
25 mm (1"):	100	99
19 mm (3/4"):	93	92
12.5 mm (1/2"):	82	84
9.5 mm (3/8"):	71	76
4.75 mm (#4):	52	57
2.36 mm (#8):	45	47
1.18 mm (#16):	35	38
0.60 mm (#30):	24	26
0.30 mm (#50):	12	15
0.15 mm (#100):	7	9
0.075 mm (#200):	3.9	5.3
Binder Content (Pb):	4.7	4.4
Eff. Binder Content (Pbe):	4.1	3.9
Dust-to-Binder Ratio:	0.9	1.4
Rice Gravity (Gmm):	2.575	2.551
Avg. Bulk Gravity (Gmb):	2.472	2.439
Avg Air Voids (Va):	4.0	4.4
Agg. Bulk Gravity (Gsb):	2.737	2.695
Avg VMA:	13.9	13.5
Avg. VFA:	71	68

Construction Diary

Relevant Conditions for Construction

Completion Date:	July 14, 2009
24 Hour High Temperature (F):	93
24 Hour Low Temperature (F):	72
24 Hour Rainfall (in):	0.00
Planned Subot Lift Thickness (in):	2.8
Paving Machine:	Roadtec

Plant Configuration and Placement Details

Component	% Setting
Asphalt Content (Plant Setting)	4.7
78 Opelika Limestone	30.0
57 Opelika Limestone	18.0
M10 Columbus Granite	25.0
Shorter Coarse Sand	27.0

As-Built Sublot Lift Thickness (in):	2.8
Total Thickness of All 2009 Sublots (in):	7.0
Approx. Underlying HMA Thickness (in):	0.0
Type of Tack Coat Utilized:	NTSS-1HM
Target Tack Application Rate (gal/sy):	0.07
Approx. Avg. Temperature at Plant (F):	335
Avg. Measured Mat Compaction:	92.8%

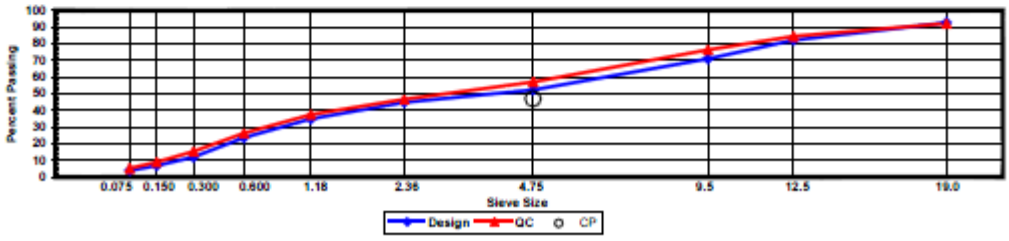

General Notes:
1) Mixes are referenced by quadrant (E=East, N=North, W=West, and S=South), section # (sequential) and sublot (top=1);
3) The total HMA thickness of all structural study sections (N1-N11 and S8-S12) ranges from 5-3/4 to 14 inches by design;
3) All non-structural sections are supprted by a uniform perpetual foundation in order to study surface mix performance;
4) SMA and OGFC refer to stone matrix asphalt and open-graded friction course, respectively; and
5) All liquid asphalt purchased for use in Track reconstruction contained LOF 6500 antistrip additive at a rate of 0.5 percent

10/5/2009

Quadrant: S
Section: 9
Sublot: 3

Mix Type = Base - Control

Laboratory Diary

General Descoription of Mix and Materials

Design Method:	Super
Compactive Effort:	80 gyrations
Binder Performance Grade:	67-22
Modifier Type:	NA
Aggregate Type:	Lms/Sand/Grn
Design Gradation Type:	Fine

Avg. Lab Properties of Plant Produced Mix

Sieve Size	Design	QC
25 mm (1"):	100	99
19 mm (3/4"):	93	95
12.5 mm (1/2"):	84	87
9.5 mm (3/8"):	73	77
4.75 mm (#4):	55	56
2.36 mm (#8):	47	46
1.18 mm (#16):	36	37
0.60 mm (#30):	25	26
0.30 mm (#50):	14	15
0.15 mm (#100):	8	9
0.075 mm (#200):	4.6	5.1
Binder Content (Pb):	4.6	4.7
Eff. Binder Content (Pbe):	4.1	4.2
Dust-to-Binder Ratio:	1.1	1.2
Rice Gravity (Gmm):	2.574	2.540
Avg. Bulk Gravity (Gmb):	2.471	2.439
Avg Air Voids (Va):	4.0	4.0
Agg. Bulk Gravity (Gsb):	2.738	2.699
Avg VMA:	13.9	13.9
Avg. VFA:	71	71

Construction Diary

Relevant Conditions for Construction

Completion Date:	July 3, 2009
24 Hour High Temperature (F):	92
24 Hour Low Temperature (F):	69
24 Hour Rainfall (in):	0.00
Planned Subot Lift Thickness (in):	3.0
Paving Machine:	Roadtec

Plant Configuration and Placement Details

Component	% Setting
Asphalt Content (Plant Setting)	4.9
78 Opelika Limestone	30.0
57 Opelika Limestone	18.0
M10 Columbus Granite	25.0
Shorter Coarse Sand	27.0
As-Built Sublot Lift Thickness (in):	3.0
Total Thickness of All 2009 Sublots (in):	7.0
Approx. Underlying HMA Thickness (in):	0.0
Type of Tack Coat Utilized:	NA
Target Tack Application Rate (gal/sy):	NA
Approx. Avg. Temperature at Plant (F):	325
Avg. Measured Mat Compaction:	92.6%

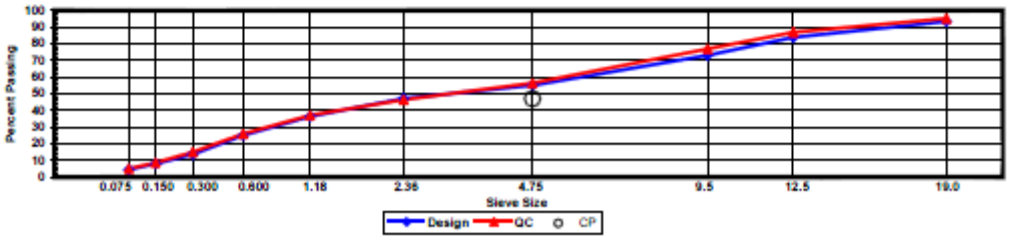

General Notes:

1) Mixes are referenced by quadrant (E=East, N=North, W=West, and S=South), section # (sequential) and sublot (top=1);
3) The total HMA thickness of all structural study sections (N1-N11 and S8-S12) ranges from 5-3/4 to 14 inches by design;
3) All non-structural sections are supprted by a uniform perpetual foundation in order to study surface mix performance;
4) SMA and OGFC refer to stone matrix asphalt and open-graded friction course, respectively; and
5) All liquid asphalt purchased for use in Track reconstruction contained LOF 6500 antistrip additive at a rate of 0.5 percent

APPENDIX B **– IDT DATA**

Table E1: Creep Compliance Data Determined through AASHTO T 322-07

Test Temperature (°C)	Loading Time (sec)	Thiopave - Intermediate	Thiopave - Base	Control - Surface	Control - Base
-20	1	0.032	0.043	0.044	0.028
-20	2	0.033	0.045	0.046	0.029
-20	5	0.035	0.047	0.048	0.032
-20	10	0.037	0.05	0.052	0.033
-20	20	0.038	0.052	0.054	0.035
-20	50	0.041	0.056	0.058	0.037
-20	100	0.043	0.06	0.062	0.039
-10	1	0.045	0.061	0.066	0.049
-10	2	0.048	0.065	0.073	0.053
-10	5	0.052	0.073	0.08	0.059
-10	10	0.056	0.079	0.088	0.063
-10	20	0.06	0.087	0.096	0.07
-10	50	0.067	0.099	0.111	0.08
-10	100	0.074	0.111	0.12	0.09
0	1	0.055	0.084	0.092	0.072
0	2	0.06	0.094	0.102	0.084
0	5	0.066	0.107	0.12	0.1
0	10	0.074	0.121	0.134	0.117
0	20	0.082	0.139	0.16	0.14
0	50	0.097	0.171	0.197	0.181
0	100	0.113	0.205	0.235	0.224

Table E2: Indirect Tensile Strength (ITS) (psi) Values determined at -10°C

Mix ID	Thiopave - Intermediate	Thiopave - Base	Control - Surface	Control - Base
Sample 1 ITS (psi)	619.21	578.89	685.33	643.51
Sample 2 ITS (psi)	612.29	539.03	681.26	572.93
Sample 3 ITS (psi)	595.02	591.18	683.34	596.15
Average ITS (psi)	608.84	569.70	683.31	604.20
Standard Deviation ITS (psi)	12.46	27.26	2.04	35.97